European Journal of Taxonomy 898: 1–61
https://doi.org/10.5852/ejt.2023.898.2295
ISSN 2118-9773
www.europeanjournaloftaxonomy.eu
2023 · Laville T. *et al.*

Monograph

urn:lsid:zoobank.org:pub:87EE2C76-1DDC-40DE-87E7-4D0E11A312DC

Re-appraisal of thylacocephalans (Euarthropoda, Thylacocephala) from the Jurassic La Voulte-sur-Rhône Lagerstätte

Thomas LAVILLE [1,*], Marie-Béatrice FOREL [2] & Sylvain CHARBONNIER [3]

[1,2,3] Muséum national d'Histoire naturelle, Centre de Recherche en Paléontologie – Paris (CR2P, UMR 7207), Sorbonne Université-MNHN-CNRS, 57 rue Cuvier, 75005 Paris, France.
[1] Biogéosciences, UMR 6282 CNRS, Université de Bourgogne, 6 boulevard Gabriel, 2100 Dijon, France.

[*] Corresponding author: thomas.laville2@mnhn.fr
[2] Email: marie-beatrice.forel@mnhn.fr
[3] Email: sylvain.charbonnier@mnhn.fr

[1] urn:lsid:zoobank.org:author:EDDB1B51-2017-405B-9A92-52EA900A13CA
[2] urn:lsid:zoobank.org:author:063C1F7E-6D26-48F9-A8B1-2AFA496B5FB8
[3] urn:lsid:zoobank.org:author:2B4CC15F-FB7A-4AAF-8CB5-365E976850FA

Abstract. Thylacocephalans are enigmatic euarthropods, known at least from the Silurian to the Cretaceous. Despite remaining uncertainties concerning their anatomy, key features can be recognised such as a shield enveloping most of the body, hypertrophied compound eyes, three pairs of raptorial appendages and a posterior trunk consisting of eight up to 22 segments bearing appendages and eight pairs of gills. Well-known for its euarthropod diversity, the La Voulte-sur-Rhône Lagerstätte (Callovian, Middle Jurassic, France) has provided many remains of four thylacocephalan species so far: *Dollocaris ingens*, *Kilianicaris lerichei*, *Paraostenia voultensis* and *Clausocaris ribeti*. In this paper, we study the type material as well as undescribed material. The re-description of La Voulte thylacocephalans reveals an unexpected diversity, with the description of two new species, *Austriocaris secretanae* sp. nov. and *Paraclausocaris harpa* gen. et sp. nov., and of specimens of *Mayrocaris*, a taxon originally described from Solnhofen Lagerstätten. We also reassign *Clausocaris ribeti* to *Ostenocaris*. The reappraisal of La Voulte thylacocephalans also provides important insight into the palaeobiology of Thylacocephala. New key anatomical features are described, such as an oval structure or a putative statocyst, which indicate a nektonic or nektobenthic lifestyle. Finally, we document a juvenile stage for *Paraostenia voultensis*.

Keywords. Euarthropoda, Jurassic, anatomy, disparity, morphometrics.

Laville T., Forel M.-B. & Charbonnier S. 2023. Re-appraisal of thylacocephalans (Euarthropoda, Thylacocephala) from the Jurassic La Voulte-sur-Rhône Lagerstätte. *European Journal of Taxonomy* 898: 1–61. https://doi.org/10.5852/ejt.2023.898.2295

Introduction

Thylacocephala Pinna, Arduini, Pesarini & Teruzzi, 1982 is a group of intriguing fossil euarthropods which are characterised by particular body features: a folded shield enveloping most of the body, large

compound eyes, three pairs of raptorial appendages, a set of eight pairs of gills, and from eight up to 22 posterior trunk segments bearing appendages (Schram 2014). Known from at the least the Silurian to the Cretaceous (Schram 2014), thylacocephalans have a scarce fossil record in the Jurassic. They have only been reported from four different European localities (Table 1): Osteno Lagerstätte (Italy, Sinemurian, Early Jurassic: Arduini *et al*. 1980; Pinna *et al*. 1982, 1985), Strawberry Bank Lagerstätte (England, Toarcian, Early Jurassic: Williams *et al*. 2015), La Voulte-sur-Rhône Lagerstätte (France, Callovian, Middle Jurassic: Van Straelen 1923a; Secrétan & Riou 1983; Secrétan 1985; Charbonnier *et al*. 2010) and Solnhofen Limestones (Germany, Tithonian, Late Jurassic: e.g., Oppenheim 1888; Polz 1990, 1994, 2001; Braig *et al*. 2019). Despite this limited distribution during the Jurassic, 11 thylacocephalan species have been described so far (Table 1).

In addition to this important diversity, Jurassic representatives are among the best-preserved thylacocephalans. While most species are essentially described based on their shield, Jurassic representatives are often preserved with soft-parts. For instance, the organisation of the digestive, respiratory and visual systems has been reported for *Dollocaris ingens* Secrétan, 1985 (La Voulte Lagerstätte; Vannier *et al*. 2016). Moreover, cephalic appendages have been described from Solnhofen representatives of *Clausocaris lithographica* (Oppenheim, 1888) (see Laville *et al*. 2021a) and *Mayrocaris bucculata* Polz, 1994 (see Haug *et al*. 2014). These anatomical details are important for resolving the phylogenetic affinities of Thylacocephala (e.g., Haug *et al*. 2014; Vannier *et al*. 2016; Broda & Zatoń 2017). Even though many morphological details point out to a pancrustacean affinity, the position of Thylacocephala relative to other pancrustacean ingroups is uncertain. Affinities with cirripeds (Pinna *et al*. 1982, 1985), malacostracans (Secrétan 1985; Vannier *et al*. 2016) and remipeds (Haug *et al*. 2014) have been suggested but no consensus exists on this topic.

In this paper, we revise known species from the La Voulte-sur-Rhône Lagerstätte and describe new species. This descriptive work provides new important insight into the diversity, morphology and palaeobiology of thylacocephalans. Furthermore, the exceptional preservation of the La Voulte specimens clarifies key aspects of the anatomy of thylacocephalans.

Geological setting

The La Voulte-sur-Rhône Lagerstätte (Middle Jurassic, early Callovian, *Gracilis* Biozone) is located in Ardèche, France and belongs to the eastern sedimentary cover of the Massif Central (Fig. 1A–B). Following the onset of the transgression in the late Bathonian, the Tethys Ocean was characterised by a high eustatic level during the Callovian (Jacquin & Graciansky 1999; Hallam 2001). This event was associated with an important period of rifting which led to the overflow of epicontinental seas on the peri-tethyan domain and to well-developed terrigenous platforms with only few, small carbonate platforms in Western Europe (Enay *et al.* 1993). The deposits of the La Voulte-sur-Rhône Lagerstätte are particularly linked to this context. During the Callovian, La Voulte-sur-Rhône was located on the Ardèche palaeomargin, adjacent to the submerged Hercynian Massif Central and the Subalpine Basin. This latest was connected to the Tethys Ocean (Enay 1993).

The La Voulte Lagerstätte corresponds to about 5–6 m of marls, mainly composed of a clay mineralogy (60–70% of montmorillonite), and topped by 15 m of iron carbonate deposits (Fig. 1C). Described for the first time by Fournet (1843), the La Voulte Lagerstätte has yielded a well-diversified non-vertebrate fauna with few vertebrate remains (actinopterygians, sarcopterygians and reptiles; Charbonnier 2009). This Lagerstätte is famous for its fossils with soft-tissues preservation, especially among pancrustaceans and cephalopods (Wilby *et al.* 1996). Fossils are either preserved in 3D in sideritic nodules uncovered from the basal marls, or compressed in other marly layers (Fischer *et al*. 2003; Charbonnier *et al*. 2014). Jauvion *et al*. (2019) studied in detail the preservation sequence of Thylacocephala in nodules from La Voulte and highlighted the important role of the early precipitation of fluoroapatite and pyrite in soft-tissue preservation and the various mineralogies associated with the different tissue types.

Table 1. Diversity of Jurassic thylacocephalans.

Series	Age	Locality	Species	References
Early Jurassic	Sinemurian	Osteno, Lombardy, Italy	*Ostenocaris cypriformis* (Arduini, Pinna & Teruzzi, 1980)	Arduini *et al*. 1980; Pinna *et al*. 1982, 1985
	Toarcian	Strawberry Bank Lagerstätte, Ilminster, Somerset, UK	No described or figured specimens	Williams *et al*. 2015
Middle Jurassic	Callovian	La Voulte-sur-Rhône, Ardèche, France	*Austriocaris secretanae* sp. nov.	This paper
			Dollocaris ingens Van Straelen, 1923	Van Straelen 1923; Secrétan & Riou 1983; Secrétan 1985; Charbonnier *et al*. 2010; Vannier *et al*. 2016
			Kilianicaris lerichei Van Straelen, 1923	Van Straelen 1923; Secrétan & Riou 1983; Secrétan 1985; Charbonnier *et al*. 2010; This paper
			Mayrocaris sp.	This paper
			Ostenocaris ribeti (Secrétan, 1985)	Secrétan & Riou 1983; Secrétan 1985; Charbonnier *et al*. 2010; This paper
			Paraclausocaris harpa gen. et sp. nov.	This paper
			Paraostenia voultensis Secrétan, 1985	Secrétan & Riou 1983; Secrétan 1985; Charbonnier *et al*. 2010; This paper
Late Jurassic	Tithonian	Solnhofen Lagerstätten, Bavaria, Germany	*Clausocaris lithographica* (Oppenheim, 1888)	Oppenheim 1888; Polz 1988, 1989, 1990, 1993; Haug *et al.* 2014; Laville *et al*. 2021a
			Dollocaris michelorum Polz, 2001	Polz 2001
			Falcatacaris bastelbergeri Braig, Haug J.T, Schädel & Haug C., 2019	Braig *et al*. 2019
			Mayrocaris bucculata Polz, 1994	Polz 1994, 1997; Haug *et al*. 2014; Laville *et al*. 2021a

Sixty species have been described, including bivalves, cephalopods (Fischer & Riou 1982, 2002; Fuchs 2014; Kruta *et al.* 2016), annelids (Alessandrello *et al.* 2004), pycnogonids (Charbonnier *et al*. 2007b), pancrustaceans (cumaceans: Bachmayer 1960; mysidaceans: Secrétan & Riou 1986; decapods: Van Straelen 1922, 1923b, 1925; Carriol & Riou 1991; Charbonnier *et al.* 2013; Audo *et al.* 2014; Jauvion

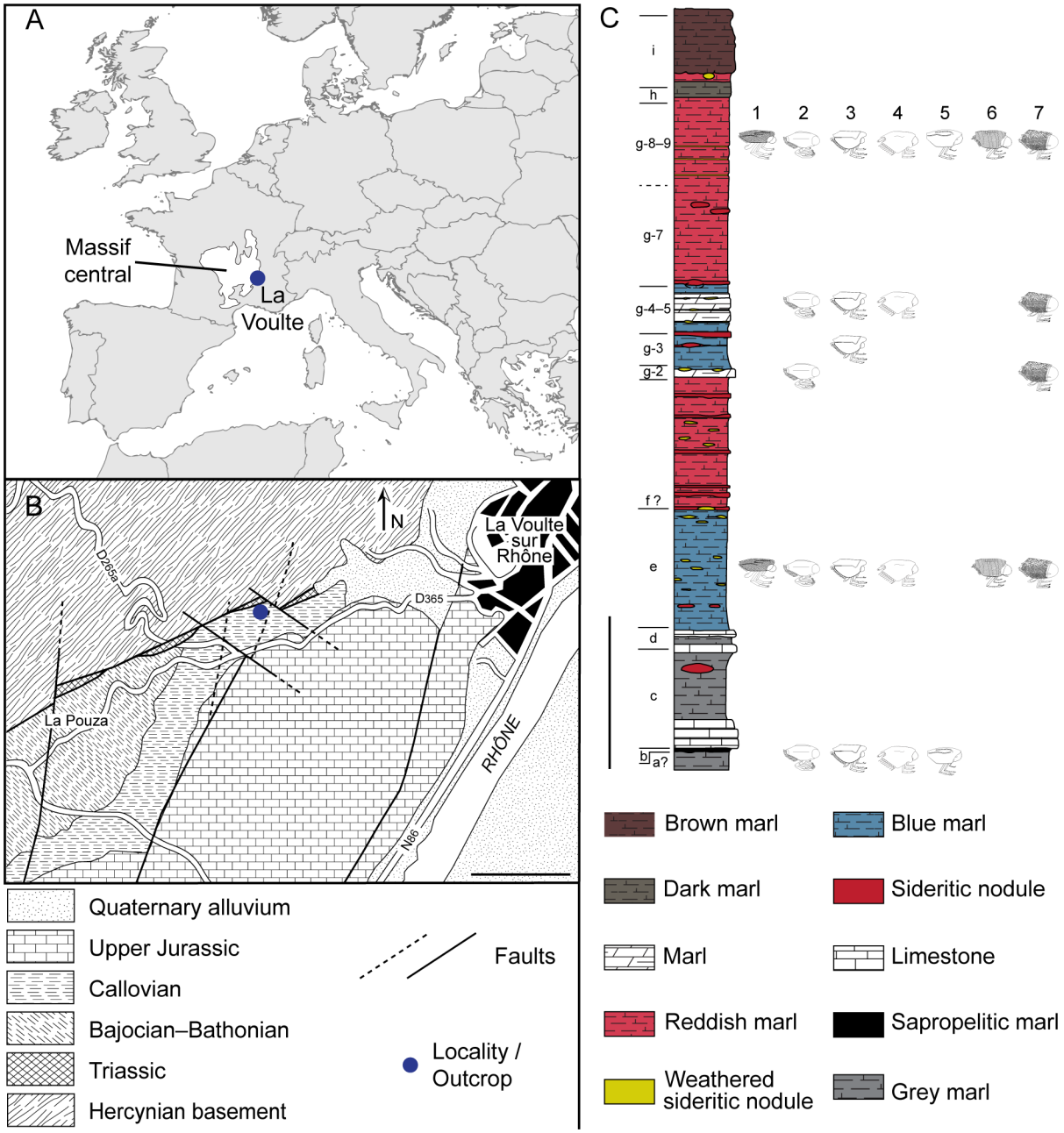

Fig. 1. Geological settings of La Voulte-sur-Rhône Lagerstätte. **A**. Location of La Voulte Lagerstätte. **B**. Geological map of the La Voulte area. **C**. Stratigraphic column of the La Voulte Lagerstätte, with the distribution of thylacocephalan taxa. Abbreviations: 1 = *Austriocaris secretanae* sp. nov.; 2 = *Dollocaris ingens* Van Straelen, 1923; 3 = *Kilianicaris lerichei* Van Straelen, 1923; 4 = *Mayrocaris* sp; 5 = *Ostenocaris ribeti* (Secrétan, 1985) comb. nov.; 6 = *Paraclausocaris harpa* gen. et sp. nov.; 7 = *Paraostenia voultensis* Secrétan, 1985. Scale bars: B = 500 m; C = 1 m. A–B modified after Charbonnier *et al*. (2010), C modified after Charbonnier (2009).

et al. 2016, 2017, 2020; Audo & Schweigert 2018), brachiopods, echinoderms (e.g., Villier *et al*. 2009) and hemichordates (Alessandrello *et al*. 2004). Euarthropoda Lankester, 1904 is the most diverse taxon, representing nearly 50% of all taxa described from La Voulte (Charbonnier 2009). Among euarthropods, thylacocephalans are the most abundant fossils, representing 32.3% of the euarthropods recovered in nodules (Charbonnier *et al*. 2010). Up to now, four species had been described: *Dollocaris ingens* Van Straelen, 1923, *Kilianicaris lerichei* Van Straelen, 1923, *Paraostenia voultensis* Secrétan, 1985 and *Clausocaris ribeti* Secrétan, 1985.

Based on structural, sedimentary and faunal evidences, the La Voulte Lagerstätte corresponds to the upper part of the bathyal zone, near the slope-basin transition, with a water depth most probably exceeding 200 m (Elmi 1967; Charbonnier *et al.* 2007a). However, recent discoveries place doubts on this statement, providing arguments for an illuminated and thus shallower environment (Vannier *et al.* 2016).

Material and methods

Material

We investigated 211 specimens in this study (exhaustive list in Supp. file 1), most being preserved in compression. The studied specimens are deposited in the collections of the Muséum national d'histoire Naturelle, Paris, France (197 specimens; acronym: MNHN.F), the Observatoire des Sciences de l'Univers de Grenoble, France (three specimens; acronym: OSUG-UJF-ID), the Museo Civico di Storia Naturale, Milano, Italy (11 specimens; acronym: MSNM).

We do not include the species *Dollocaris ingens* in this study, as it has been extensively studied in the past (Secrétan & Riou 1983; Secrétan 1985; Fröhlich *et al*. 1992; Charbonnier 2009; Vannier *et al*. 2016; Jauvion *et al*. 2019).

Documentation methods

General view

Six specimens (MNHN.F.A29301, A29310, A29327, A53329, A53335, A53342) were imaged using a Keyence VHX-6000 digital microscope at the Zoomorphologie group, Ludwig-Maximilians Universität (LMU), München. Three different illumination settings were used: cross-polarised ring-light illumination, cross-polarised co-axial illumination or co-axial illumination. A 50 times magnification was used. The built-in high dynamic range (HDR) function was used to cope with issues of under- or over-exposure. Every image is thus a composite of several images taken under different exposure times. To overcome limitations in depth of field and in field of view, several adjacent images were recorded, each with a Z-stack of images.

All other MNHN specimens were documented using either a Nikon d700 camera equipped with a Nikon AF-S Nikkor 35 mm f/1.8g ED lens or a Nikon d5300 camera equipped with a Nikon AF-S Nikkor 35 mm f/1.8g ED lens and a Hoya HD polarising filter. Specimens were illuminated with a Kaiser RB 218n HF lighting unit. The camera was controlled for remote shooting using DigiCamControl (Duka Istvan, MIT license). To overcome limitations in depth of field, some specimens were recorded with a Z-stack of images.

MSNM specimens were recorded using a Pentax KS-2 camera equipped with a Pentax D-FA Macro 50 mm f/2.8 lens.

Pictures of anatomical details were taken either with a Canon EOS 60D camera equipped with a Canon MPE-65 mm macrolens and a Hoya HD polarising filter, illuminated with a Kaiser RB 218n HF lighting unit or with an Axio ZOOM.V16 stereo microscope equipped with a DeltaPix Invenio-20EIII camera under cross-polarised ring light at the Centre de Recherche en Paléontologie – Paris (CR2P).

Fluorescence imaging

Specimen MNHN.F.A53342 was photographed with a Keyence BZ-9000 inverse epifluorescence microscope using green light at the Zoomorphologie group, LMU, München (TRITC filter, band-pass width: 532–554 nm, with a maximal excitation wavelength of 543 nm; detection ranges: 570–613 nm) with lens magnification of ×2. Together with the magnification of the camera, this results in a magnification of about 20×. To overcome limitations in depth of field and in field of view, several adjacent images were recorded, each with a Z-stack of images. Only the luminescence was collected.

Image processing

For specimens documented with the Keyence VHX-6000 digital microscope, focus stacking and panoramic stitching were performed with the software implemented in the digital microscope. For the other specimens, Z-stacks of fluorescence images were digitally fused to single in-focus images using CombineZP (Alan Hadley, GNU).

For the specimen documented under fluorescence settings using Keyence BZ-9000 inverse epifluorescence microscope, stitching of the adjacent images was made with the Photomerge plug-in from Adobe Photoshop CS5.

Post-processing of every image (histogram optimisation, contrast, brightness and sharpness adjustment) was performed with GIMP 2.10 (GNU). Additionally, areas of interest were colour-marked to highlight morphological structures. Line drawings were made using Adobe Illustrator CS6.

Morphometric analyses

Measurements

Shield, eyes and appendages were measured directly on digital photographs with ImageJ2 (Schneider *et al.* 2012). Descriptive statistics are given in Table 2, which was computed using the gtsummary R package (Sjoberg *et al.* 2021). Measurement data are available at the following link (Supp. file 2): https://doi.org/10.5281/zenodo.6341180.

Measurement abbreviations

Aad = anterodorsal angle
Aav = anteroventral angle
Apd = posterodorsal angle
Apv = posteroventral angle
H = height
Ha = anterior shield height
Hmax = maximum shield height
Hp = posterior shield height
L_n = length of podomere n (appendages)
Lr = length of the rostrum
Ls = length of the shield
Lw = length of the shield without the rostrum
w = width
w_n = width of podomere n (appendages; Fig. 2)

Simple allometry

The allometry between shield height (Hmax) and shield length (Ls) was studied by running a standardised major axis analysis (SMA) for each species using the R package smatr ver. 3.4.8 (Warton *et al.* 2012). A major axis analysis is a type-II regression, which is used to find a line of best fit that summarises the relationships between two variables but not to predict the value of one variable using the other as in

a linear regression (Warton *et al.* 2006). The major axis is the line that minimises the sum of squares of the shortest distances from the data points to the line. Log-transformed data were used to study the relationships between both variables (see Packard 2018 and Pélabon *et al*. 2018 for a discussion on the use of log-transformed data in allometry studies). Significance of the correlation for each group was tested using an analysis of variance (ANOVA) under a α-level of 0.05. This analysis was not performed for *Mayrocaris* sp. and *Austriocaris secretanae* sp. nov. as the number of specimens available for measurements was no more than two for each species.

The allometry between shield height (Hmax) and shield length (Ls) for *Paraostenia voultensis* was studied in more details as the qualitative morphological description (see Systematic Palaeontology) distinguished two morphotypes. Comparison between elevation and slope of both morphotypes was respectively done using a Wald test (Rao 1973) and a likelihood ratio test (Flury 1984) for $\alpha = 0.05$.

Complex allometry

To have a complete view of the morphological variability of *Paraostenia voultensis*, we studied the complex allometry using a principal component analysis (PCA). The first principal component (PC1) is considered an estimate of the allometric line as it represents the line of best fit under a least-square criterion for multivariate dataset (Jolicoeur 1963). Log-transformed data were used for this analysis. Not all measures being assessable on all the specimens due to preservation, we applied an iterative PCA method, also known as EM-PCA algorithm (Kiers 1997), to estimate the missing values for the PCA. The Burnaby back-projection method was applied to remove the effect of size on the data (Burnaby 1966).

Estimation of missing values was done with the R package missMDA ver. 1.18 (Josse & Husson 2016). Burnaby back-projection method algorithm developed by Blankers *et al*. (2012) and modified by Eberle *et al*. (2014) was used for the size correction.

The PCA was performed with the R package FactoMineR ver. 2.4 (Lê *et al.* 2008) and the results were plotted using R packages factoextra ver. 1.0.7 (Kassambara & Mundt 2019) and cowplot ver. 1.1.1 (Wilke 2019). Table of eigenvalues and factor loadings was done with gridExtra ver. 2.3 (Auguie 2017).

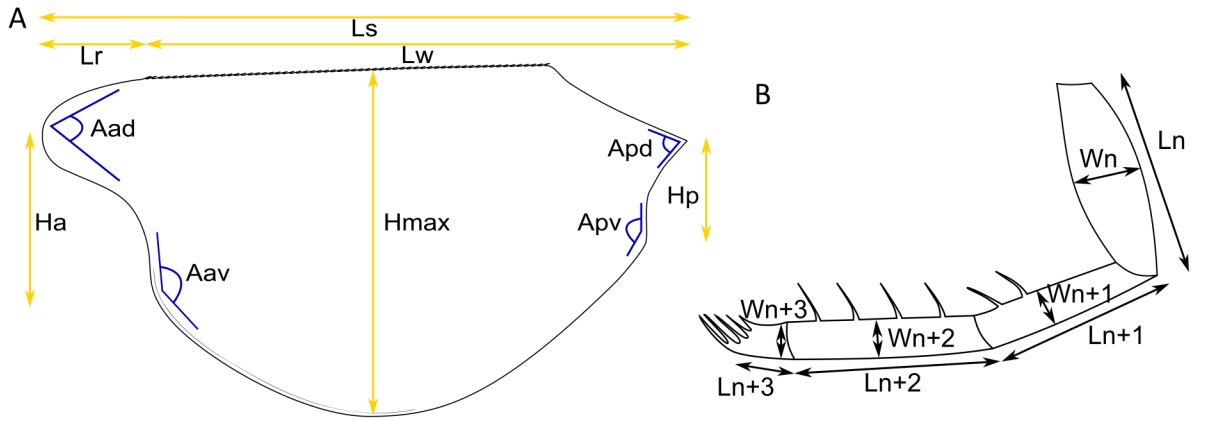

Fig. 2. Scheme of measurements for thylacocephalans. **A**. Shield. **B**. Raptorial appendages. Abbreviations: Aad = anterodorsal angle; Aav = anteroventral angle; Apd = posterodorsal angle; Apv = posteroventral angle; Ha = anterior shield height; Hmax = maximum shield height; Hp = posterior shield height; Ln = length of podomere (appendages); Lr = length of the rostrum; Ls = length of the shield; Lw = length of the shield without the rostrum; w_n = width of podomere n (appendages).

Table 2 (continued on nex page). Descriptive statistics on the shield measurements. Abbreviations: Aad = anterodorsal angle; Aav = anteroventral angle; Apd = posterodorsal angle; Apv = posteroventral angle; Ha = anterior shield height; Hmax = maximum shield height; Hp = posterior shield height; Inf = unknown data; Lr = length of the rostrum; Ls = length of the shield; Lw = length of the shield without the rostrum; N = number of measured specimens; NA = non-applicable; SD = standard deviation.

Measurements	*Austriocaris secretanae* sp. nov. (N = 4)	*Kilianicaris lerichei* (N = 15)	*Mayrocaris* sp. (N = 2)	*Ostenocaris ribeti* (N = 8)	*Paraclausocaris harpa* gen. et sp. nov. (N = 9)	*Paraostenia voultensis* (N = 44)
Ls (mm)						
Mean (SD)	66.29 (47.98)	37.27 (8.69)	18.27 (1.25)	17.16 (5.46)	33.73 (12.34)	24.27 (7.76)
Minimum–Maximum	32.36–100.22	25.06–57.01	17.39–19.15	10.03–23.24	24.29–51.87	10.66–39.92
Missing data	2	5	0	4	5	9
Lr (mm)						
Mean (SD)	9.10 (5.74)	13.96 (14.65)	NA (NA)	NA (NA)	NA (NA)	NA (NA)
Minimum–Maximum	5.04–13.16	3.30–50.91	Inf–Inf	Inf–Inf	Inf–Inf	Inf–Inf
Missing data	2	1	2	8	9	44
Lw (mm)						
Mean (SD)	27.38 (NA)	19.18 (12.46)	NA (NA)	NA (NA)	NA (NA)	NA (NA)
Minimum–Maximum	27.38–27.38	5.72–36.44	Inf–Inf	Inf–Inf	Inf–Inf	Inf–Inf
Missing data	3	6	2	8	9	44
Ha (mm)						
Mean (SD)	13.22 (8.38)	10.76 (3.46)	6.42 (0.69)	7.64 (1.82)	12.45 (2.29)	12.75 (3.47)
Minimum–Maximum	7.29–19.15	6.56–20.85	5.93–6.91	4.75–10.10	9.83–15.98	6.26–20.32
Missing data	2	1	0	0	0	6
Hmax (mm)						
Mean (SD)	29.03 (11.91)	21.15 (3.63)	11.79 (0.37)	8.52 (2.11)	16.45 (4.84)	15.26 (4.74)
Minimum–Maximum	11.20–35.85	15.74–28.27	11.53–12.05	5.33–11.93	11.77–27.83	7.28–26.55
Missing data	0	4	0	0	0	8
Hp (mm)						
Mean (SD)	5.84 (3.16)	6.19 (1.21)	4.10 (0.34)	2.66 (0.70)	7.07 (4.75)	5.23 (1.74)
Minimum–Maximum	3.60–8.07	4.53–8.10	3.86–4.34	1.54–3.73	3.33–15.20	2.55–9.02
Missing data	2	9	0	1	4	8
Aad (°)						
Mean (SD)	67.15 (0.06)	59.93 (9.66)	71.60 (6.76)	89.53 (47.37)	75.69 (8.55)	73.67 (7.18)
Minimum–Maximum	67.10–67.21	44.36–76.30	66.82–76.38	47.20–180.00	66.42–91.98	55.61–86.40
Missing data	1	3	0	2	0	5

Table 2 (continued). Descriptive statistics on the shield measurements. Abbreviations: Aad = anterodorsal angle; Aav = anteroventral angle; Apd = posterodorsal angle; Apv = posteroventral angle; Ha = anterior shield height; Hmax = maximum shield height; Hp = posterior shield height; Inf = unknown data; Lr = length of the rostrum; Ls = length of the shield; Lw = length of the shield without the rostrum; N = number of measured specimens; NA = non-applicable; SD = standard deviation.

Measurements	*Austriocaris secretanae* sp. nov. (N = 4)	*Kilianicaris lerichei* (N = 15)	*Mayrocaris* sp. (N = 2)	*Ostenocaris ribeti* (N = 8)	*Paraclausocaris harpa* gen. et sp. nov. (N = 9)	*Paraostenia voultensis* (N = 44)
Aav (°)						
Mean (SD)	108.10 (7.17)	140.07 (5.38)	108.52 (17.77)	106.68 (14.05)	99.92 (12.68)	74.03 (10.27)
Minimum–Maximum	103.03–113.17	130.69–145.15	95.95–121.09	85.39–124.34	86.55–122.78	43.99–95.12
Missing data	2	1	0	1	0	3
Apv (°)						
Mean (SD)	148.26 (0.96)	140.07 (25.37)	81.13 (14.63)	142.80 (6.94)	138.71 (21.00)	104.02 (10.34)
Minimum–Maximum	147.58–148.94	68.14–162.39	70.79–91.47	136.33–156.35	108.52–153.23	81.10–128.82
Missing data	2	4	0	1	5	4
Apd (°)						
Mean (SD)	74.50 (9.70)	76.59 (6.50)	80.77 (14.83)	105.09 (9.34)	93.07 (7.67)	90.02 (9.55)
Minimum–Maximum	67.64–81.36	65.16–82.50	70.29–91.26	94.33–120.08	84.22–102.03	71.11–113.71
Missing data	2	7	0	1	5	8
Hmax/Ls ratio						
Mean (SD)	0.35 (0.00)	0.57 (0.04)	0.65 (0.06)	0.52 (0.03)	0.57 (0.06)	0.65 (0.06)
Minimum–Maximum	0.34–0.35	0.50–0.63	0.60–0.69	0.48–0.55	0.50–0.64	0.52–0.79
Missing data	2	6	0	4	5	15

Clustering analyses

In addition to the SMA to compare the allometry of the two morphotypes of *Paraostenia voultensis*, we ran a K-means analysis to see if the morphotypes can be recovered using a quantitative morphological method. K-means is a partitioning clustering analysis in which a dataset is separated into a set of K groups, where K is specified by the analyst (here K = 3). Samples are classified in multiple groups, using the minimisation of the within-cluster sum-of-squares (also known as inertia). Each group is represented by its centroid, which corresponds to the means of the samples assigned to the group. Prior to the analysis, we analysed the clustering tendency of the dataset using the Hopkins statistic and the visual assessment of cluster tendency method using the factoextra package. The optimal number of clusters was assessed using the NbClust function from the R package NbClust ver. 3.0 (Charrad *et al.* 2014). The K-means analysis was run with functions implemented in the R environment (R Core Team 2021).

Results

Systematic palaeontology

Class **Thylacocephala** Pinna, Arduini, Pesarini & Teruzzi, 1982

Original diagnosis (Schram 1990)

These are arthropods with a small to large bilobed carapace enclosing the entire body. Compound eyes very well developed as either large, sessile bodies situated in optic notches or as organs that virtually cover the surface of a protrudent, sac-like cephalon. Body appendages are of two types: anteriorly 3 pairs of subchelate, raptorial limbs, and posteriorly a set of from 8 to 16 pairs of apparently paddle-like limbs. Eight sets of well-developed gills are associated with the subchelate limbs. The posterior trunk is marked with pronounced pleurites, probably developed internally as an endrophragmal skeleton, associated with the posterior limbs.

Remarks

We decide not to follow the attempt of classification proposed by Schram (2014) as it has been shown to present many issues (e.g., polyphyly of Concavicarida Briggs & Rolfe, 1983 and Conchyliocarida Secrétan, 1983, problems with the definition of autapomorphies for many taxa; see Hegna *et al.* 2014 and Laville *et al.* 2021a, 2021b for detailed explanations).

Genus ***Austriocaris*** Glaessner, 1931

Type species

Austriocaris carinata Glaessner, 1931 by monotypy.

Original diagnosis (Rolfe 1969)

Carapace only known, posterior excavation arcuate or irregular, anterior margin concave or produced into small beak; posteroventral or ventromedian V-shaped furrow; surface smooth with mid-dorsal granulations or posteroventral pits, or dorso-ventrally striate.

Emended diagnosis

Thylacocephala with an optic notch occupying only the ventral part of the anterior margin, presence of a straight mid-dorsal line and a sharp postero-ventral corner.

Remarks

Rolfe (1969) inversed the orientation of the shield of *Austriocaris*, the posterior being identified as the anterior. This influenced his diagnosis, with the optic notch being described as a posterior notch.

Austriocaris secretanae sp. nov.
urn:lsid:zoobank.org:act:1AE5E1E4-F48D-4D36-BD5B-3CDC7225DE95
Figs 3–4

Dollocaris ingens – Secrétan 1985: 381–386, fig. 5a–b. — Charbonnier *et al*. 2010: 119, fig. 6d; 2014: 375, fig. 4a.

Diagnosis

Austriocaris with stout and long raptorial appendages, the third pair having spines on the second and third podomeres of the distal part, and a posterior trunk consisting of 12 segments bearing rod-like appendages. Absence of ventro-lateral structure.

Etymology

In reference to Sylvie Secrétan (CNRS, Paris), for her important contribution to the study of La Voulte-sur-Rhône thylacocephalans.

Material examined

Holotype

FRANCE • La Boissine, La Voulte-sur-Rhône, Ardèche; Callovian, Middle Jurassic; MNHN.F.R50963.

Paratypes

FRANCE • 6 specs; same collection data as for holotype; MNHN.F.A29249, A29257, A29286, A84029, R06203, R50971 • 3 specs; same collection data as for holotype; MSNM i7591, i13276, i13603.

Measurements

See Table 2.

Description

Shield morphology

Sub-oval shield in lateral view with a short, sinuous anterior margin, a sharp antero-dorsal corner, a straight and horizontal dorsal midline, endings posteriorly in a sharp postero-dorsal corner, a posterior margin divided into a very short and straight dorsal part antero-ventrally oriented and a straight, sub-vertical ventral part, a rounded postero-ventral corner, a ventral margin divided into a posterior half, steeply descending antero-ventrally and a horizontal anterior part merging approximately at the posterior third of the length, a rounded antero-ventral corner (Fig. 3A–D). Rim of all free margins delimiting a marginal fold.

Shield macro-ornamentation

Shield with a dorso-lateral carina located on its anterior area and a medio-lateral carina protruding from the postero-ventral angle (Fig. 3). Dorso-lateral carina horizontal until mid-length of the shield where it folds down on itself. Presence of a row of 33 pores on the top of the carina (Fig. 3E). Medio-lateral carina horizontal until mid-length then becoming antero-ventrally oriented. Rim of all free margins delimiting the marginal fold. Shield also ornamented with horseshoe-like ridges (Fig. 4A, C).

Sensory structures

Large, oval, stalked compound eyes protruding from the anterior margin and occupying the entire margin (Fig. 3H–I). Eyes tilted in the same orientation as the anterior margin, formed by hexagonal ommatidia (w = ~65 µm; l = ~70 µm, about 196 per mm²; Fig. 4A, F).

Cephalic appendages

Cephalic appendages not preserved.

Raptorial appendages

Presence of three pairs of stout raptorial appendages recognised by preservation of muscles, protruding from the anterior part of the ventral margin (Fig. 3A, C). Raptorial appendages consisting in two parts: a proximal postero-ventrally oriented and a distal one, antero-ventrally oriented. Articulation between both parts forming an elbow.

First pair of raptorial appendages (Fig. 3H–I), the shortest, consisting of a proximal part with two rectangular podomeres: podomere 1 being 4.2 times as long as wide; podomere 2 being 4.7 times as long as wide. Distal part of the appendages formed by three rectangular podomeres: podomere 3 being 3.4 times as long as wide, bearing six spines on its medial margin; podomere 4 being 2.3 times as long as wide; podomere 5, the shortest, being 1.4 times as long as wide and ending in a cluster of three spines.

Second pair of raptorial appendages consisting of a proximal part with two podomeres (Fig. 3A, C): podomere 1 being 4.7 times as long as wide; podomere 2, the longest, being 5.3 times as long as wide. Distal part of the appendage consisting of three podomeres: podomere 3 being 3.2 times as long as wide; podomere 4 being 3.1 times as long as wide; podomere 5 being 1.5 times as long as wide and ending distally in a cluster of five spines.

Third pair of raptorial appendages, the longest, consisting of a proximal part formed by two rectangular podomeres (Figs 3A–C, 4I–J): podomere 1 being 3.2 times as long as wide; podomere 2, the longest, being 7.9 times as long as wide. Distal part consisting of three podomeres: podomere 3 being 5.2 times as long as wide; podomere 4 being 4.5 times as long as wide and bearing eight spines on its medial margin, the first two being close to the proximal margin (Fig. 4I–J), followed by two stout spines, surrounding a more gracile one, and then by three short spines and a long, stout spine. Distal part of the third raptorial appendages ending with a square-shaped podomere (podomere 5), bearing a cluster of three spines.

Oval structure

Long, oval structure protruding from the anterior part of the ventral margin, between raptorial and trunk appendages (Fig. 3A–D, H–I). Two elongate and sinuous rectangular structures visible on this feature. The nature of this structure is unknown.

Posterior trunk

Posterior trunk consisting of eleven elongate, rectangular structures (i.e., pleural parts of the segments; Figs 3A–D, 4D, G), slightly curved upward at their distal end and surrounding a long rectangular structure (i.e., tergal part of posterior trunk segments). Last pleural part thinner than the other ones. Presence of a square-shaped element (i.e., telson) at the posterior extremity of the trunk, bearing a circular structure formed by two circular parts: an outer one, delimiting the entire feature, and an inner smaller one.

Posterior trunk appendages

Eleven pairs of rod-like trunk appendages posteriorly oriented and protruding from the posterior part of the ventral margin (Figs 3A–D, 4E, H).

Gills

Four long lamellar gills preserved under the posterior area of the shield below the medio-lateral carina (Fig. 3H–I).

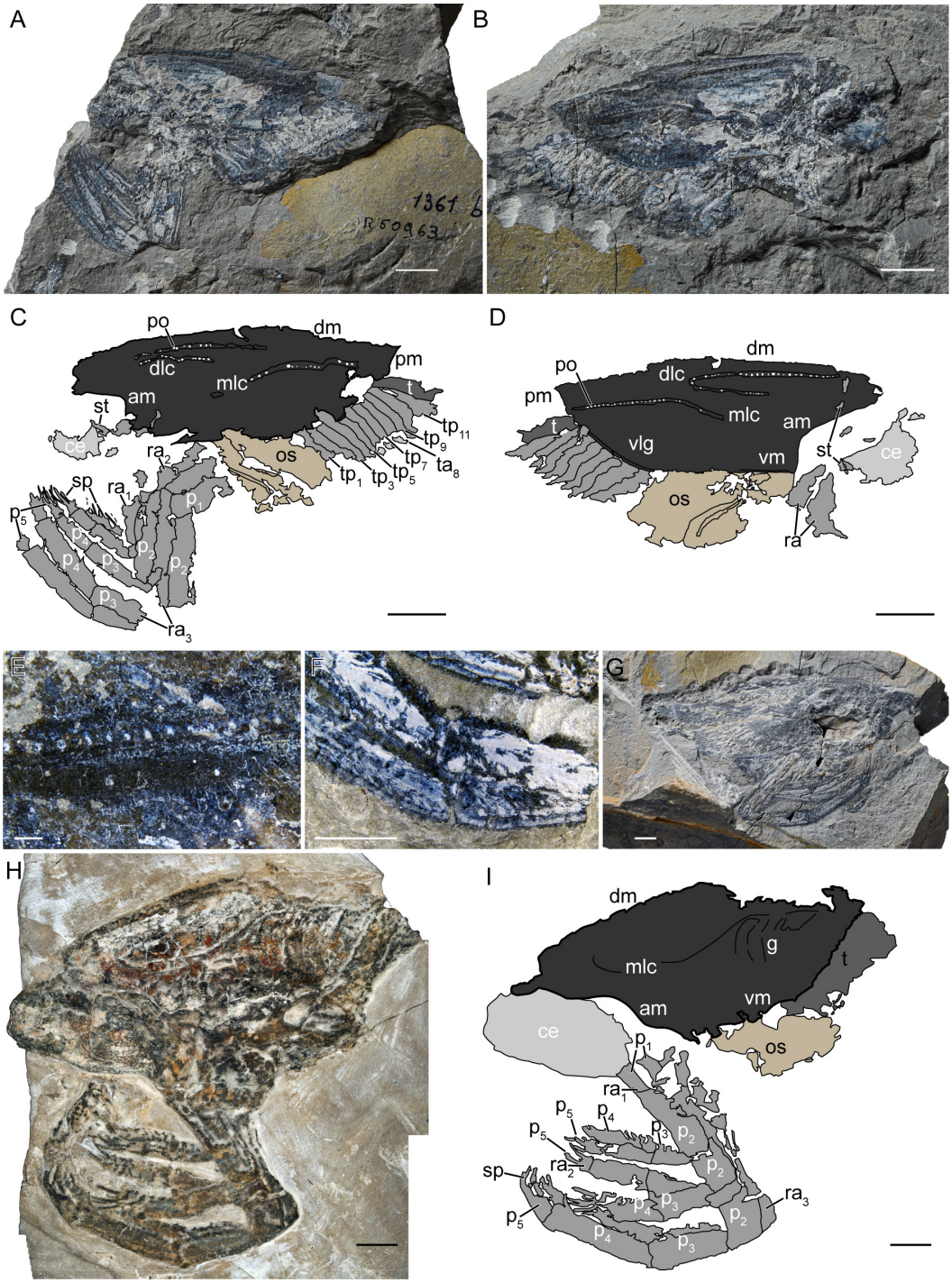

Fig. 3. *Austriocaris secretanae* sp. nov. **A–F**. Holotype MNHN.F.R50963. **A**. General view (part). **B**. General view (counter-part). **C**. Drawing (part). **D**. Drawing (counter-part). **E**. Close-up of pores. **F**. Close-up of muscles of raptorial appendages. **G**. Paratype MNHN.F.A29257. **H–I**. Paratype MNHN.F.R06203. **H**. General view. **I**. Drawing. Abbreviations: am = anterior margin; ce = compound eye; dlc = dorso-lateral carina; dm = dorsal midline; g = gills; mlc = medio-lateral carina; os = oval structure; $p_{1–5}$ = podomeres of raptorial appendages; pm = posterior margin; po = pores; $ra_{1–3}$ = raptorial appendages; sp = spines; st = stalk; t = posterior trunk; ta_8 = posterior trunk appendage 8; $tp_{1–11}$ = pleural parts of posterior trunk; vlg = ventro-lateral groove; vm = ventral margin. Scale bars: A–D, G–I = 10 mm; E = 1 mm; F = 5 mm. Photos: A–B, G: L. Cazes; E–F: T. Laville. H: C. Haug & Joachim T. Haug.

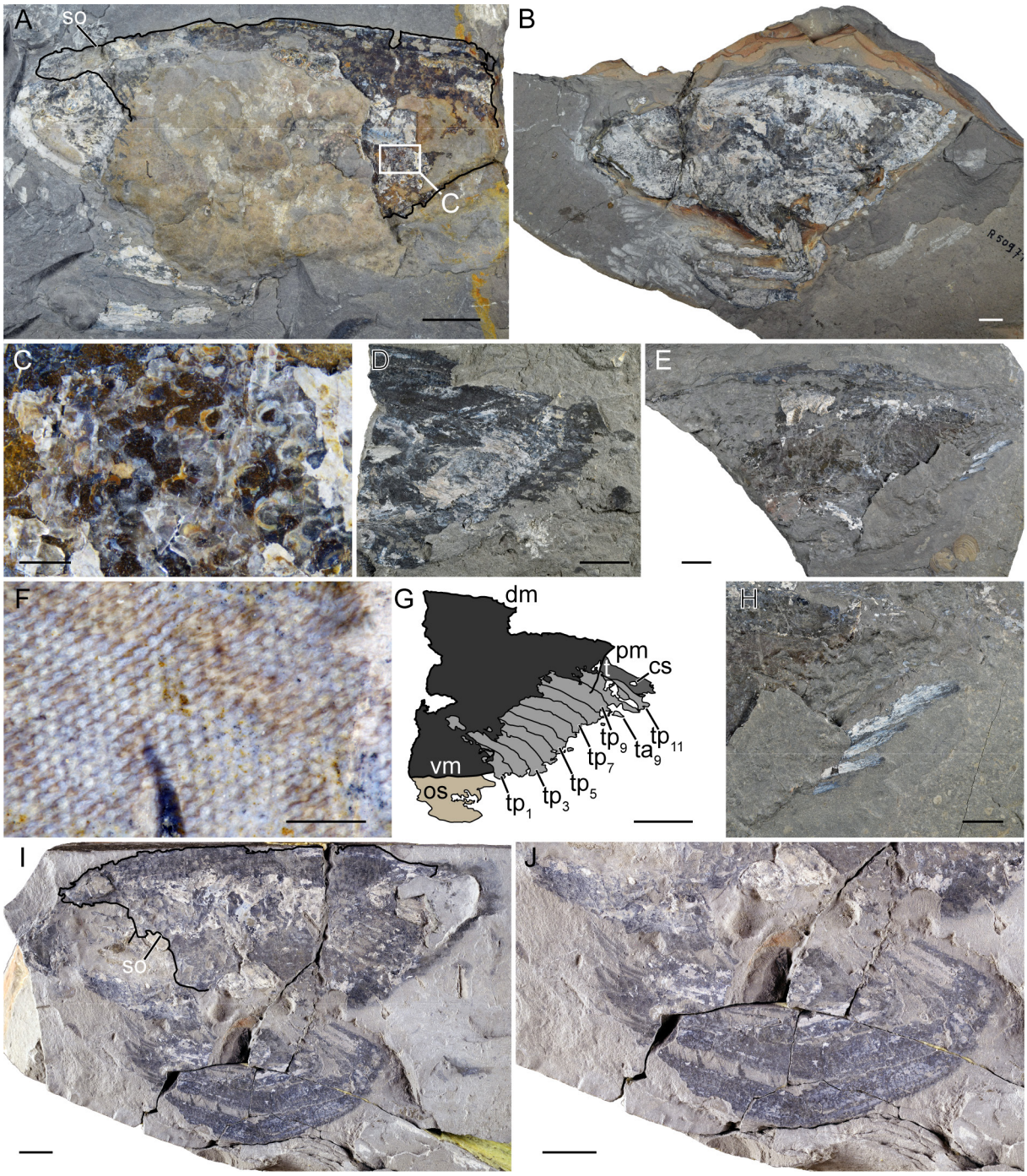

Fig. 4. *Austriocaris secretanae* sp. nov. **A, C, F**. Paratype MNHN.F.A29286. **A**. General view. **C**. Close-up of ornamentation. **F**. Close-up of compound eye. **B**. Paratype MNHN.F.R50971. **D, G**. Paratype MNHN.F.A29249. **D**. General view. **G**. Drawing. **E–H**. Paratype MNHN.F.A84029. **E**. General view. **H**. Close-up of posterior trunk appendages. **I–J**. Paratype MSNM i7591. **I**. General view. **J**. Close-up of raptorial appendages. Abbreviations: cs = circular structure; dm = dorsal midline; os = oval structure; pm = posterior margin; t = posterior trunk; $tp_{1–11}$ = pleural parts of posterior trunk appendages. Scale bars: A–B, D–E, G, I = 10 mm; C = 1 mm; F = 400 µm; H, J = 5 mm. Photos: A, C–F, H–J: T. Laville; B: L. Cazes.

Remarks

The specimens described above display typical characters of *Austriocaris* such as the well-developed optic notch restricted to the ventral part of the anterior margin, the large triangular rostrum, a straight dorsal mid-line ending in a spinous postero-dorsal corner. They differ from the type species, *Austriocaris carinata*, by the hook-shaped and tuberculate dorso-lateral carina, by the presence of horseshoe-like ridges and by the absence of a Y-shaped ventro-lateral carina. Thus, we consider these specimens as belonging to a new species: *Austriocaris secretanae* sp. nov.

Genus ***Kilianicaris*** Van Straelen, 1923

Type species

Kilianicaris lerichei Van Straelen, 1923 by monotypy.

Original diagnosis (literal translation from Van Straelen 1923a)

The overall shape is more angular, sub-quadratic in the posterior region and with a large rostrum expressed anteriorly. Tergal carina rises, especially in the rostral region. Lateral carinas are quite low. The rostrum is proportionally wider than long. The spiny posterior process is poorly delineated. Likewise for the postero-lateral processes that are slightly expressed.

Emended diagnosis

Thylacocephala with a rounded shield in lateral view, a rounded rostrum, a convex posterior part of the ventral margin, a falciform, tuberculate, dorso-lateral carina, eleven styliform, posterior trunk appendages, including elongate terminal trunk appendages.

Remarks

Schram (2014) suggested that *Kilianicaris* might be related to *Ostenocaris* Arduini, Pinna & Teruzzi, 1984, forming the Ostenocarididae Schram, 2014. He proposed that both taxa "have fused the posterior-most 8 trunk somites of the series of 16 into a posteriorly directed lobe". This lobe corresponds to the putative telson that we describe in most of La Voulte-sur-Rhône taxa (see below) and is therefore not only present in *Kilianicaris* and *Ostenocaris*. In addition to this misconception, many morphological differences exist between both taxa. As pointed out by Schram (2014), *Ostenocaris* lacks a rostrum while *Kilianicaris* has a rounded rostrum. Moreover, they present differences in the overall shape of the shield (trapezoidal for *Ostenocaris* vs rounded for *Kilianicaris*), in the morphology of their anterior margin (proverse vs straight), in the ornamentation of their dorsal margin (serrate and carinate in *Kilianicaris*), in the morphology of their dorso-lateral carina and in the number of posterior trunk appendages (9 vs 11).

Kilianicaris lerichei Van Straelen, 1923
Figs 5B, 6–9

Kilianicaris lerichei Van Straelen, 1923a: 434–435, pl. XIV figs 4–5.

Kilianicaris lerichei – Secrétan & Riou 1983: 84, pl. III figs 1–4. — Secrétan 1985: 386–387, fig. 2e. — Schram *et al*. 1999: 772. — Charbonnier 2009: 205–206, figs 249, 337, 367, tab. 14. — Charbonnier *et al*. 2010: 115, 117, 121, fig. 5c, tabs 1–2; 2014: 375, fig. 4b, tab. 1. — Schram 2014: 353. — Ji *et al*. 2017: 174. — Rak *et al*. 2018: 268. — Van Roy *et al*. 2021: 1737. — Schram & Koenemann 2022: tab. 41.2.

Material examined

Holotype

FRANCE • La Boissine, La Voulte-sur-Rhône, Ardèche, France; Callovian, Middle Jurassic; OSUG-UJF-ID.11545.

Paratype

FRANCE • same collection data as for holotype; OSUG-UJF-ID.1752.

Additional material

FRANCE • 48 specs; same collection data as for holotype; MNHN.F.A29246, A29253, A29301 to A293016, A29318, A29374, A29375, A53334, A53335, A53338, A53339, A53342, A83991 to A85013, A84073, R50942, R50961, R50967, R50969, R50972, R50973, R50975, R50976 • 1 spec.; same collection data as for holotype; OSUG-UJF-ID.1751 • 3 specs; same collection data as for holotype; MSNM i7593, i7596, i20704.

Measurements

See Table 2.

Description

Shield morphology

Rounded shield in lateral view with a straight and sub-vertical anterior margin, an antero-dorsal corner expressed as a large, rounded and horizontal rostrum, a slightly convex dorsal midline bearing a dorsal carina in its posterior third (Fig. 6). Presence of serrations along the first two thirds of the dorsal midline, until the dorsal carina (Fig. 6H–I). Postero-dorsal corner expressed as a small spine; straight and vertical posterior margin ending in a rounded postero-ventral corner; ventral margin divided into a posterior half steeply descending antero-ventrally and an anterior one ascending antero-dorsally; both parts merged approximately at mid-length; rounded antero-ventral corner. Rim of all free margins forming a marginal fold.

Shield macro-ornamentation

Dorso-lateral carina protruding from the posterior margin, running straight until the anterior third of the shield and forming a depression (Figs 6–7); carina then ascending to the dorsal midline and merging with the dorso-lateral carina from the other side of the shield; carina associated with a row of at least 19 pores (d = ~0.5 mm) in its posterior part (Fig. 8H–K). Marginal fold delimited by a ventro-lateral groove (Fig. 6C–D).

Sensory structures

Oval, stalked compound eyes protruding from the anterior margin and occupying the entire margin (Figs 7F–G, 9E, G).

Cephalic appendages

Cephalic appendages not preserved.

Raptorial appendages

Presence of three pairs of raptorial appendages recognised by preservation of muscles, protruding from the ventral margin (Figs 9H–I, 11). Raptorial appendages consisting of two parts: a proximal postero-ventrally oriented and a distal one, antero-ventrally oriented. Articulation between both parts forming an elbow.

First pair of raptorial appendages (Fig. 9A–D), the shortest, consisting of a proximal part with two podomeres: a rectangular podomere 1 being 3.4 times as long as wide; a stout podomere 2 being 5.9 times

as long as wide. Distal part of the appendages formed by three podomeres: podomere 3 being 4 times as long as wide; podomere 4 being 5.6 times as long as wide and bearing two medial spines; podomere 5, the most distal and shortest one, being 4.8 times as long as wide.

Second pair of raptorial appendages consisting of a proximal part with two podomeres (Fig. 9): podomere 1 not well preserved; podomere 2 being 4.7 times as long as wide (Fig. 9A–B, D). Distal part of the appendage consisting of three podomeres: podomere 3, the longest, being 5.2 times as long as wide and bearing two medial spines; podomere 4 being 5.3 times as long as wide and bearing four medial spines; podomere 5 being 3.5 times as long as wide and ending distally in a cluster of five long spines, the medial one being the smallest.

Third pair of raptorial appendages, the longest, consisting of a proximal part with two poorly preserved rectangular podomeres (Fig. 9). Distal part consisting of three podomeres: podomeres 3 being 4.8 times as long as wide; podomere 4 being 6.1 times as long as wide; podomere 5 being 5.3 times as long as wide and ending in a cluster of two spines.

Oval structure

Long oval structure, protruding from the anterior part of the ventral margin, between raptorial and trunk appendages (Fig. 9E–F).

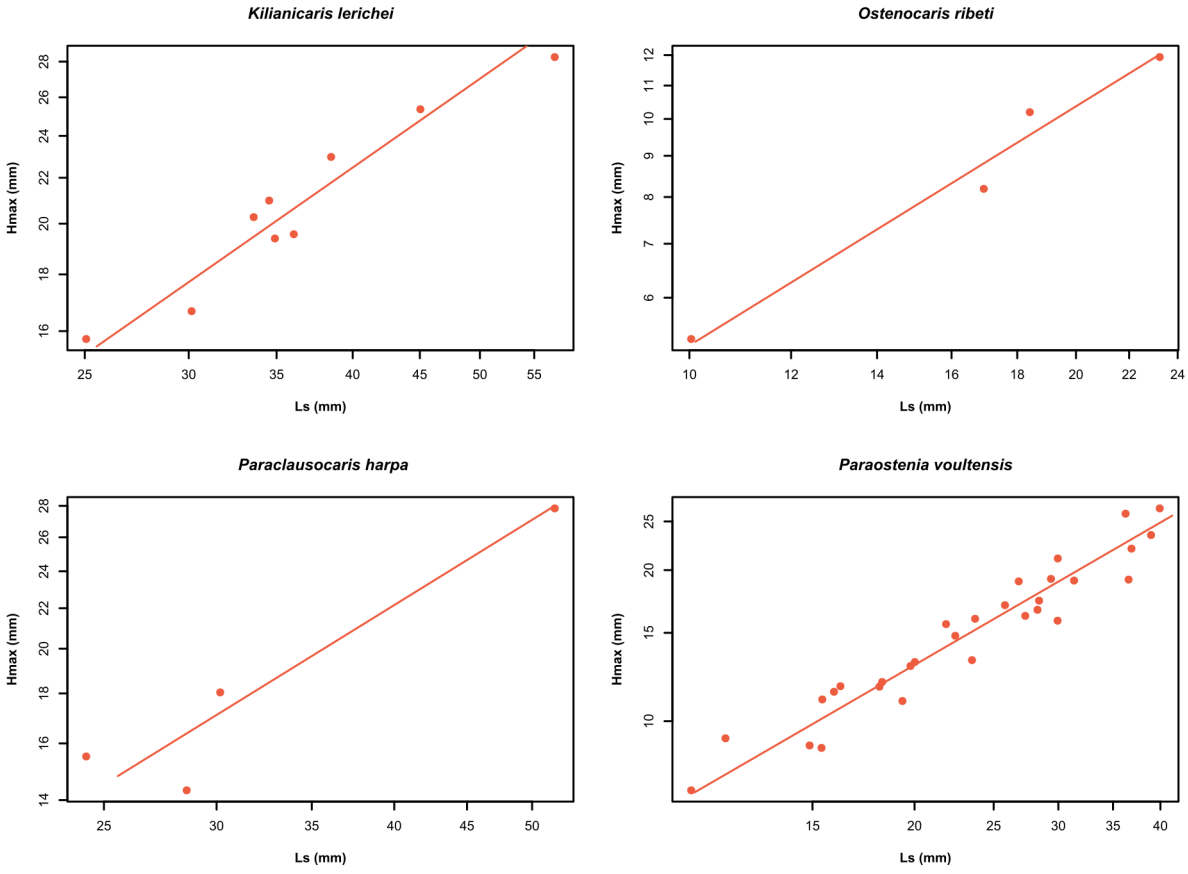

Fig. 5. Scatter plots of length of the shield against maximal height of the shield. **A**. *Kilianicaris lerichei* Van Straelen, 1923. **B**. *Ostenocaris ribeti* (Secrétan, 1985) comb. nov. **C**. *Paraclausocaris harpa* gen. et sp. nov. **D**. *Paraostenia voultensis* Secrétan, 1985. Abbreviations: Hmax = maximal shield height; Ls = length of the shield.

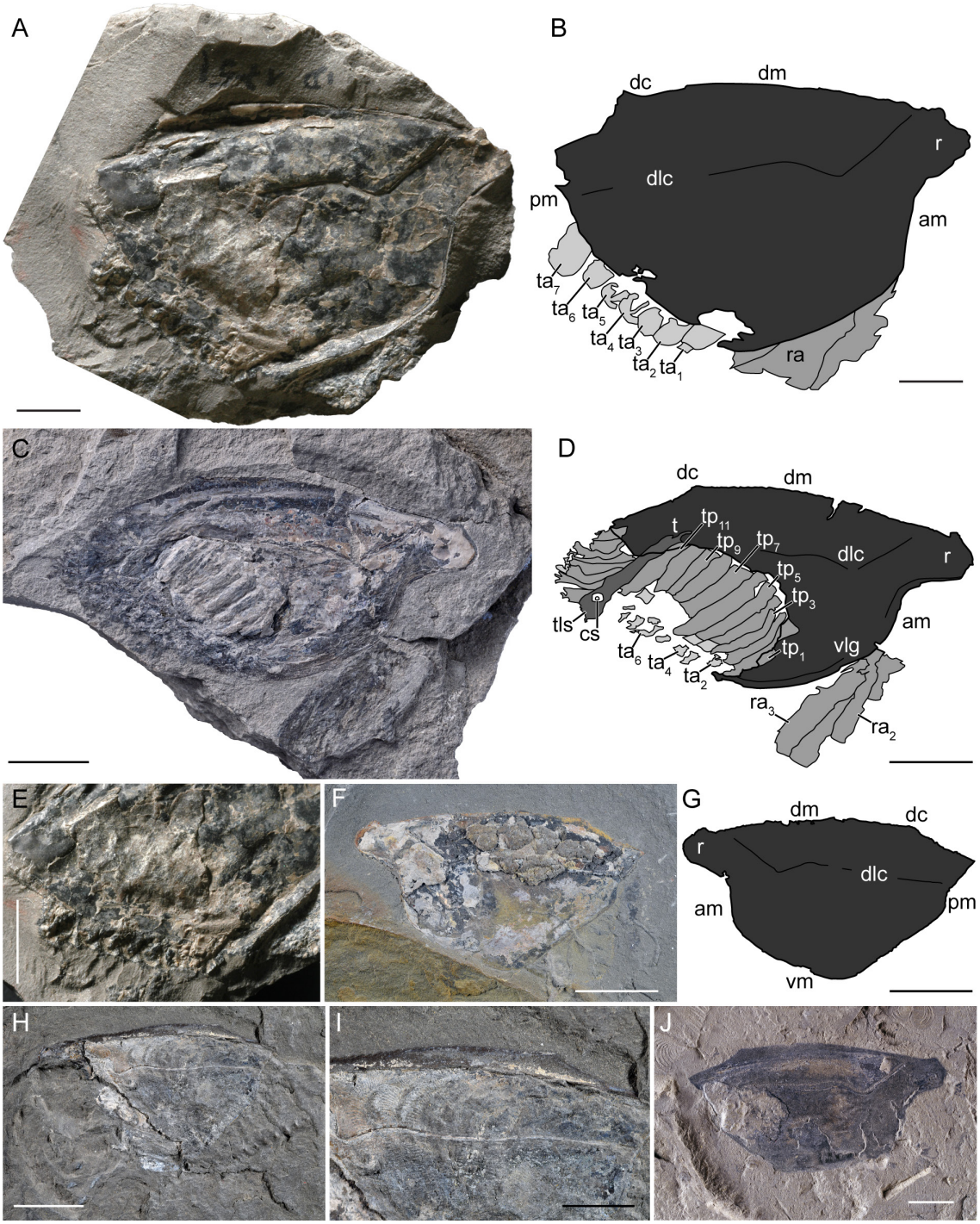

Fig. 6. *Kilianicaris lerichei* Van Straelen, 1923. **A, B, E**. Holotype OSUG-UJF-ID.11545. **A**. General view. **B**. Drawing. **E**. Close-up of posterior trunk appendages. **C–D**. Specimen MNHN.F.R50973. **C**. General view. **D**. Drawing. **F–G**. Specimen MNHN.F.A29315. **F**. General view. **G**. Drawing. **H–I**. Specimen MNHN.F.A29304. **H**. General view. **I**. Drawing. **J**. Specimen MSNM i7593. Abbreviations: am = anterior margin; cs = circular structure; dc = dorsal carina; dlc = dorso-lateral carina; dm = dorsal midline; pm = posterior margin; r = rostrum; $ra_{2, 3}$ = raptorial appendages; t = trunk; ta_{1-7} = posterior trunk appendages; tls = telson; $tp_{1–11}$ = pleural part of posterior trunk; vm = ventral margin; vlg = ventro-lateral groove. Scale bars: A–B, E, I = 5 mm; C–D, F–H, J = 10 mm. Photos: A, E: S. Charbonnier; C: L. Cazes; F–J: T. Laville.

Posterior trunk

Eleven, elongate rectangular structures (i.e., pleural part of posterior trunk segments) surrounding a long rectangular structure (i.e., possible tergal part; Fig. 8A–D). Pleural parts slightly curved downward at their distal end (Fig. 8D). Last pleura thinner than the others. Posterior extremity of the trunk expressed as a rhomboidal element (i.e., telson) bearing a rounded structure, formed by two circular parts (Fig. 6C–D): an outer one, delimiting the entire feature, and an inner smaller one.

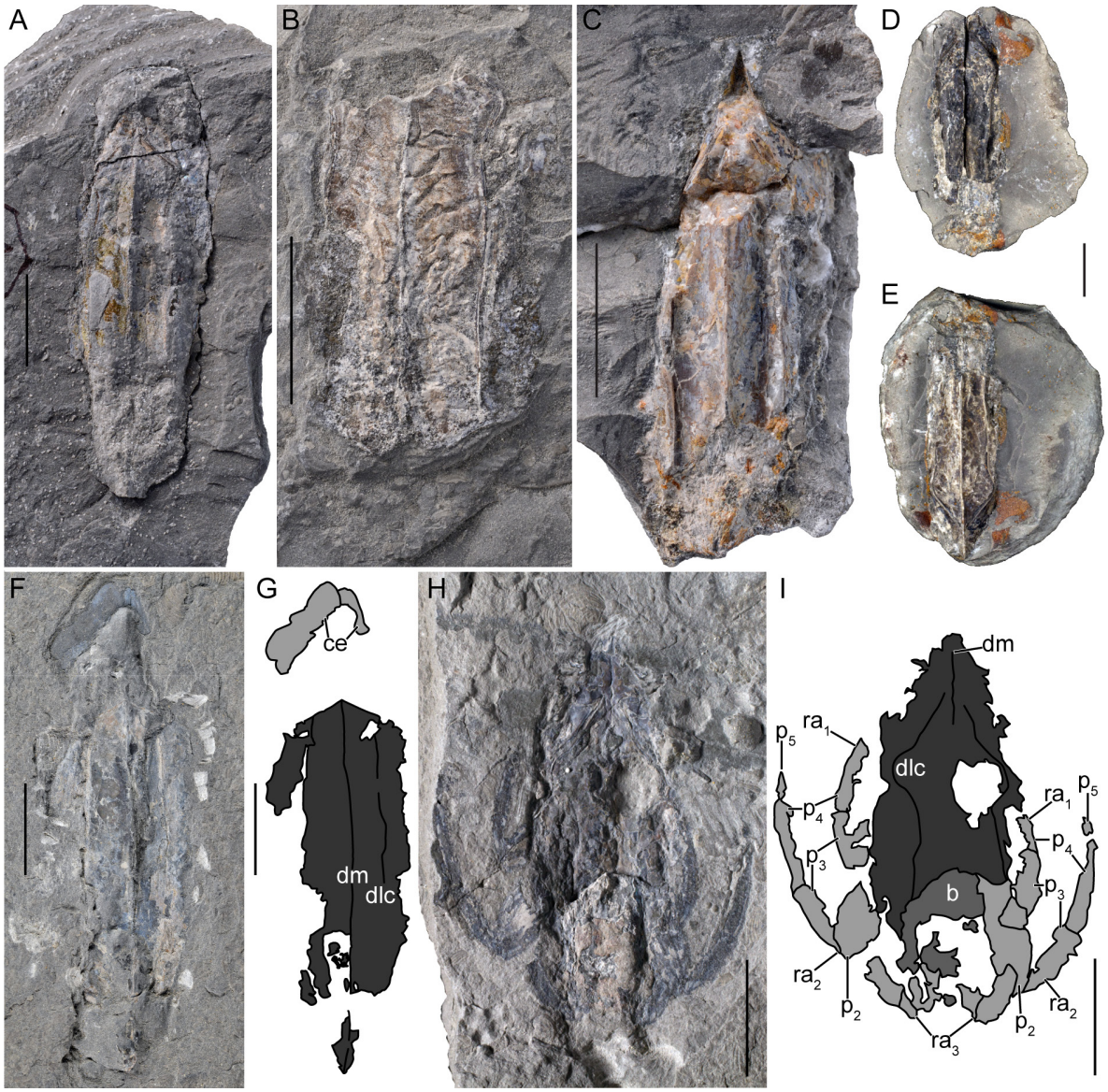

Fig. 7. *Kilianicaris lerichei* Van Straelen, 1923 preserved dorso-ventrally. **A**. Specimen MNHN.F.A83998 (sliced after the photograph). **B**. Specimen MNHN.F.A84012. **C**. Specimen MNHN.F.A29307. **D–E**. Specimen MNHN.F.R50969. **D**. Counter-part. **E**. Part. **F–G**. Specimen MNHN.F.A84009. **F**. General view. **G**. Drawing. **H–I**. Specimen MNHN.F.R50975. **H**. General view. **I**. Drawing. Abbreviations: b = body; ce = compound eye; dlc = dorso-lateral carina; dm = dorsal midline; $p_{2–5}$ = podomeres of raptorial appendages; $ra_{1, 2}$ = raptorial appendages. Scale bars = 10 mm. Photos: A–C: L. Cazes; D–E: Elise Porez (RECOLNAT – MNHN); F: T. Laville; H: Jocelyn Falconnet (RECOLNAT – MNHN).

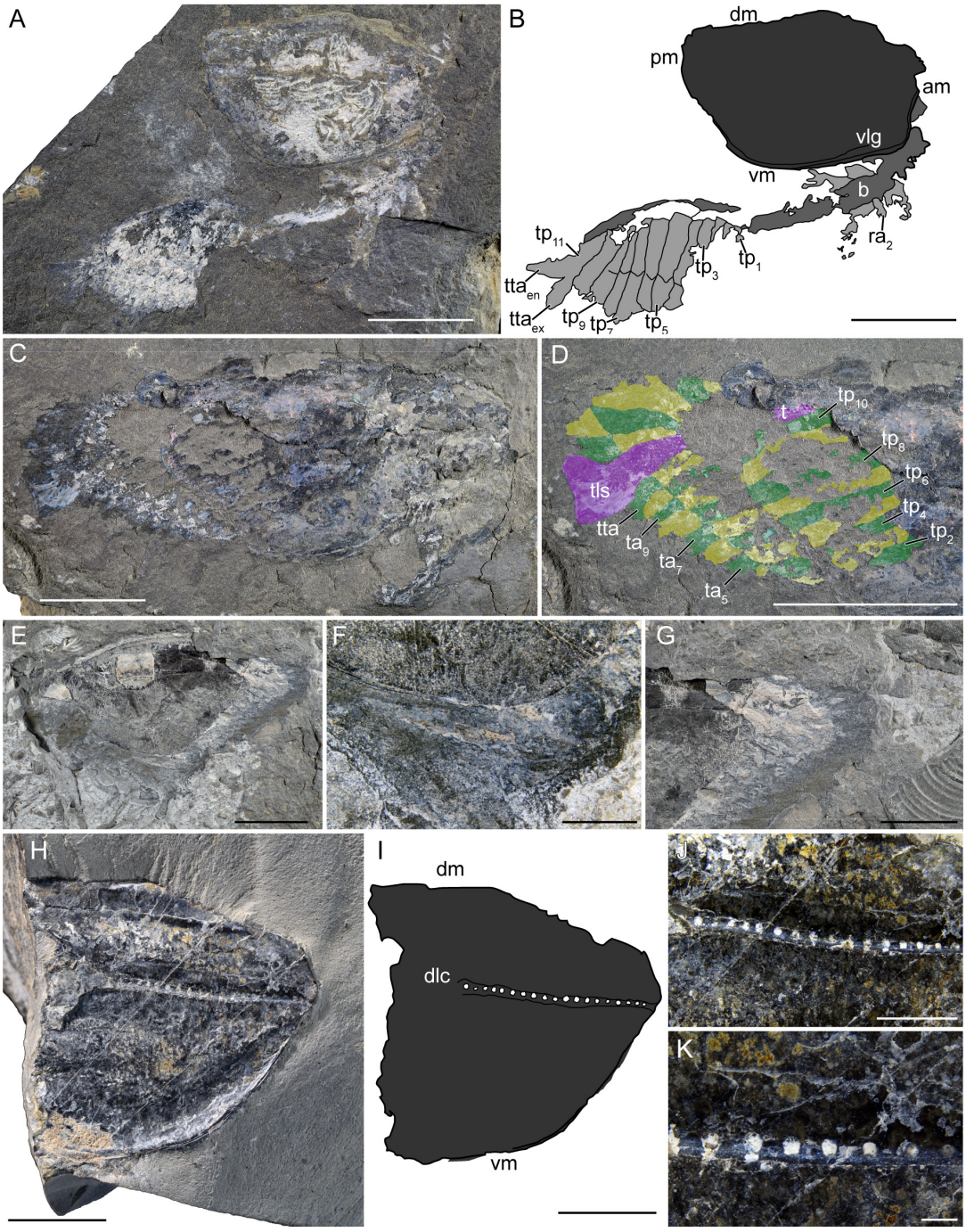

Fig. 8. *Kilianicaris lerichei* Van Straelen, 1923. **A–B**. Specimen MNHN.F.A29375. **A**. General view. **B**. Drawing. **C–D**. Specimen MNHN.F.A29309. **C**. General view. **D**. Close-up of posterior trunk. **E–G**. Specimen MNHN.F.A29246. **E**. General view. **F**. Close-up of oval structure. **G**. Close-up of posterior trunk. **H–K**. Specimen MNHN.F.A29374. **H**. General view. **I**. Drawing. **J**. Close-up of dorso-lateral carina. **K**. Close-up of pores. Abbreviations: am = anterior margin; b = body; dlc = dorso-lateral carina; dm = dorsal midline; pm = posterior margin; ra_2 = raptorial appendage 2; tls = telson; $tp_{1–11}$ = pleural part of posterior trunk segments; tta = terminal trunk appendages; ttaen = endopod of terminal trunk appendages; ttaex = exopod of terminal trunk appendages; vlg = ventro-lateral groove; vm = ventral margin. Scale bars: A–C, E, H–I = 10 mm; D, G = 5 mm; F, J = 4 mm; K = 1 mm. Photos: T. Laville.

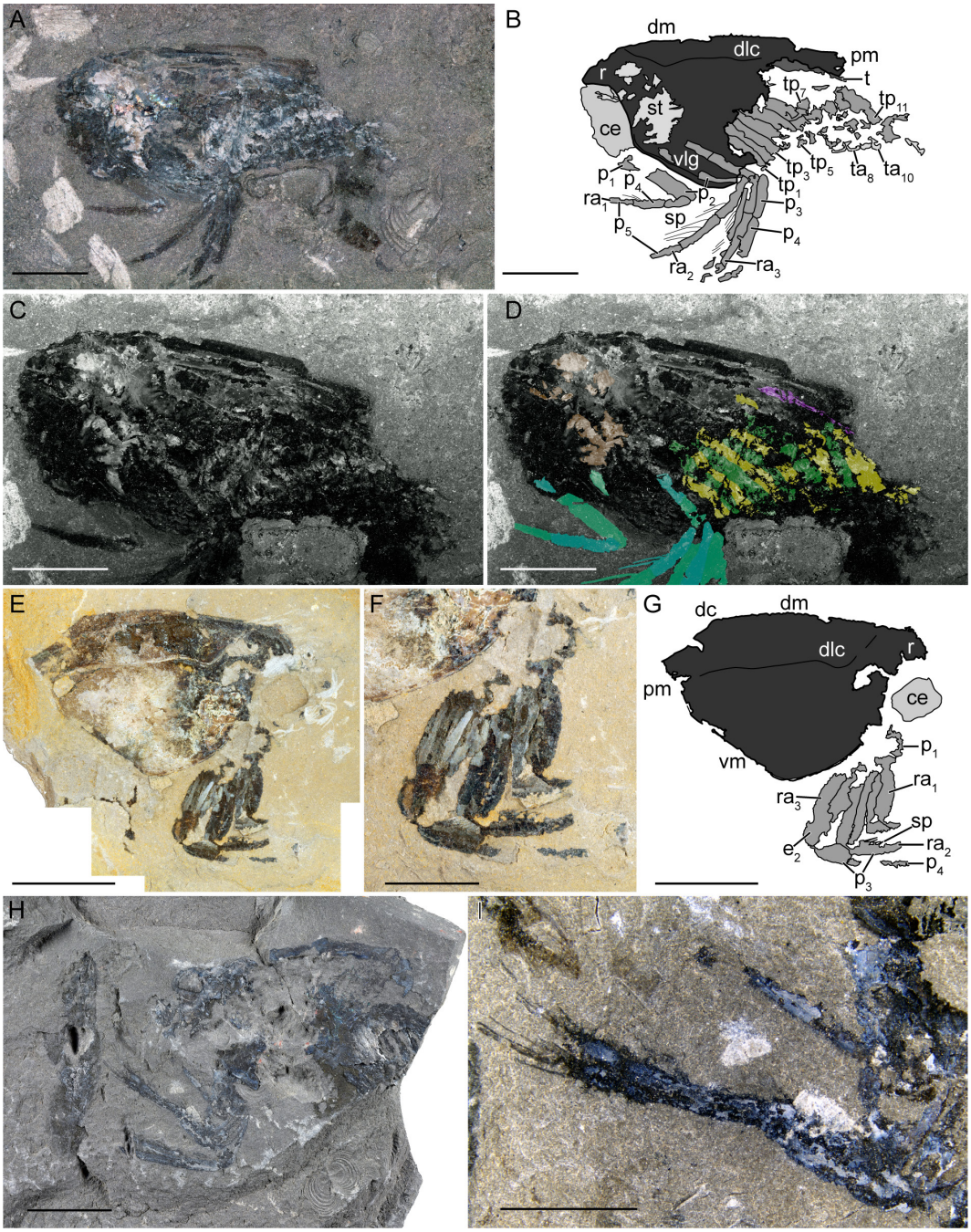

Fig. 9. *Kilianicaris lerichei* Van Straelen, 1923. **A–D**. Specimen MNHN.F.A53342. **A**. General view (natural light). **B**. Drawing. **C**. General view (green fluorescence; band-pass width: 532–554 nm, with a maximal excitation wavelength of 543 nm; detection ranges: 570–613 nm). **D**. General view (green fluorescence; colour marked). **E–G**. Specimen MNHN.F.R50972. **E**. General view. **F**. Close-up of raptorial appendages. **G**. Drawing. **H–I**. Specimen MNHN.F.A29253. **H**. General view. **I**. Close-up of raptorial appendages. Abbreviations: ce = compound eye; dc = dorsal carina; dlc = dorso-lateral carina; dm = dorsal midline; $p_{1–5}$ = podomeres of raptorial appendages; pm = posterior margin; r = rostrum; $ra_{1–3}$ = raptorial appendages; sp = spines; st = stalk; t = posterior trunk; $ta_{8, 10}$ = posterior trunk appendages; $tp_{1–11}$ = pleural part of posterior trunk segments; vlg = ventro-lateral groove; vm = ventral margin. Scale bars: A–E, G–H = 10 mm; F, I = 5 mm. Photos: A–D, H–I: T. Laville; E–F: Carolin Haug & Joachim T. Haug.

Posterior trunk appendages

Eleven pairs of trunk appendages, postero-dorsally oriented, protruding from the posterior part of the ventral margin (Fig. 8). First ten appendages formed by two parts: a square-shaped proximal one with a rounded distal margin and a styliform distal one (Fig. 6E). Last pair of trunk appendages formed by two paddle-like parts and being longer than the rest (Fig. 8A–B).

Gills

Eight long lamellar gills preserved under the central part of the shield below the dorso-lateral carina (Fig. 6H–I). Gills with an elliptic shape, becoming arcuate near the dorsal midline.

Genus ***Mayrocaris*** Polz, 1994

Type species

Mayrocaris bucculata Polz, 1994 by monotypy.

Original diagnosis (literal translation from Polz 1994)

Carapace subtrapezoid, without a clearly delineated optic notch, however, with a pronounced subquadratic notch; ventral line from here slopping down at 45° angle, almost equally ascending from the middle of the carapace, forming, together with the lowest part of the anterior margin, a characteristic U-shaped bulge; hinge line on the whole slightly convex, terminating in a pointed spine; rostrum inconspicuous; carapace surface roughly sculptured only by a short horizontal, very delicate ridge, and by eight small bases of spines, micro-relief in the form of single, very small arched lines on an ultrafine faveolated surface; anterior lobes larger than in comparable genera, protruding from the carapace not only anteriorly, but even projecting over its antero-ventral section; abdomen segmented. Kind of large appendages not clausocarid, course of anterior carapace margin conchyliocarid.

Emended diagnosis

Thylacocephala with a slightly developed optic notch, a serrate dorsal margin consisting of a carina, a rounded postero-dorsal spine, a posterior notch, and an anterior part of the ventral margin oriented antero-dorsally and bearing a square notch.

Mayrocaris sp.
Fig. 10

Dollocaris sp. – Secrétan & Riou 1983: text-fig. 14c.

Material examined

FRANCE • 11 specs; La Boissine, La Voulte-sur-Rhône, Ardèche, France; Callovian, Middle Jurassic; MNHN.F.A29366, A84014 to A84022, R50964.

Measurements

See Table 2.

Description

Shield morphology

Sub-trapezoidal shield in lateral view with an anterior margin formed by a weakly developed optic notch bent in its central part, a sharp antero-dorsal corner, a slightly convex dorsal midline ascending until a carina located in the last third of the margin. (Fig. 10); dorsal midline with small serrations in the anterior part of the midline; posterior margin consisting of a notch delimited dorsally by a postero-dorsal corner

expressed as a spine with a rounded tip and ventrally by a rounded postero-ventral corner; ventral margin divided into a steep posterior half descending antero-ventrally and an anterior one slightly ascending antero-dorsally and bearing a pronounced subquadratic notch; ventral margin ending anteriorly as a rounded antero-ventral corner. Rim of all free margins delimiting a marginal fold.

Shield macro-ornamentation

Presence of a medio-lateral carina in the central part of the shield, above the gills (Fig. 10A–D). One rounded pore, formed by a canal-like structure, sitting close to the anterior end of the carina (Fig. 11A–D).

Sensory structures

Oval, stalked compound eyes protruding from the optic notch and occupying all of it (Fig. 10).

Cephalic appendages

One antenniform structure protruding from the anterior margin of the shield, becoming thinner distally (Fig. 10I–J). Three rectangular elements preserved distally.

Raptorial appendages

Presence of three pairs of raptorial appendages recognised by preservation of muscles, protruding from the ventral margin, posterior to the presumed cephalic appendages. Raptorial appendages consisting of two parts: a proximal postero-ventrally oriented and a distal one, antero-ventrally oriented. Articulation between both parts forming an elbow.

First pair of raptorial appendages protruding from the ventral notch (Fig. 10E–F). Proximal part formed by two rectangular podomeres (podomeres 1 and 2). Distal part consists of at least one podomeres (podomere 3).

Second pair of raptorial appendages consisting of a proximal part with at least two rectangular podomeres (Fig. 10E–F). Distal part of the second raptorial appendages ending distally in a cluster of three spines.

Third pair of raptorial appendages ending distally in a cluster of five spines (Fig. 10E–F).

Posterior trunk

Long, tubular-like structure consisting of longitudinal muscles, extending from the anterior part of the shield to the posterior notch, interpreted as part of the posterior trunk (Fig. 10A–D). Nine trunk segments preserved under the shield, consisting of a rectangular pleural part, slightly curved downward at its distal end (Fig. 10H). Pleural parts decreasing in length toward the last segment. Presence of a circular structure at the posterior extremity of the trunk (Fig. 10A–D).

Posterior trunk appendages

Remnants of nine pairs of trunk appendages protruding from the posterior part of the ventral margin; appendages postero-dorsally oriented and poorly preserved, preventing their morphology from being determined (Fig. 10A–D).

Gills

Eight lamellar gills preserved under the central part of the shield, below the lateral carina (Fig. 10A–D). Gills becoming more arcuate toward the posterior part of the shield.

Anterior muscles

Presence of a bundle of radially arranged muscles close to the antero-ventral corner of the shield (Fig. 10A–D).

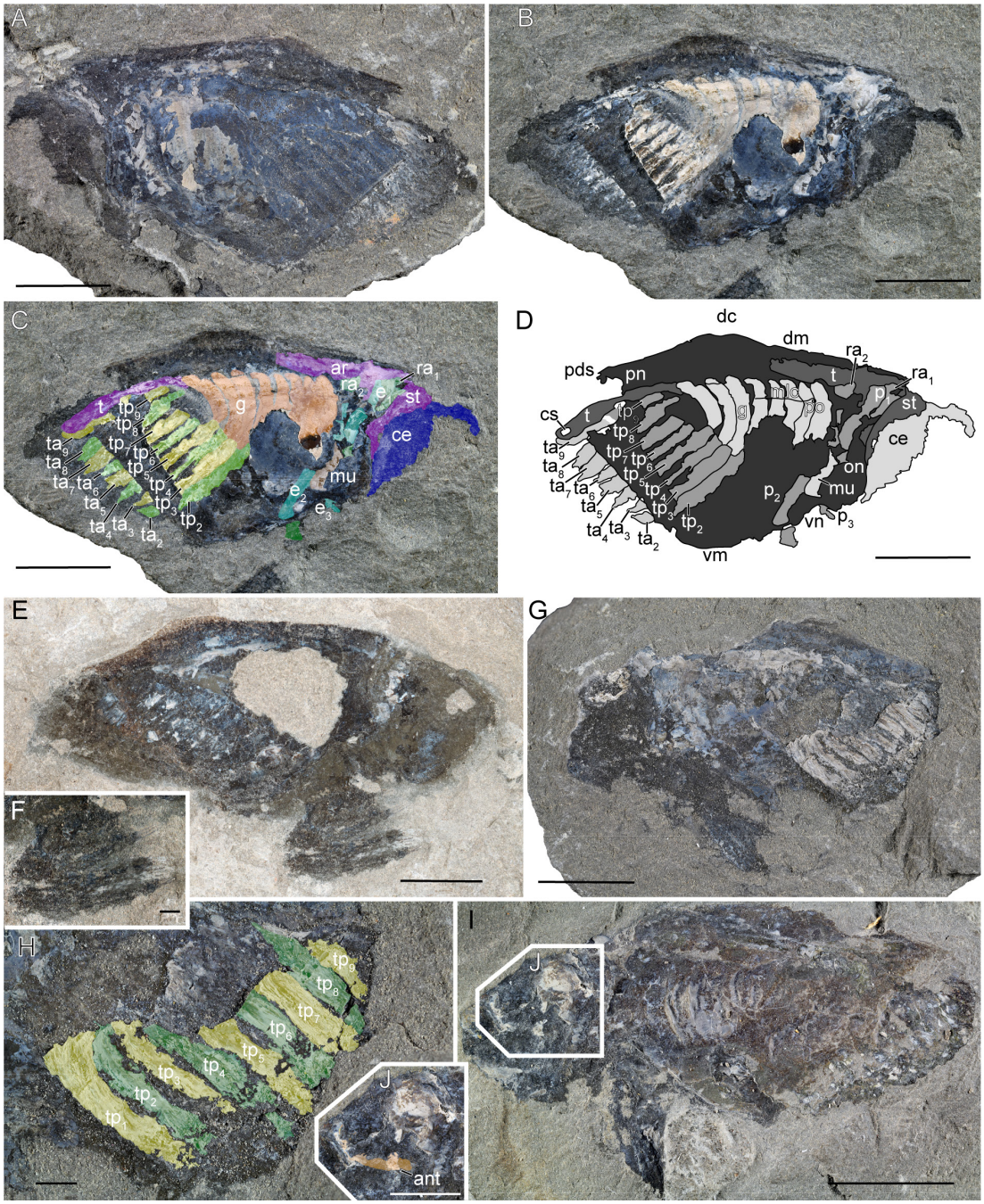

Fig. 10. *Mayrocaris* sp. **A–D**. Specimen MNHN.F.A84015. **A**. General view (counter-part). **B**. General view (part). **C**. General view (part; colour-marked). **D**. Drawing (part). **E–F**. Specimen MNHN.F.R50964. **E**. General view. **F**. Close-up of raptorial appendages. **G–H**. Specimen MNHN.F.A84014. **G**. General view. **H**. Close-up of posterior trunk. **I–J**. Specimen MNHN.F.A29366. **I**. General view. **J**. Close-up of cephalic appendages. Abbreviations: ant = antenniform structure; ar = anterior body region; ce = compound eye; cs = circular structure; dc = dorsal carina; dm = dorsal midline; g = gills; mlc = mediolateral carina; mu = muscles; on = optic notch; $p_{1–3}$ = podomeres of raptorial appendages; pds = posterodorsal spine; pn = posterior notch; po = pore; $ra_{1–2}$ = raptorial appendages; st = stalk; t = posterior trunk; $ta_{2–9}$ = posterior trunk appendages; $tp_{1–9}$ = pleural part of posterior trunk; vm = ventral margin; vn = ventral notch. Scale bars: A–E, G, I = 5 mm; E, H, J = 1 mm. Photos: A–C, G–J: T. Laville; E–F: C. Haug & J.T. Haug.

Remarks

The morphology of *Mayrocaris* sp. from La Voulte-sur-Rhône Lagerstätte is similar to that of *Mayrocaris bucculata* from Solnhofen-type Lagerstätten (Laville *et al*. 2021a): presence of a carina and of serrations on the dorsal midline, postero-dorsal corner expressed as a rounded spine, posterior and ventral notches, morphology and orientation of trunk segments, raptorial and trunk appendages, and of gills. The main difference is the ornamentation: no scale-like structures are visible on the shield of the La Voulte specimens. However, this might be due to poor preservation. Until better-preserved specimens are discovered, these specimens cannot be unambiguously assigned to a particular species.

Genus ***Ostenocaris*** Arduini, Pinna & Teruzzi, 1984

Type species

Ostenia cypriformis Arduini, Pinna & Teruzzi, 1980 by monotypy.

Diagnosis

Thylacocephalan with a sinuous anterior margin ending in a sharp antero-dorsal corner. Large oval eyes protruding from the anterior margin. Medio and dorso-lateral carina present on the shield. Large raptorial appendages bearing short spines.

Other included species

Ostenocaris ribeti (Secrétan, 1985) comb. nov. – Callovian, Middle Jurassic, France.

Remarks

Arduini *et al* (1980) did not provide a diagnosis for *Ostenocaris*. They just mentioned that the description of *Ostenocaris* was "coinciding with that of the type species" (Arduini *et al*. 1980: 362). Concerning the type species, they just described the original species without providing a proper diagnosis.

Ostenocaris ribeti (Secrétan, 1985) comb. nov.
Figs 5C, 11–12

Clausia ribeti Secrétan, 1985: 388, fig. 5d, i–j.

Clausia sp. – Secrétan & Riou 1983: 85, pl. IV figs 2, 4–5.
Clausia ribeti – Arduini 1992: 266.
Clausocaris ribeti – Schram *et al*. 1999: 772. — Charbonnier 2009: 205–206. — Charbonnier *et al*. 2010: 115, 117, 121, tab. 1, fig. 5d. — Schram 2014: 351. — Rak *et al*. 2018: 268, tab. 1.

Original diagnosis (Secrétan 1985)

The new species differs from the type species *Clausia lithographica* Oppenheim in its much stronger anterior appendages. Like the type species, *C. ribeti* is small, has a rounded carapace and large eye with oval lateral aspect. The appendages, however, have very fine paintbrush like extremities and are very much shorter and very much more massive than these of *C. lithographica.*

Emended diagnosis

Ostenocaris with a tuberculate, club-shaped dorso-lateral carina and hook-shaped first raptorial appendages.

Material examined

Holotype

FRANCE • La Boissine, La Voulte-sur-Rhône, Ardèche, France; Callovian, Middle Jurassic; MNHN.F.R50981.

Additional material

FRANCE • 11 specs; same collection data as for holotype; MNHN.F.A29349, A29365, A29368, A29372, A84023 to 84028, R50970.

Measurements

See Table 2.

Description

Shield morphology

Sub-oval shield in lateral view with a sinuous and proverse anterior margin, a sharp, antero-dorsal corner, a convex dorsal midline with a short flattening near the rounded postero-dorsal corner, a straight and vertical posterior margin, a rounded postero-ventral corner a ventral margin consists of a posterior half steeply descending antero-ventrally and of a horizontal anterior one (Figs 11–12). Rim of all free margins delimiting a marginal fold.

Shield macro-ornamentation

Shield adorned by two large, tuberculate carinae on its lateral sides: a club-shaped horizontal dorso-lateral carina and a sinuous medio-lateral carina (Figs 11A, 12A–C, G).

Sensory structures

Two oval, sessile compound eyes protruding from the optic notch, occupying most (Fig. 11).

Cephalic appendages

One elongate structure, consisting of at least three elements, lying in front of the raptorial appendages (Fig. 12A–C).

Raptorial appendages

Presence of three pairs of raptorial appendages recognised by preservation of muscles, protruding from the ventral margin, posterior to the presumed cephalic appendages (Fig. 12A–D). Raptorial appendages consisting of two parts: a proximal postero-ventrally oriented and a distal one, antero-ventrally oriented. Articulation between both parts forming an elbow.

First pair of raptorial appendages, the shortest, having a hook-shaped morphology (Fig. 12D). Proximal part consisting of two rectangular podomeres: podomere 1 being 2.5 times as long as wide; podomere 2 being 8 times as long as wide. Distal part formed by three rectangular podomeres: podomere 3 being 3.4 times as long as wide; podomere 4 being 3.4 times as long as wide; podomere 5 being 1.7 times as long as wide and ending in a spiny tip.

Second pair of raptorial appendages consisting of a proximal part with two rectangular podomeres (Fig. 12D): podomere 1 not being well preserved; podomere 2 being 4.6 times as long as wide. Distal part of the appendage consisting of three podomeres: podomere 3 being 3.8 times as long as wide; podomere 4 being 5 times as long as wide; podomere 5 being 2.7 times as long as wide and ending in a spiny tip.

Third pair of raptorial appendages, the longest, consisting of a proximal part with two long rectangular podomeres (Fig. 12D): podomere 1 being 1.8 times as long as wide; podomeres 2 being 5.2 times as long as wide. Distal part consisting of three podomeres: podomere 3 being 4.7 times as long as wide; podomere 4 being 5 times as long as wide and bearing a row of spine on its medial and lateral sides; podomere 5 being slightly curved and 2.9 times as long as wide.

Posterior trunk

Presence of seven rectangular posterior trunk segments, with only three rectangular pleural parts preserved (Fig. 11F–G). Trunk appendages not preserved.

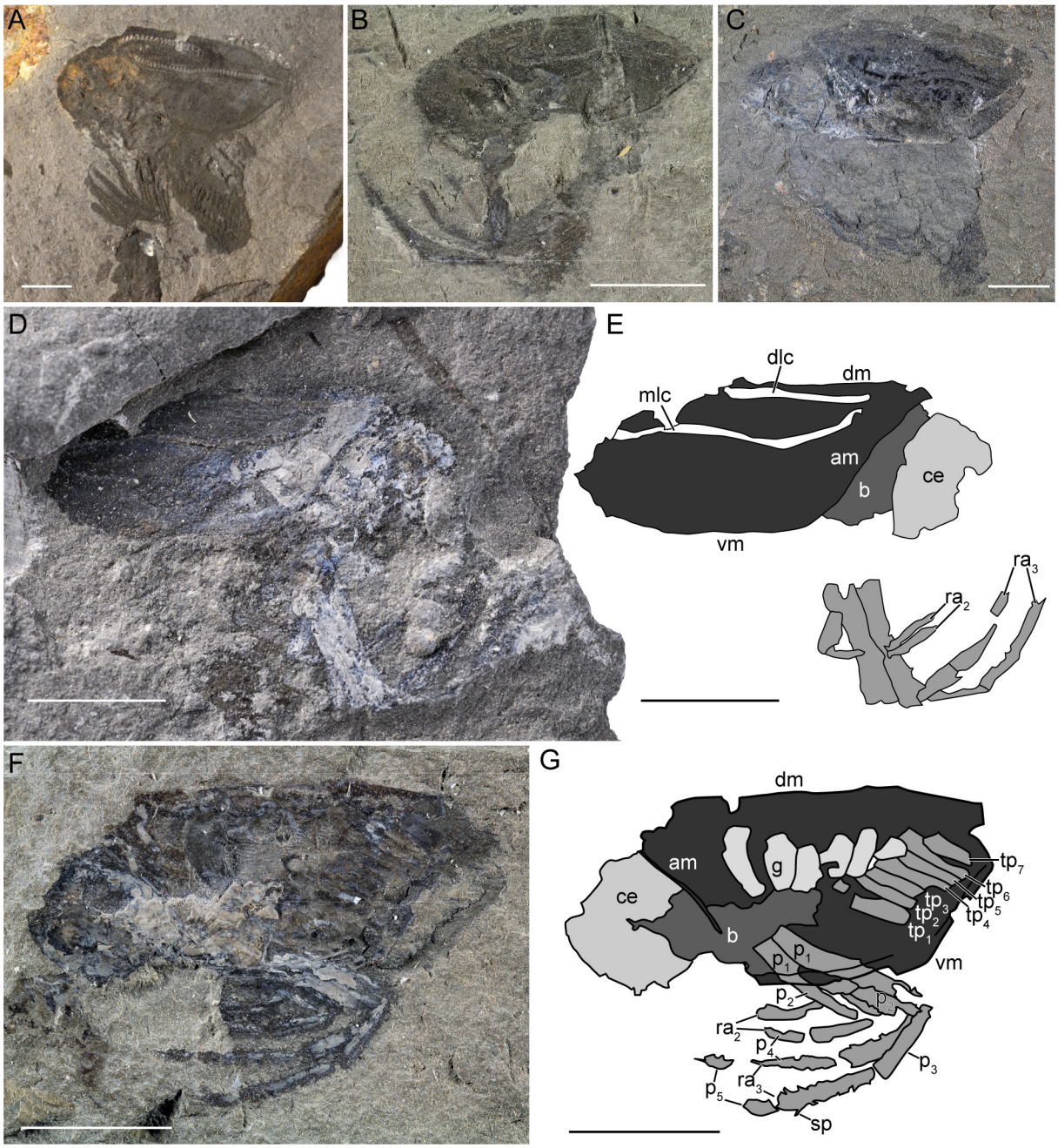

Fig. 11. *Ostenocaris ribeti* (Secrétan, 1985) comb. nov. **A**. Holotype MNHN.F.R50981. **B**. Specimen MNHN.F.A29349. **C**. Specimen MNHN.F.A29368. **D–E**. Specimen MNHN.F.A84023. **D**. General view. **E**. Drawing. **F–G**. Specimen MNHN.F.A29365. **F**. General view. **G**. Drawing. Abbreviations: am = anterior margin; b = body; ce = compound eye; dlc = dorso-lateral carina; dm = dorsal midline; g = gills; mlc = medio-lateral carina; $p_{1–5}$ = podomeres of raptorial appendages; $ra_{2–3}$ = raptorial appendages; $tp_{1–7}$ = pleural part of the posterior trunk; vm = ventral margin. Scale bars: 5 mm. Photos: A: J. Falconnet (RECOLNAT – MNHN); B–C, F: T. Laville; D: L. Cazes.

Gills

Six oval, short gills located below the median part of the shield (Fig. 11F–G).

Remarks

New observations of the holotype of *Clausocaris ribeti* indicate that this species has the general morphology of *Ostenocaris*: a proverse anterior margin with a sharp antero-dorsal angle, a convex dorsal midline, a straight posterior margin, a marginal fold on all free margins, presence of rows of spines on

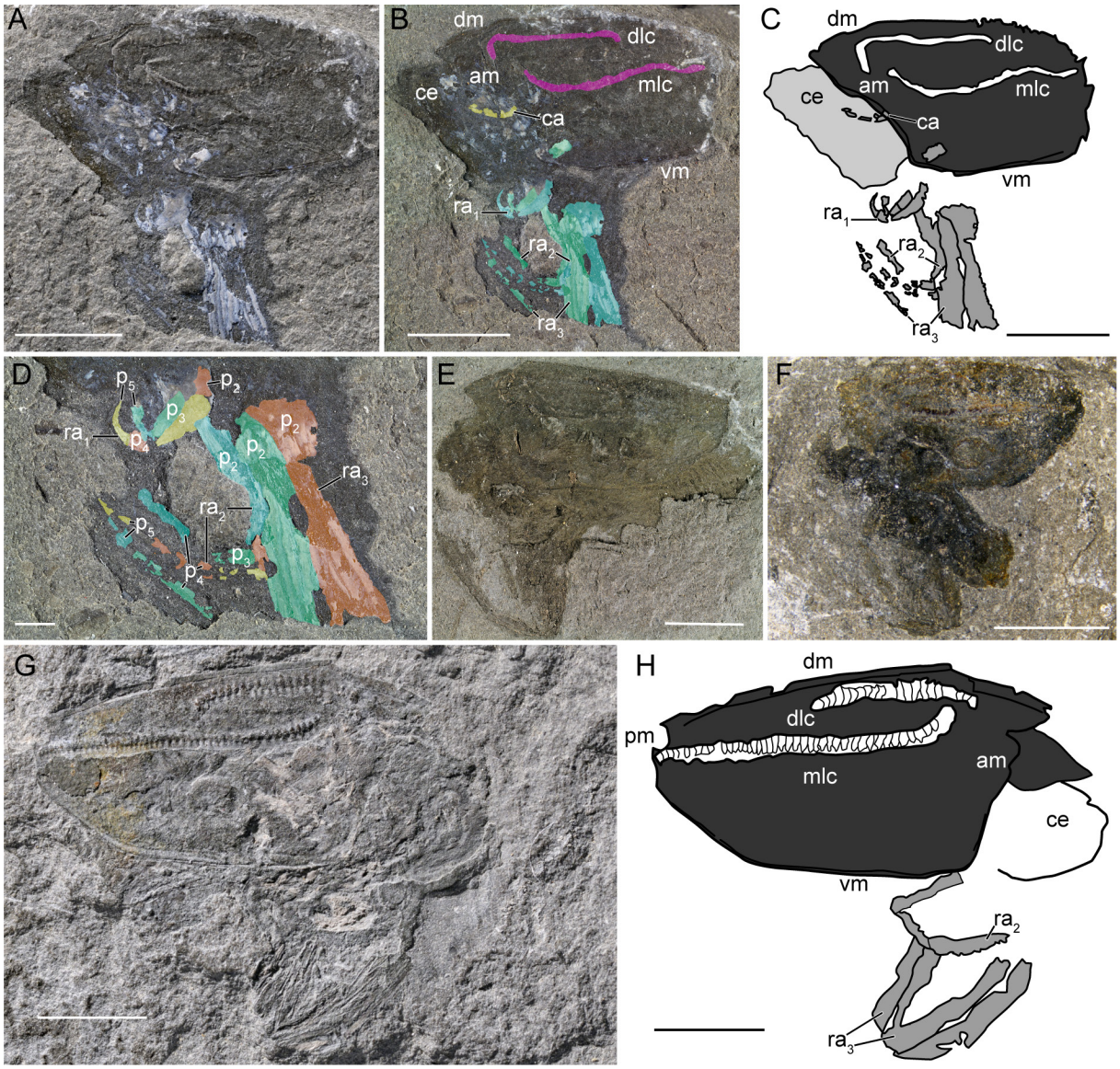

Fig. 12. *Ostenocaris ribeti* (Secrétan, 1985) comb. nov. **A–D**. Specimen MNHN.F.A29372. **A**. General view. **B**. General view (colour-marked). **C**. Drawing. **D**. Close-up of raptorial appendages. **E**. Specimen MNHN.F.R50970. **F**. Specimen MNHN.F.A84024. **G–H**. Specimen MNHN.F.A84027. **G**. General view. **H**. Drawing. Abbreviations: am = anterior margin: ca = cephalic appendage; ce = compound eye; dlc = dorso-lateral carina; dm = dorsal midline; mlc = medio-lateral carina; p_{2-5} = podomeres of raptorial appendages; pm = posterior margin; ra_{1-3} = raptorial appendages; vm = ventral margin. Scale bars: A–C, E–H = 5 mm; D = 1 mm. Photos: A–B, G: L. Cazes; D–F: T. Laville.

the medial and lateral end of podomere 4 of the third pair of raptorial appendages. This species also displays major differences with *Clausocaris*: absence of an optic notch and of serrations on the dorsal margin, presence of a posterior margin, differentiation of the ventral margin into a posterior and an anterior parts, short and stout raptorial appendages. Thus, we propose the new combination *Ostenocaris ribeti* (Secrétan, 1985) comb. nov.

Here, it is also important to note that the paratype of *C. ribeti* (MNHN.F.R50978) is no longer considered to be a representative of this species. Based on its morphology, it is now considered to belong to *Paraostenia voultensis*. As pointed out by Laville *et al*. (2021c), there has been a lot of confusion between *Paraostenia* Secrétan, 1985 and *Ostenocaris* due the wrong assignement of specimens of *Paraostenia* from the Osteno Lagerstätte, Italy, to *Ostenocaris* (see Arduini *et al*. 1980). Both taxa differ from each other based on the morphology of their anterior margin (sinuous for *Ostenocaris* vs large optic notch for *Paraostenia*), of their dorsal margin (presence of carina in *Paraostenia*) and of their posterior margin (straight vs concave).

Ostenocaris ribeti is the second species of *Ostenocaris* described. The main difference with the type species is the size: *O. ribeti* is only 1.7 cm long while *O. cypriformis* can reach a length of 20 cm. *Ostenocaris ribeti* also differs from *O. cypriformis* by its large, tuberculate and elongate dorso-lateral and medio-lateral carinae and its hook-shaped first raptorial appendages. Its dorsal midline also appears less convex.

Genus ***Paraclausocaris*** gen. nov.
urn:lsid:zoobank.org:act:BE0312F9-B192-4581-A2CB-3CC408857206

Type species

Paraclausocaris harpa gen. et sp. nov. by monotypy.

Diagnosis

Thylacocephala with a well-developed optic notch restricted to the ventral margin, a sharp antero-ventral angle, small sinuous ridges on the shield and raptorial appendages 3 having spines on the second and third podomeres of the distal part.

Etymology

From the Latin '*par*, *paris*' ('close to') and *Clausocaris* Polz, 1989.

Remarks

Paraclausocaris gen. nov. has many similarities with *Clausocaris*: a cone-shaped shield in lateral view, a dorsal midline with sharp, short serrations and long, thin raptorial appendages relative to the shield. However, it also displays some differences, including a well-developed posterior margin and an anterior margin with an optic notch limited to the ventral part of the margin for *Paraclausocaris*, while in *Clausocaris* the posterior margin is absent and the optic notch occupies the whole margin. As a result of these differences, we erect *Paraclausocaris*.

One last morphological trait should also be discussed here: the number of posterior trunk appendages. In *Paraclausocaris* gen. nov., we recognize nine pairs of posterior trunk appendages. Arduini (1992) described eight posterior trunk appendages in *Clausocaris pinnai*, but based on pictures from Dalla Vecchia (2012), there may actually be nine as in *Paraclausocaris*. However, it is different from the number reported by Polz (1990) or Haug *et al.* (2014) for *Clausocaris lithographica*. They respectively reported 10 or 11 posterior trunk appendages for this species. Interspecific variation in the number of

posterior trunk appendages is not uncommon among Thylacocephala (Schram 2014). However, it is quite unusual to find such variation among closely related forms: for instance, eight posterior trunk appendages are usually reported in *Concavicaris* species (Schram 2014). Thus, it will be necessary to revise *C. pinnai* to confirm its assignment to *Clausocaris*.

Paraclausocaris harpa gen. et sp. nov.
urn:lsid:zoobank.org:act:4F007D44-251E-496D-818B-9C3065947B0D
Figs 5A, 13–15

Clausia sp. – Secrétan & Riou 1983: 85–86, pl. 4 figs 2, 17.
Clausia ribeti – Secrétan 1985*:* 388, fig. 5j.
Clausocaris ribeti – Polz 1989: 73. — Charbonnier 2009: 158, fig. 250. — Charbonnier *et al*. 2010: 118, fig. 5d; 2014: 375, fig. 5c.
Dollocaris ingens – Charbonnier *et al*. 2010: 113, fig. 3e.

Diagnosis

Same as for *Paraclausocaris.*

Etymology

Referring to the shape of the shield, which is similar to the shape of a harp.

Material examined

Holotype

FRANCE • La Boissine, La Voulte-sur-Rhône, Ardèche; Callovian, Middle Jurassic; MNHN.F.A29295.

Paratypes

FRANCE • 22 specs; same collection data as for holotype; MNHN.F.A29148, A29149, A29264, A29267 A29295, A29323, A29327, A29345, A29348, A29353, A29356, A29358, A29360, A53341, A83986 to A83990, A84072, R50955, R50974.

Measurements

See Table 2.

Description

Shield morphology

Cone-shaped shield in lateral view with an anterior margin formed by a symmetric and concave optic notch in its ventral part and with a convex dorsal part, a sharp antero-dorsal corner, a slightly convex dorsal midline with small serrations in the last two thirds of the midline and ending in a sharp postero-dorsal corner (Figs 13A, C, H, 14G–H); straight posterior margin antero-ventrally oriented, ending in a rounded postero-ventral corner; ventral margin divided in a concave posterior part steeply descending antero-ventrally and in a horizontal anterior part slightly rising to the antero-ventral corner. Rims of all free margins forming a marginal fold.

Shield macro-ornamentation

Small sinuous ridges covering the entire dorsal area of the shield (Fig. 13F). Central part of the shield adorned with a straight dorso-lateral carina (Fig. 14A–B). Shield forming a hump near the antero-ventral corner (Fig. 14A–B). Thin ventro-lateral groove delimiting the marginal fold. Four rounded, canal-like pores visible in the posterior part of the shield, above the pleural part of trunk segments (Fig. 13F–G). Pores forming a rim surrounding a hollow part.

Sensory structures
Two stalked, circular compound eyes protruding from the optic notch and occupying most of the anterior margin (Fig. 14A–B). Eyes consisting of 136 hexagonal ommatidia per mm² (w = ~73 µm; h = ~130 µm; Figs 13E, 14E, 15H).

Cephalic appendages
One elongate, antenniform structure (~15 mm) lying in the anterior part of the body (Figs 13A, C, 14C–D).

Raptorial appendages
Three pairs of long and slender raptorial appendages recognised by the preservation of muscles, protruding from the ventral margin, posterior to the presumed cephalic appendages. Raptorial appendages consisting of two parts: a proximal postero-ventrally oriented and a distal one, antero-ventrally oriented. Articulation between both parts forming an elbow.

First pair of raptorial appendages (Figs 13H–I, 15F–G), the shortest, consisting of a proximal part with two podomeres: podomere 1 being 3.4 times as long as wide; podomere 2 being 4.6 times as long as wide and longer than podomere 1. Distal part of the appendages formed by three podomeres: podomeres 3 being 4.3 times as long as wide; podomere 4 being 3.3 times as long as wide; podomere 5, the most distal one, being 3 times as long as wide, ending in a cluster of three long spines.

Second pair of raptorial appendages consisting of a proximal part with two podomeres: podomere 1 being 3.4 times as long as wide, podomere 2 being 6.2 times as long as wide (Figs 14A–B, 15F, I). Distal part of the appendage consisting of three podomeres: podomere 3 being 4.7 times as long as wide; podomere 4 being 5.5 times as long as wide; podomere 5, being 3.2 times as long as wide and ending distally in a cluster of three long spines.

Third pair of raptorial appendages, the longest, consists of a proximal part formed by two podomeres: podomere 1 being 3.6 times as long as wide; podomere 2, the longest of the appendages, being 6 times as long as wide (Fig. 15A, F–G). Distal part consisting of three podomeres: podomere 3 being 4.4 times as long as wide; podomere 4 being 5.7 times as long as wide and bearing three long spines on its medial end; podomere 5 being 3.3 times as long as wide and ending with a cluster of three long spines.

Oval structure
Long oval structure, protruding from the anterior part of the ventral margin, posterior to raptorial appendages (Figs 13H–I, 15A, C, G–H).

Posterior trunk
Posterior trunk consists of nine rectangular segments, slightly tilted anteriorly. Segments consisting of a dorsal square-shaped structure (i.e., tergal part of the segments), surrounded on their lateral sides by nine elongate rectangular structures (i.e., pleural part; Fig. 15G–H, J), slightly curved downward at their distal end (Fig. 15A, D). Segments increasing in height towards the penultimate segment. Most posterior segment shorter than the previous one.

Posterior trunk ending posteriorly in a rhomboidal element (i.e., telson), bearing a circular structure formed by two circular parts (Fig. 14A–D): an outer one, delimiting the entire feature, and an inner smaller one.

Posterior trunk appendages
Nine pairs of posterior trunk appendages protruding from the posterior part of the ventral margin (Fig. 13A–D). First appendage formed by two parts: a square-shaped dorsal one (i.e., endopod) and a

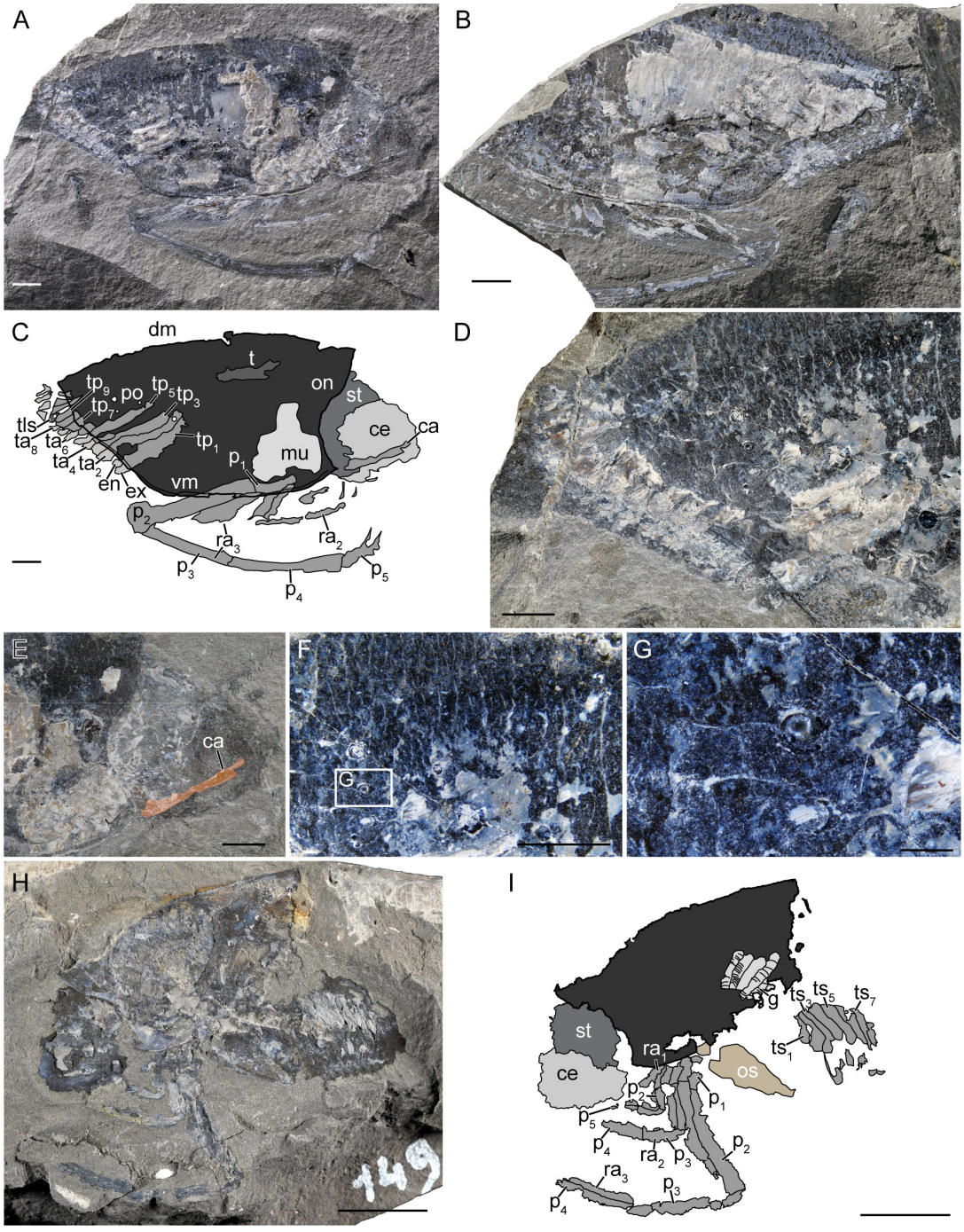

Fig. 13. *Paraclausocaris harpa* gen. et sp. nov. **A–G**. Holotype MNHN.F.A29295. **A**. General view of the part. **B**. General view of the counter-part. **C**. Drawing of the part. **D**. Close-up of the posterior trunk. **E**. Close-up of cephalic appendages. **F**. Close-up of the ornamentation. **G**. Close-up of pores. **H–I**. Paratype MNHN.F.A29148. **H**. General view. **I**. Drawing. Abbreviations: ca = cephalic appendages; ce = compound eye; dm = dorsal midline; en = putative endopod of posterior trunk appendage; ex = putative exopod of posterior trunk appendages; g = gills; mu = muscles; on = optic notch; os = oval structure; $p_{1–5}$ = podomeres of raptorial appendages; po = pore; $ra_{1–3}$ = raptorial appendages; st = stalk; t = trunk; $ta_{2–8}$ = posterior trunk appendages; tls = telson; $tp_{1–9}$ = pleural part of posterior trunk segments; $ts_{1–7}$ = trunk segments; vm = ventral margin. Scale bars: A–D, F = 5 mm; E = 2 mm; G = 1 mm; H–I = 10 mm. Photos: A–B: Lilian Cazes; D–H: T. Laville.

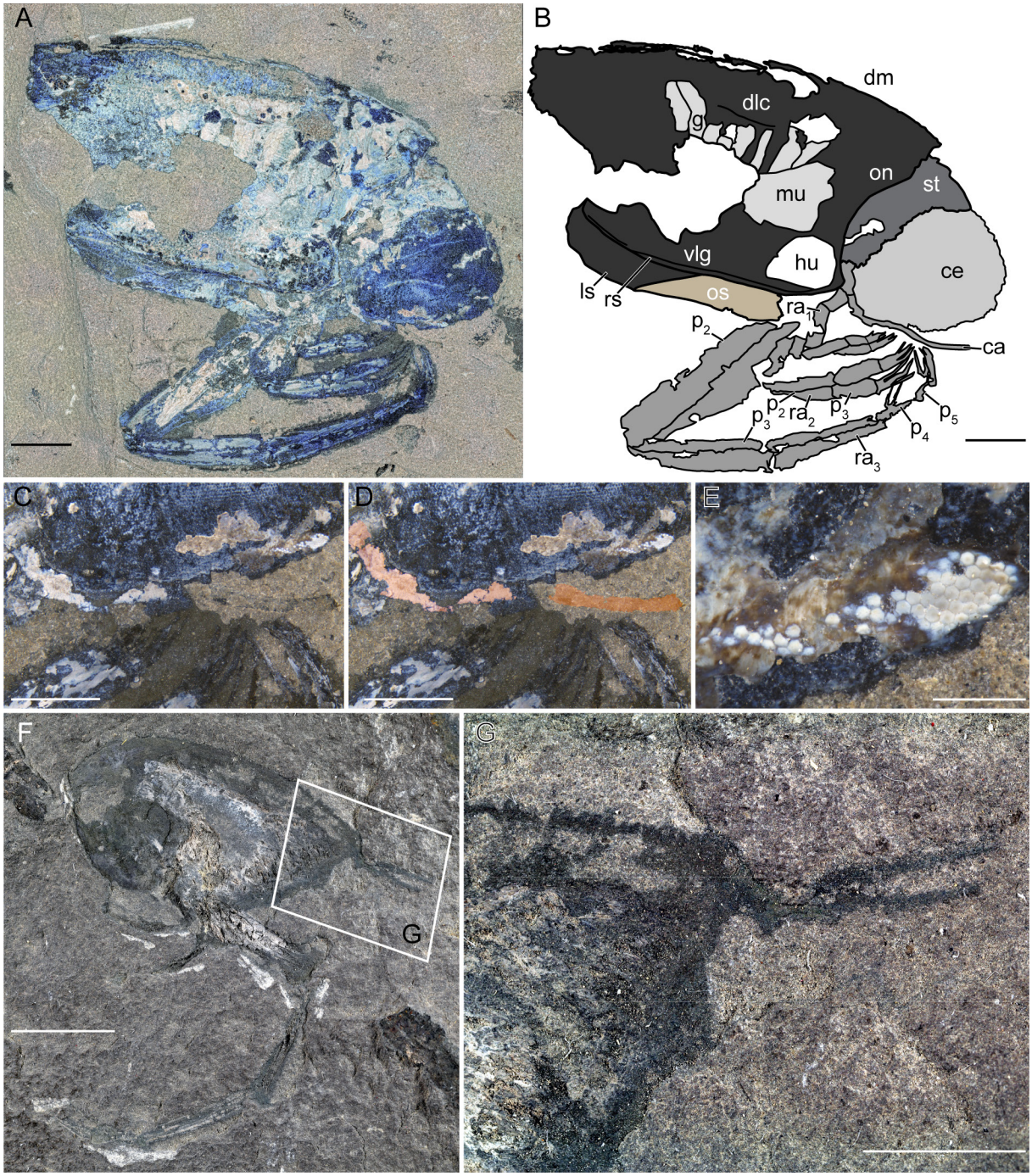

Fig. 14. *Paraclausocaris harpa* gen. et sp. nov. **A–E**. Paratype MNHN.F.A29327. **A**. General view. **B**. Drawing. **C**. Close-up of cephalic appendage. **D**. Close-up of cephalic appendage (colour-marked). **E**. Close-up of compound eyes. **F–G**. Paratype MNHN.F.A29149. **F**. General view. **G**. Close-up of posterior part. Abbreviations: ca = cephalic appendage; ce = compound eye; dm = dorsal midline; dlc = dorso-lateral carina; g = gills; hu = hump; ls = left side of the shield: mu = muscles; on = optic notch; os = oval structure; $p_{2–5}$ = podomeres of raptorial appendages; $ra_{1–3}$ = raptorial appendages; rs = right side of the shield; vlg = ventro-lateral groove. Scale bars: A–B, G = 5 mm; C–D = 2 mm; E = 500 µm; F = 10 mm. Photos: T. Laville.

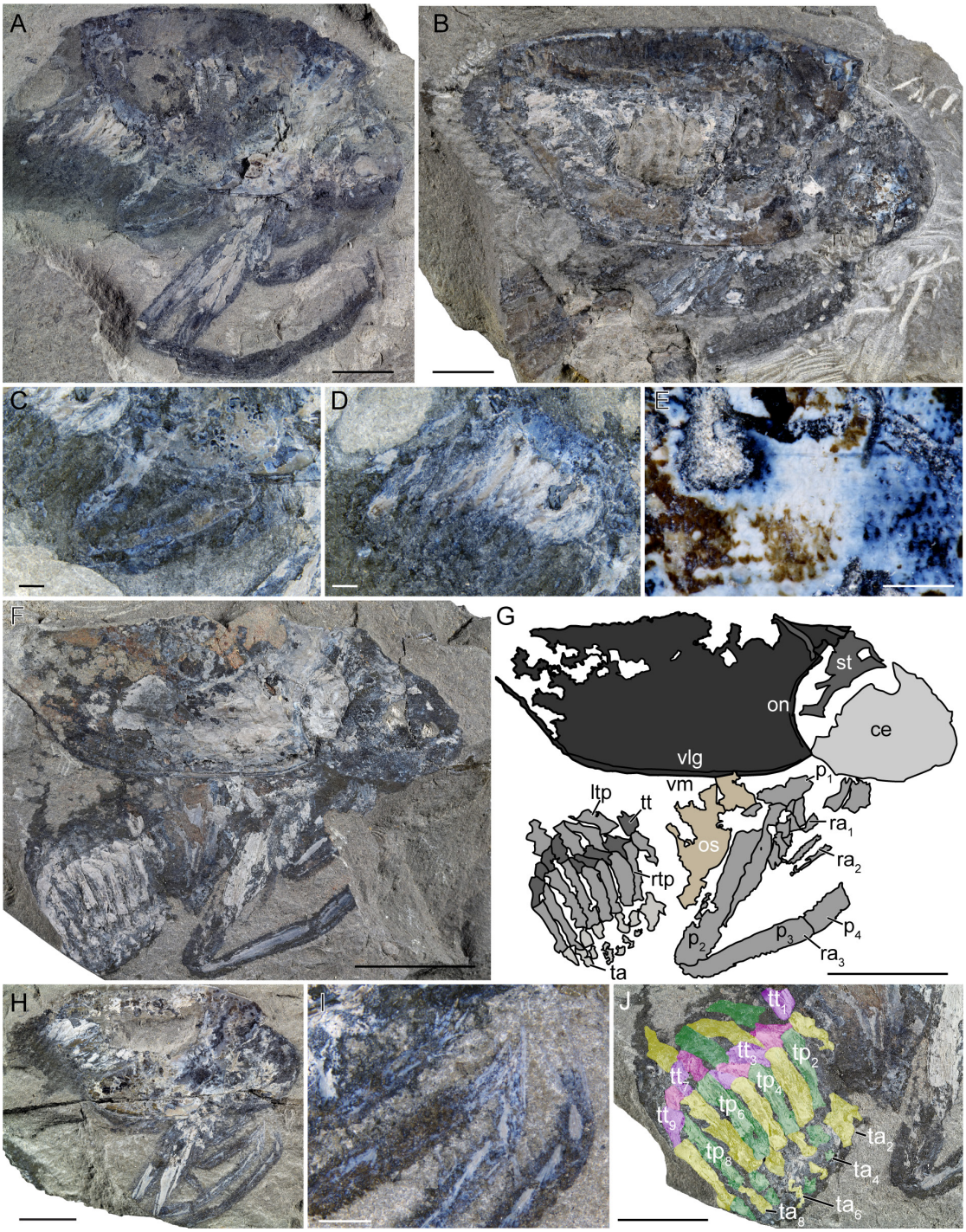

Fig. 15. *Paraclausocaris harpa* gen. et sp. nov. **A, C–D**. Paratype MNHN.F.A29356. **A**. General view. **C**. Close-up of oval structure. **D**. Close-up of posterior trunk. **B, E**. Paratype MNHN.F.A29323. **B**. General view. **E**. Close-up of compound eye. **F–G, J**. Paratype MNHN.F.R50955. **F**. General view. **G**. Drawing. **J**. Close-up of posterior trunk. **H–I**. Paratype MNHN.F.A29323. **H**. General view. **I**. Close-up of distal part of raptorial appendages. Abbreviations: ce = compound eye; on = optic notch; os = oval structure; ltp = left pleural part of posterior trunk; $p_{1–4}$ = podomeres of raptorial appendages; $ra_{1–3}$ = raptorial appendages; rtp = right pleural part of posterior trunk; $ta_{2–8}$ = trunk appendages; $tp_{2–8}$ = pleural part of posterior trunk; tt_{1-9} = tergal part of posterior trunk; vm = ventral margin; vlg = ventro-lateral groove. Scale bars: A–B, H, J = 5 mm; C–D, I = 1 mm; E = 200 µm; F–G = 10 mm. Photos: T. Laville.

ventral oval one (i.e., exopod). Trunk appendages 2–8 consist of at least two elements: a square-shaped proximal one and a rectangular distal one. Last pairs of trunk appendages being much longer than the rest (Fig. 14F–G). No square-shaped element discernible.

Gills

Eight lamellar gills preserved under the central part of the shield below the lateral carina (Fig. 14A–B). Gills arcuate with an elliptic shape.

Anterior muscles

Bundle of radially arranged muscles preserved in the antero-medial part of the shield, above the antero-ventral hump (Fig. 13A, C).

Remarks

Some specimens previously assigned to *Clausocaris ribeti* (now *Ostenocaris ribeti* comb. nov.) are now ascribed to *Paraclausocaris harpa* gen. et sp. nov. (e.g., MNHN.F.A29149; Fig. 13H–I; Charbonnier *et al*. 2010). Indeed, they differ from the type material (and thus from *Ostenocaris*) by their well-developed optic notch, their serrated dorsal margin, their concave posterior part of the ventral margin and their elongate raptorial appendages relative to the shield size.

Genus ***Paraostenia*** Secrétan, 1985

Type species

Paraostenia voultensis Secrétan, 1985 by monotypy.

Original diagnosis (Secrétan 1985)

The voluminous and rounded eyes, the gills and the anterior and posterior appendages are as in *Dollocaris*. The form of the carapace is nearly identical to that of *Ostenia* (Arduini *et al*. 1980 amend Arduini & Brasca 1984) differing in form from *Dollocaris* in the outline which is proportionally higher and shorter and devoid of suborbital spine below the orbital opening which is less deep and more gaping.

Emended diagnosis

Thylacocephala with a symmetric optic notch, a sharp antero-dorsal corner, a dorsal carina, a concave posterior margin, rounded postero-dorsal and postero-ventral corners, long and gracile appendages.

Other included species

Paraostenia ambatolokobensis (Arduini, 1990), Dienerian/Smithian, Early Triassic, Madagascar. *Paraostenia* sp. Ehiro & Kato in Ehiro *et al*., 2015, Spathian, Early Triassic, Japan.

Paraostenia voultensis Secrétan, 1985
Figs 5D, 16–20

Paraostenia voultensis Secrétan, 1985: 388–389, fig. 5c–h, l.

cf. *Ostenia* sp. – Secrétan & Riou 1983: 26–27, figs 1, 6–7.

Paraostenia voultensis – Rolfe 1985: fig. 4; 1992: fig. 1a. — Schram *et al*. 1999: 772, tab. 1. — Charbonnier 2009: 206, figs 233, 251, 339–340, tab. 14. — Charbonnier *et al*. 2010: 115, 121, fig. 5e, tabs 1–2; 2014: 375, tab. 1. — Schram 2014: 353, fig. 3d. — Ji *et al*. 2017: 174. — Ehiro *et al*. 2019: 330. — Rak *et al*. 2018: 268. — Braig *et al*. 2019: fig. 5.6, 5.31. — Van Roy *et al*. 2021: 1739. — Laville *et al.* 2021a: 310–311; 2021b: 92–94; 2021c: 305. — Schram & Koenemann 2022: fig. 41.4, tab. 41.2.

Original diagnosis (Secrétan 1985)

As for genus.

Emended diagnosis

Paraostenia with a serrate dorsal margin and a dorso-lateral row of pores.

Material examined

Holotype

FRANCE • La Boissine, La Voulte-sur-Rhône, Ardèche; Callovian, Middle Jurassic; morphotype 2; MNHN.F.R50977.

Paratype

FRANCE • 1 spec.; same collection data as for holotype; MNHN.F.R50979.

Additional material

FRANCE • 73 specs; same collection data as for holotype; morphotype 2; MNHN.F.A29150, A29231, A29256, A29300 A29320 to A29322, A29326, A29328 to A29338, A29340, A29341, A29344, A29346, A29347, A29351, A29354, A29355, A29362, A29369, A29370, A53132, A53328 to A53330, A53336, A53340, A84030 to A84038 A84041, A84043 to A84058, A84060 to A84063, A84065 to A84071, R50966, R50978 • 4 specs; same collection data as for holotype; morphotype 2; MSNM i7597, i18928, i25037, i25038 • 9 specs; same collection data as for holotype; morphotype 1; MNHN.F.A29339, A29354, A29357, A29361, A53131, A84039, A84040, A84047, A84055, A84059.

Measurements

See Table 2.

Description

Shield morphology

Square-shaped to sub-trapezoidal shield in lateral view with an asymmetric anterior margin formed on a well-developed optic notch, a rounded or sharp antero-dorsal corner, a convex dorsal midline is slightly convex, with a large fin-like (Fig. 18D–E) or flat dorsal carina, a rounded postero-dorsal corner, a vertical or postero-ventrally tilted, concave posterior margin, a rounded postero-ventral corner and a ventral margin divided into a posterior half steeply descending antero-ventrally and a horizontal anterior one (Figs 16, 17A–D). Rim of all free margin delimiting a marginal fold (Fig. 16B, D).

Shield macro-ornamentation

Presence of one straight and large medio-lateral carina, running along almost the entire length of the shield and divided into two parts by a longitudinal narrow furrow (Figs 16A, C, 21A–B). Presence of seven small serrations dorsally oriented on the anterior side of the dorsal carina and of seven serrations dorsally oriented, longer than the anterior ones on the posterior side (Fig. 18D–E).

At least 13 pores forming a sinuous row in the dorsal area of the shield, above the medio-lateral-carina (Figs 16A, C, 18D–F). Horseshoe-like ornamentation or field of punctuations covering the ventral area of the shield (Fig. 19A, C, J). Fields of punctuations also covering the surface of the dorsal area (Fig. 19E–G). Punctuations in the ventral area most probably correspond to degraded horseshoe-like ornamentation.

Presence of a hump either on the medio-ventral area of the shield or near the antero-ventral corner (Figs 16A, C, 19H–J).

Sensory structures
Rounded, stalked, compound eyes protruding from the optic notch and occupying most of it (Figs 16, 18B–C). Eyes formed of hexagonal ommatidia (w = ~80 µm; l = ~80 µm; about 236 per mm²; Fig. 17F).

Cephalic appendages
Antenniform structure only perceptible by the muscle fibres protruding from the optic notch and decreasing in diameter distally (Fig. 17E).

Raptorial appendages
Presence of three pairs of slender raptorial appendages recognised by the preservation of the muscles, protruding from the ventral margin, posterior to the presumed cephalic appendages. Raptorial appendages consisting of two parts: a proximal postero-ventrally oriented and a distal one, antero-ventrally oriented. Articulation between both parts forming an elbow.

First pair of raptorial appendages (Figs 16, 19A, C), the shortest, consisting of a proximal part with two podomeres: podomere 1 being 3.7 times as long as wide; podomere 2 being 4.7 times as long as wide and being longer than podomere 1. Distal part of the appendages formed by three podomeres: podomeres 3 being 4.4 times as long as wide; podomere 4 being 4.8 times as long as wide; podomere 5, the most distal one, being 3.1 times as long as wide.

Second pair of raptorial appendages consisting of a proximal part with two rectangular podomeres (Fig. 18M, O): podomere 1 not being well preserved; podomere 2 being 6.1 times as long as wide. Distal part of the appendage consisting of three podomeres: podomere 3 being 5.6 times as long as wide and bearing one spine on its medial side; podomere 4 being 5.2 times as long as wide and bearing three spines on its medial side; podomere 5 being 2.8 times as long as wide and ending distally in a cluster of three long spines.

Third pair of raptorial appendages, the longest, consisting of a proximal part formed by two podomeres, podomere 2 being 5.9 times as long as wide (Fig. 18I–K). Distal part consisting of three podomere: podomere 3 being 4.4 times as long as wide, bearing two spines on the distal part of its medial side; podomere 4 being 6.4 times as long as wide and bearing nine spines on its medial side, with the first four arranged in pairs; podomere 5 being 4.3 times as long as wide and ending distally with a cluster of three long spines.

Oval structure
Oval structure protruding from the ventral margin, behind the last pair of raptorial appendages (Fig. 18G–H). Structure associated with a lamellar structure in one specimen (Fig. 17G).

Posterior trunk
Nine rectangular pleural parts of trunk segments protruding from the posterior part of the ventral margin (Figs 16B, D, G, 20). In some specimens, pleural part increasing in size until tp_6, then decreasing until tp_9 (Fig. 16B, D, G). In other specimens, pleural parts decreasing in size posteriorly with last one (tp_9) thinner than the rest (Fig. 17H). Proximally, they have a postero-dorsal orientation while they are curved downward distally. Trunk ending in a square segment, i.e., the telson, bearing a rounded structure (Fig. 17I–J). Field of setae visible on the telson.

Posterior trunk appendages
Nine pairs of appendages attached to the pleural part of the posterior trunk (Fig. 20F–H). Appendages oriented postero-dorsally and proximally consisting of a curved square-shaped plate (Fig. 20H) and ending distally in a styliform part (Fig. 20I–J). Last pair of appendages with a rounded distal plate.

Gills
Eight arcuate, lamellar gills preserved below the medio-lateral carina (Fig. 19A–B).

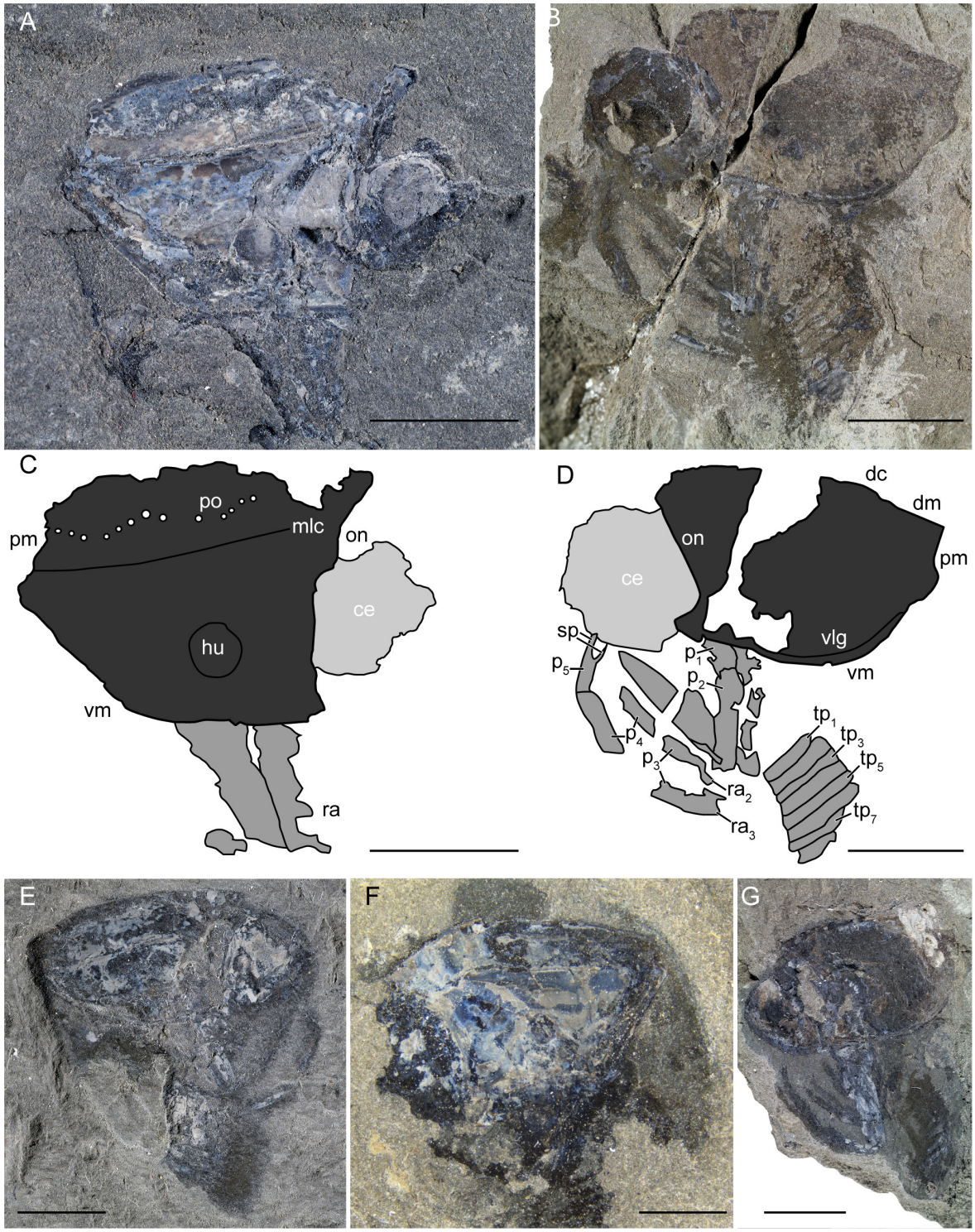

Fig. 16. Juvenile of *Paraostenia voultensis* Secrétan, 1985 (morphotype 1). **A–C**. Specimen MNHN.F.A84040. **A**. General view. **C**. Drawing. **B–D**. Specimen MNHN.F.A29357. **B**. General view. **D**. Drawing. **E**. Specimen MNHN.F.A29354. **F**. Specimen MNHN.F.A84039. **G**. Specimen MNHN.F.A29261. Abbreviations: ce = compound eye; dc = dorsal carina; dm = dorsal midline; hu = hump; mlc = medio-lateral carina; on = optic notch; $p_{1–5}$ = podomeres of raptorial appendages; pm = posterior margin; po = pore; $ra_{2–3}$ = raptorial appendages; sp = spines; $tp_{1–7}$ = pleural part of posterior trunk segments; vlg = ventro-lateral groove; vm = ventral margin. Scale bars = 5 mm. Photos: T. Laville.

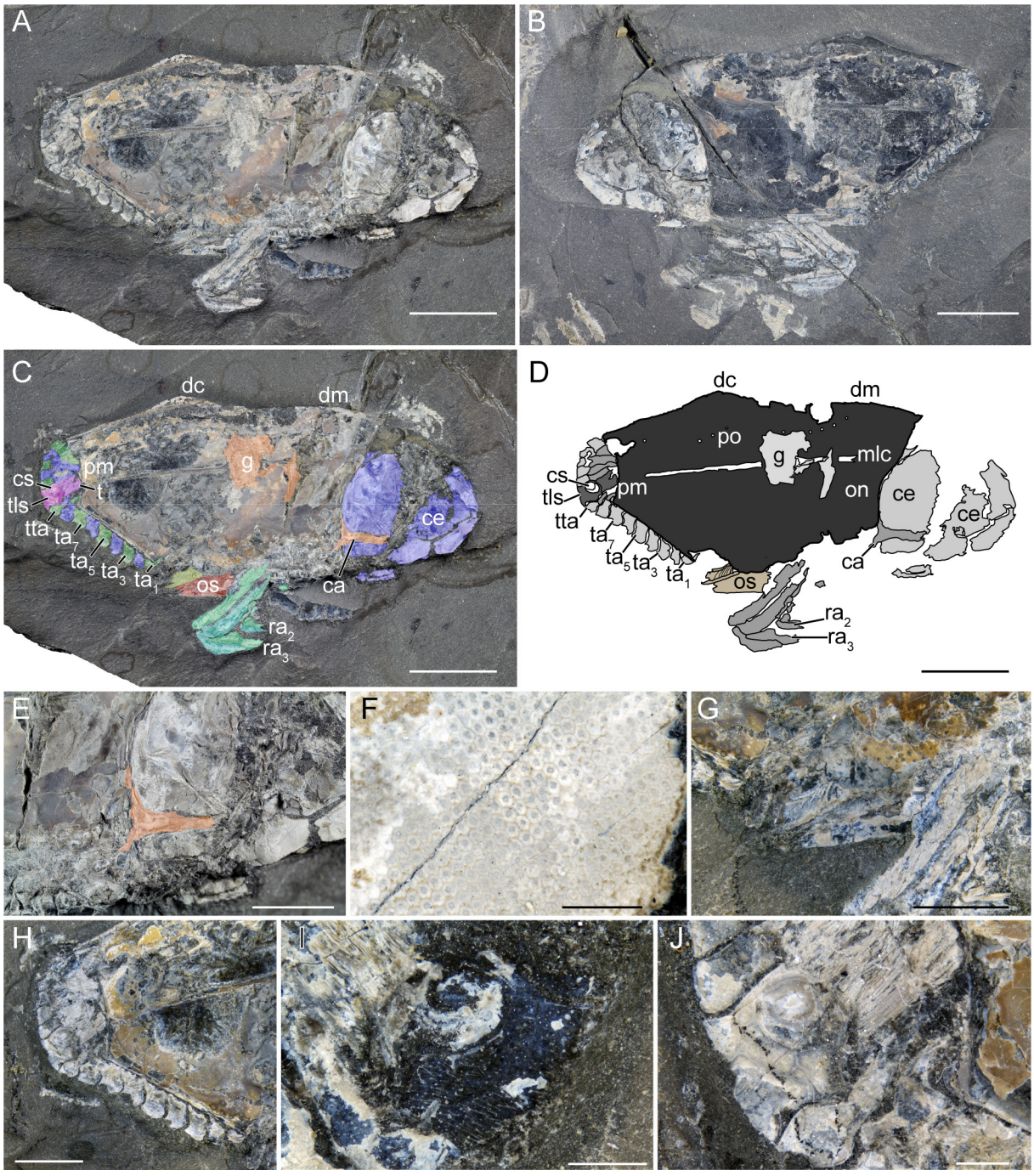

Fig. 17. Adult of *Paraostenia voultensis* Secrétan, 1985 (morphotype 2; MNHN.F.A29300). **A, C–H, J**. Counter-part. **A**. General view. **C**. General view (colour-marked). **D**. Drawing. **E**. Close-up of cephalic appendage (colour-marked). **F**. Close-up of compound eye. **G**. Close-up of oval structure. **H**. Close-up of posterior trunk. **J**. Close-up of telson. **B, I**. Part. **B**. General view. **I**. Close-up of telson. Abbreviations: ca = cephalic appendage; ce = compound eye; cs = circular structure; dc = dorsal carina; dm = dorsal midline; g = gills; mlc = medio-lateral carina; on = optic notch; os = oval structure; pm = posterior margin; po = pore; ra_{2-3} = raptorial appendages; t = trunk; tls = telson; ta_{1-7} = posterior trunk appendages; tta = terminal trunk appendages. Scale bars: A–D = 10 mm; E, G–H = 5 mm; F = 500 µm; I–J = 1 mm. Photos: T. Laville.

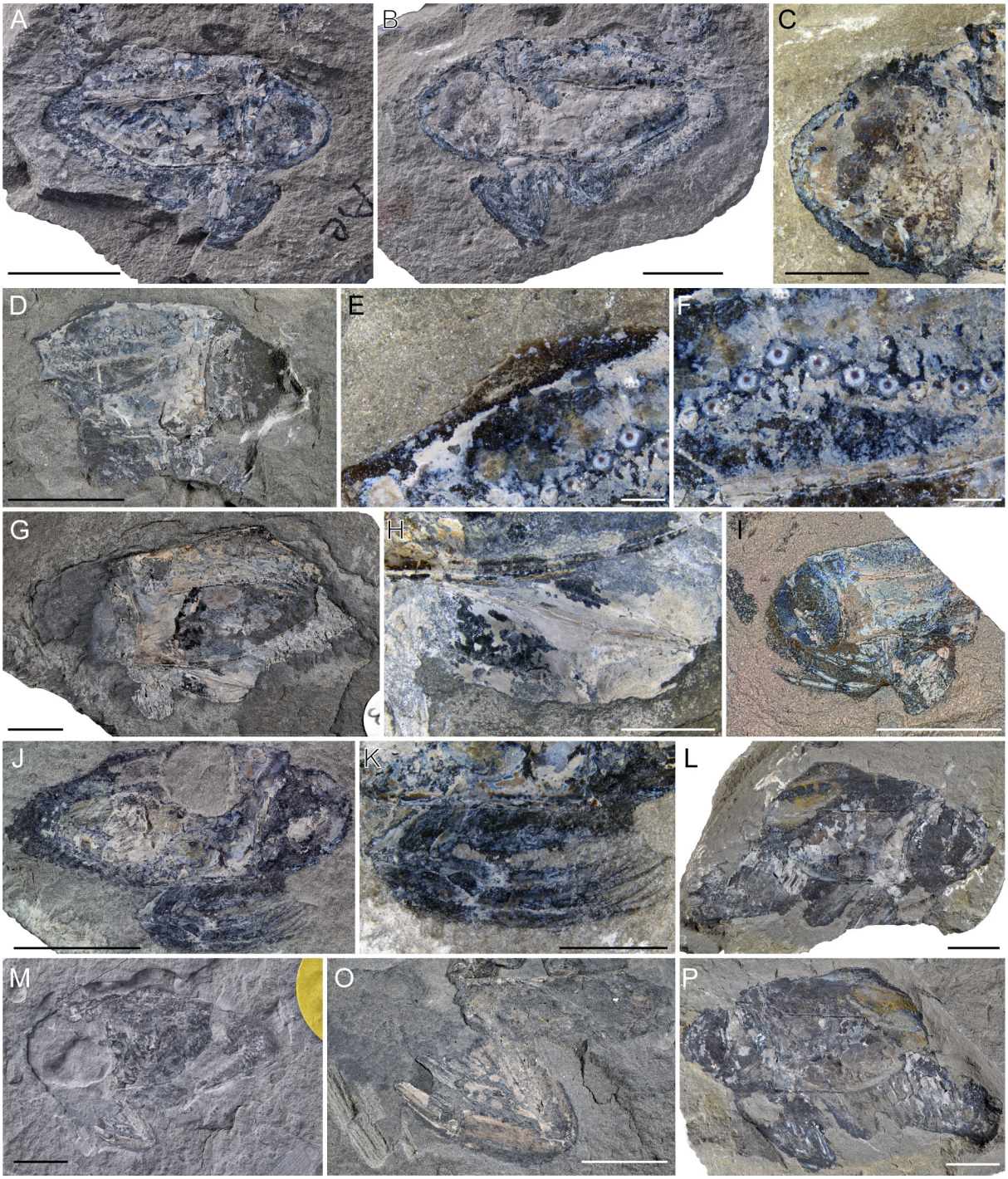

Fig. 18. Adults of *Paraostenia voultensis* Secrétan, 1985 (morphotype 2). **A–C**. Specimen MNHN.F.A29347. **A**. General view (counter-part). **B**. General view (part). **C**. Close-up of compound eye with stalk (counter-part). **D–F**. Specimen MNHN.F.A29341. **D**. General view. **E**. Close-up of dorsal carina. **F**. Close-up of pores. **G–H**. Specimen MNHN.F.A29329. **G**. General view. **H**. Close-up of oval structure. **I**. General view of MNHN.F.A53329. **J–K**. Specimen MNHN.F.A29351. **J**. General view. **K**. Close-up of raptorial appendages. **L, P**. Specimen MNHN.F.A29256. **L**. General view (part). **P**. General view (counter-part). **M, O**. Specimen MNHN.F.A29325. **M**. General view. **P**. Close-up of raptorial appendages. Scale bars: A–B, D, G, I–J, L–M, P = 10 mm; C, H, K, O = 5 mm; E–F = 1 mm. Photos: A–B, M: L. Cazes; C–L, O–P: T. Laville.

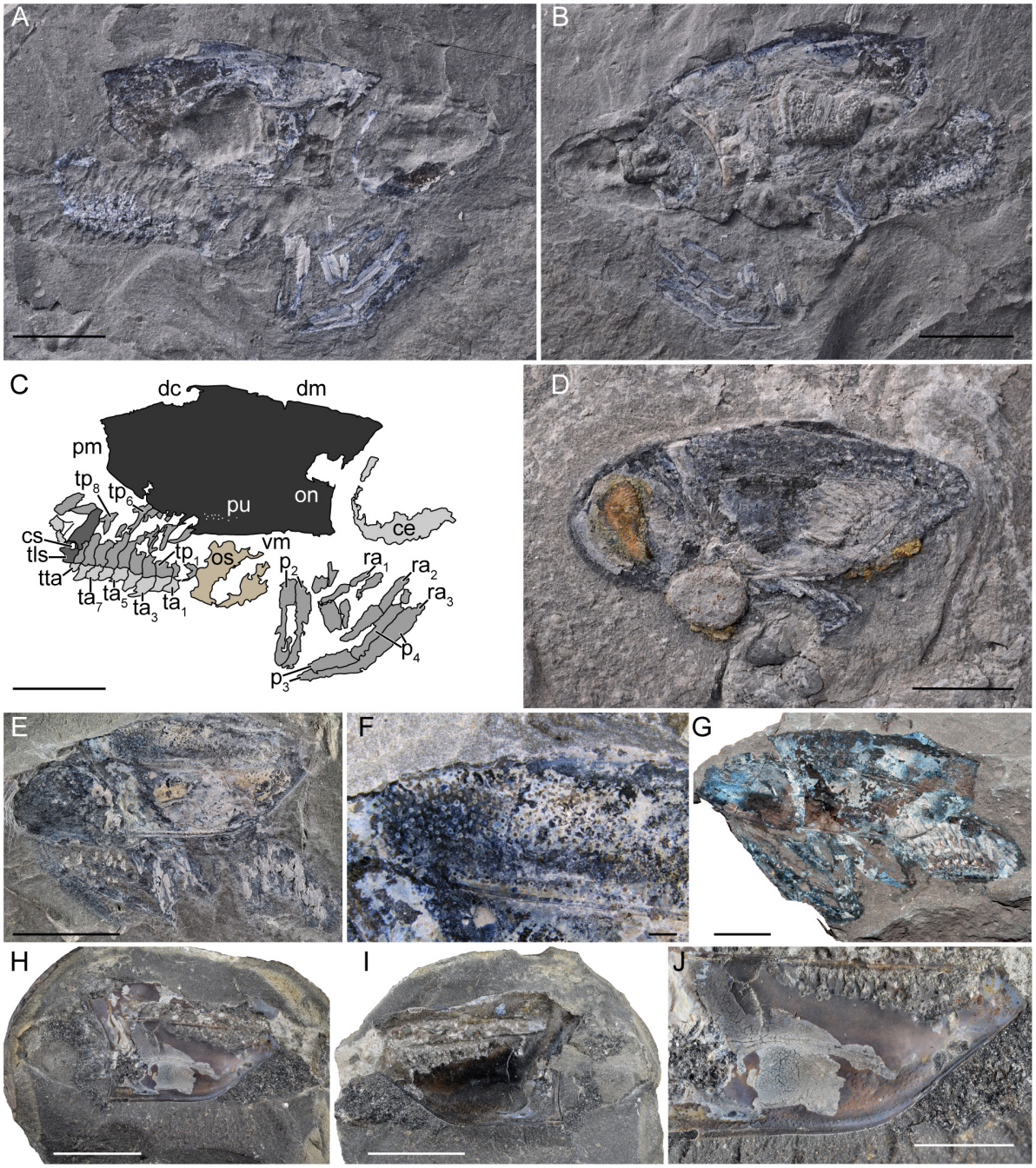

Fig. 19. Adults of *Paraostenia voultensis* Secrétan, 1985 (morphotype 2). **A–C**. Specimen MNHN.F.A29321. **A**. General view (part). **B**. General view (counter-part). **C**. Drawing (part). **D**. Specimen MNHN.F.A29275, general view. **E–F**. Specimen MNHN.F.A84058. **E**. General view. **F**. Close-up of dorsal area with ornamentation. **G**. Specimen MSNM i25038, general view. **H–J**. Specimen MNHN.F.A84036. **H**. General view. **I**. General view. **J**. Close-up of ventral area with ornamentation. Abbreviations: ce = compound eye; cs = circular structure; dc = dorsal carina; dm = dorsal midline; on = optic notch; os = oval structure; $p_{2–4}$ = podomeres of raptorial appendages; pm = posterior margin; pu = punctuations; $ra_{1–3}$ = raptorial appendages; $ta_{1–7}$ = posterior trunk appendages; tls = telson; $tp_{2–8}$ = pleural part of posterior trunk segments; tta = terminal trunk appendages; vm = ventral margin. Scale bars: A–E, G–I = 10 mm; F = 1 mm; J = 5 mm. Photos: A–B, D: L. Cazes; E–F, H–J: T. Laville; G: S. Charbonnier.

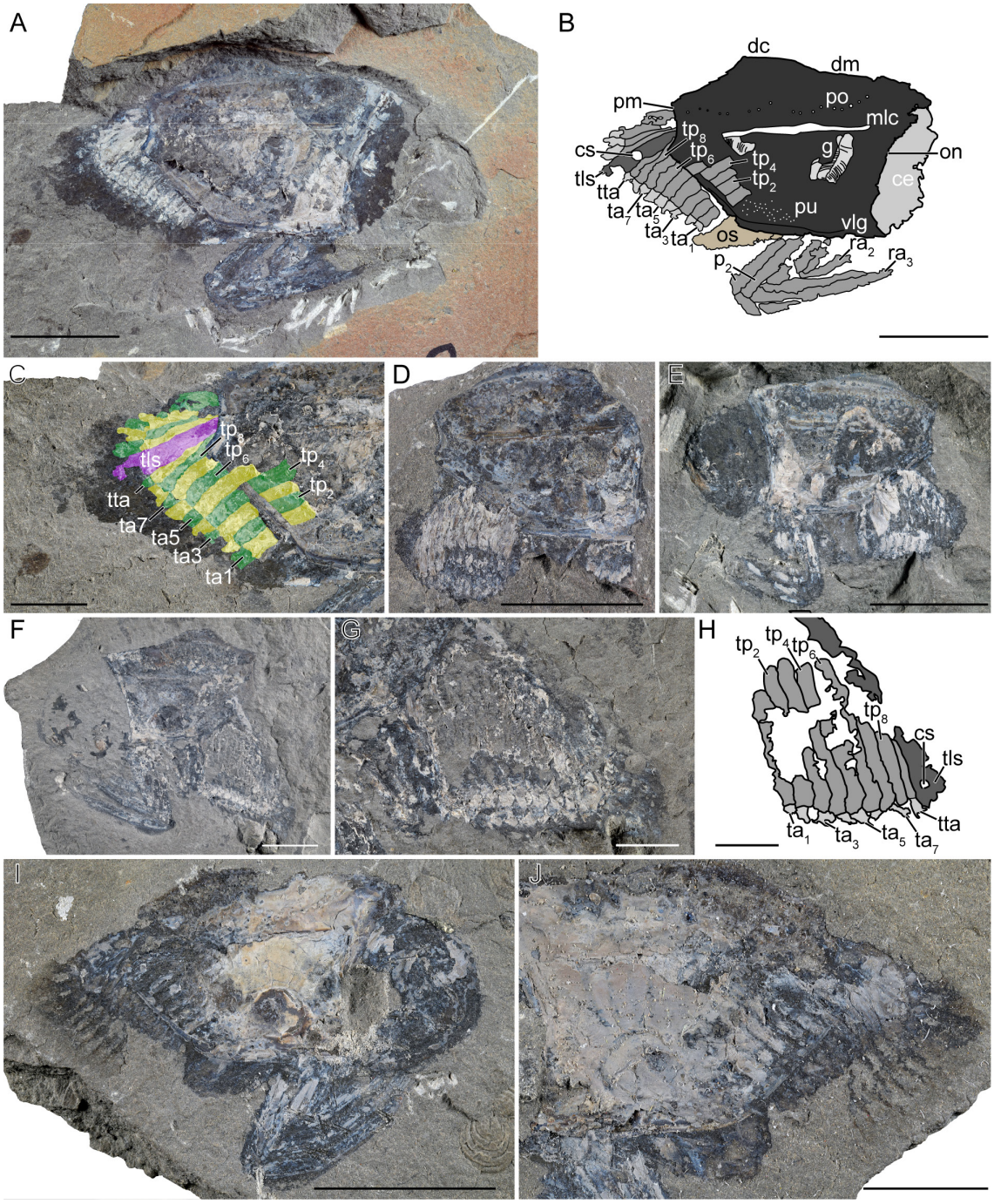

Fig. 20. Adults of *Paraostenia voultensis* Secrétan, 1985 (morphotype 2). **A–C**. Specimen MNHN.F.A29320. **A**. General view. **B**. Drawing. **C**. Close-up of posterior trunk. **D**. Specimen MNHN.F.A84038, general view. **E**. Specimen MNHN.F.A29332, general view. **F–H**. Specimen MNHN.F.A29330. **F**. General view. **G**. Close-up of posterior trunk. **H**. Drawing of posterior trunk. **I–J**. Specimen MNHN.F.A29337. **I**. General view. **J**. Close-up of posterior trunk. Abbreviations: ce = compound eye; cs = circular structure; dc = dorsal carina; dm = dorsal midline; mlc = medio-lateral carina; on = optic notch; os = oval structure; p_2 = podomere 2 of raptorial appendages; pm = posterior margin; po = pore; pu = punctuations; $ra_{1–3}$ = raptorial appendages; $ta_{1–7}$ = posterior trunk appendages; tls = telson; $tp_{2–8}$ = pleural part of posterior trunk segments; tta = terminal trunk appendages; vlg = ventro-lateral groove. Scale bars: A–B, D–E, I = 10 mm; C, F, J = 5 mm; G–H = 1 mm. Photos: T. Laville.

Table 3. Coefficients of standardised major axis analyses and dependence parameters.

	Kilianicaris lerichei	***Ostenocaris ribeti***	***Paraclausocaris harpa*** gen. et sp. nov.	***Paraostenia voultensis***		
				General	morphotype 1	morphotype 2
elevation	0.027	-0.267	-0.096	-0.115	-0.117	-0.0574
slope	0.827	0.986	0.9	0.943	0.88	0.88
R^2	0.93	0.973	0.894	0.923	0.605	0.892
p-Value	2.75e-05	0.0134	0.0547	4.21e-17	0.222	4.06e-13

Remarks

Paraostenia voultensis displays an important variability for some features. For instance, some specimens have a trapezoidal shield with a vertical posterior margin and a horseshoe-like ornamentation (Figs 17–20), while others have a square-shaped shield with a postero-ventrally tilted posterior margin and no ornamentation (Fig. 16). Moreover, it seems there is a slight difference in total length (Fig. 21A): the histogram shows a bimodal distribution that might indicate the presence of two different morphotypes.

Morphometry

In order to characterise the variability of *Paraostenia voultensis* and to confirm the presence of two morphotypes, we ran various morphometric and statistical analyses. In this section, we consider separately both *P. voultensis* putative morphotypes in order to test for their differences. Morphotype 1 corresponds to the small specimens with a square-shaped shield, a postero-ventrally tilted posterior margin, and no ornamentation. Morphotype 2 corresponds to bigger specimens having a square-shaped shield with a postero-ventrally tilted posterior margin and no ornamentation.

Descriptive statistics

The measurements made on *Paraostenia voultensis* allow us to test the homogeneity of the sample. With the exception of the length of the shield (Ls), histograms appear normally distributed for all measurements (Fig. 21A). According to the results of the Shapiro-Wilk test ($W > 0.95$; $p > 0.13$), all measurements probably follow a normal law.

Simple allometry

For *Paraostenia voultensis* (Fig. 21; Table 3), a strong and significant correlation has been found for morphotype 2 ($R^2 = 0.892$, p-value < 0.05) while it is non-significant for morphotype 1 ($R^2 = 0.605$, p-value = 0.222). The slope (likelihood ratio statistic equal to 0.4298, p-value = 0.5121) and the elevation (Wald statistic equal to 0.7178, p-value = 0.39687) are equal between the allometric line of both morphotypes. This indicates that there is no difference in static allometry of both morphotypes and that they are located on a similar allometric line.

For all other species, a strong and significant positive correlation has been found between shield length and shield height ($R^2 > 0.86$, p-value < 0.02; Table 3).

Complex allometry

The first two principal components account for 89.0% of the variance (Fig. 22A). PC1 accounts mostly for variation in height and angle measurements while PC2 accounts mostly for variation in shield length (Supp. file 3). Size measurements appear to be correlated between them (Fig. 22B), but not with angles measurements, which also appear correlated between them.

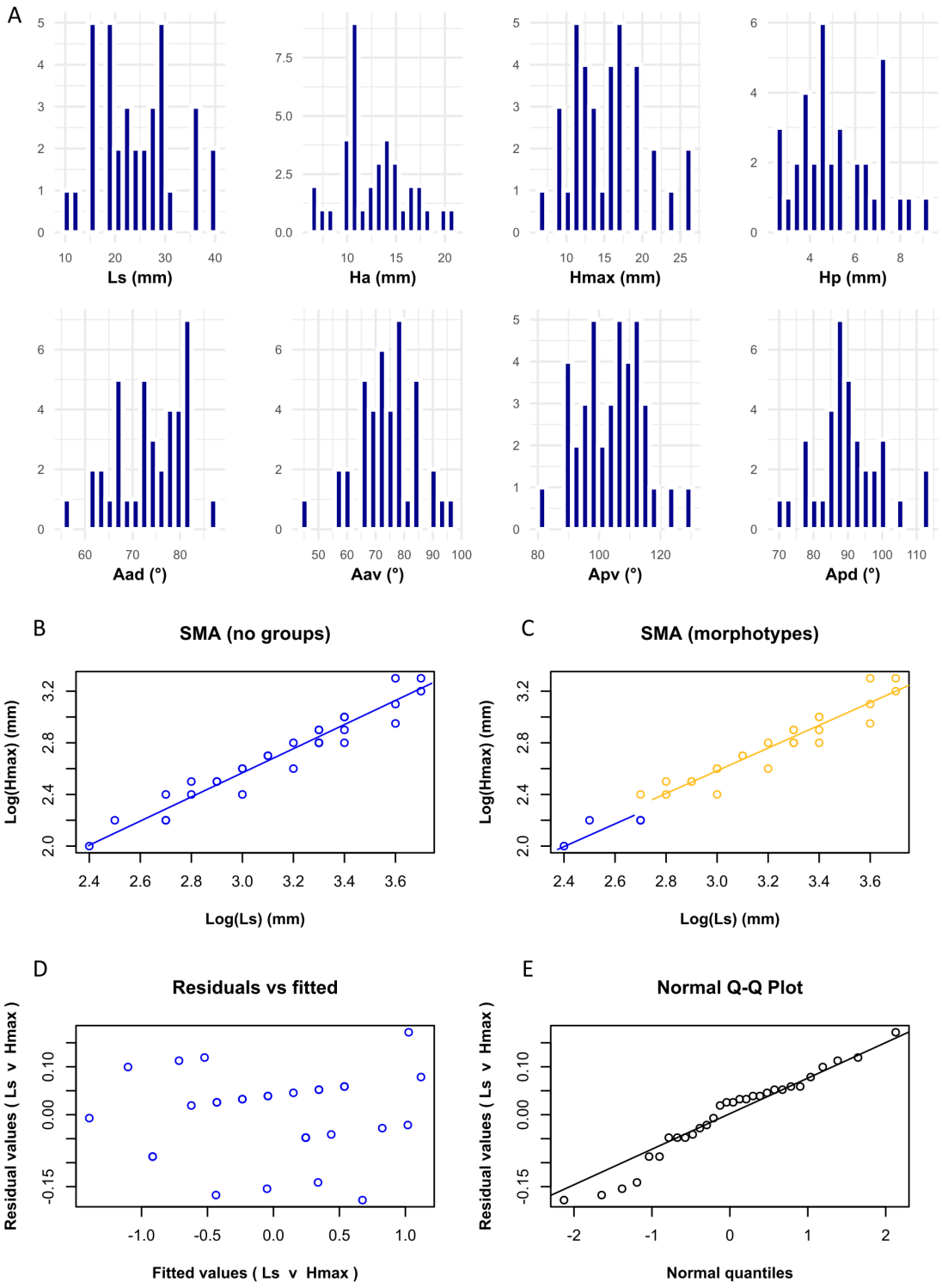

Fig. 21. Frequency distribution and simple allometry of shield measurements for *Paraostenia voultensis* Secrétan, 1985. **A**. Histograms of shield measurements. **B**. Standardised major axis (no groups). **C**. Standardised major axis (morphotypes 1 and 2). **D**. Residuals vs fitted data plot. **E**. Q-Q plot. Abbreviations: Aad = antero-dorsal angle; Aav = antero-ventral angle; Apd = postero-dorsal angle; Apv = postero-ventral angle; Ha = anterior height; Hmax = maximal shield height; Hp = posterior height; Ls = shield length; SMA = standardised major axis.

Clustering analysis (*Paraostenia voultensis*)

Based on the VAT, the dataset presents a good clustering tendency that is not confirmed by the Hopkins statistic (0.57), which indicates a low clustering tendency. An optimal number of three clusters for the K-Means analysis was determined. Results of the prediction are presented in Figure 22. Cluster 1 corresponds to specimens identified as morphotype 1 while specimens identified as morphotype 2 are split between clusters 2 and 3.

Discussion

Intraspecific variability in *Paraostenia voultensis*

The clustering analysis confirms that at least two morphotypes of *Paraostenia voultensis* co-occur in La Voulte. All specimens of morphotype 1 are part of the same cluster (1 in Fig. 22A) while specimens assigned to morphotype 2 are split into two other clusters (2–3 in Fig. 22A). There are no clear morphological differences between clusters of morphotype 2 and we thus consider these specimens as belonging to the same morphotype.

The dimorphism noticed here could have different origins: sex-related differential growth (sexual dimorphism), interspecific differential growth (interspecific variation) or ontogeny. Here, it is unlikely that the morphotypes represent two different taxa or sexual dimorphism. Indeed, in case of sexual dimorphism or interspecific variation, we would have noticed differences in allometric shape due to different growth (e.g., Fairbairn 1997; Gidasweski *et al*. 2009). Instead, both morphotypes share a common allometric line, which most probably represents the ontogenetic allometry of *P. voultensis*. This corresponds to the covariation among traits across ontogenetic stages of an individual or in a population (mean ontogenetic allometry) of a given species (Gould 1966; Klingenberg 1998; Pélabon *et al.* 2013). In a classic case, the various ontogenetic stages are distributed along the common allometric line. For *P. voultensis*, all the specimens of morphotype 1 form a cluster in the lower part of the allometric line, indicating a smaller absolute size, while morphotype 2 specimens form a cluster in the upper part of the allometric line, indicating a larger absolute size. Based on these results, it is most probable that the two morphotypes correspond to two different ontogenetic stages of the same taxa, with morphotype 1 being a juvenile stage while morphotype 2 would represent an adult stage.

Another interesting fact here is the similarity in the number of segments and appendages described in both ontogenetic stages. As there is only size difference between both stages, *P. voultensis* displays, at least partly during its post-embryonic development, an epimorphic growth, i.e., a growth between stages without increment in segment numbers (Minelli & Fusco 2013).

Morphological and anatomical interpretations

Compound eyes

With the exception of the oldest species (*Thylacares brandonensis*: Haug *et al*. 2014), thylacocephalans possess hypertrophied compound eyes. These eyes have been initially interpreted as cephalic pouches, i.e., an extension of the cephalon containing the stomach (Arduini *et al.* 1980; Pinna *et al.* 1985). However, Fröhlich *et al.* (1992) and Vannier *et al.* (2016) later demonstrated that these presumed cephalic pouches were actually compound eyes. Vannier *et al*. (2016) were even able to describe the micro-structure of the ommatidia of *Dollocaris ingens*: they are formed of a corneal lens which sits on the top of a crystalline cone, and of rhabdom surrounded by four to five retinula cells. The eyes described here for other La Voulte thylacocephalans seem to have a comparable morphology: they consist of densely packed, hexagonal ommatidia. However, the ommatidia are larger than those of *D. ingens* and less densely packed. Here, it was not possible to determine the visual parameters of the eyes as they are poorly preserved compared to those of *D. ingens*.

In La Voulte thylacocephalans, with the exception of *Ostenocaris ribeti*, the compound eyes are followed by longitudinal muscles that are attached to the posterior edge of the eyes. This suggests the presence of a massive, tubular stalk. Presence of a stalk is not uncommon in thylacocephalans: it has been documented multiple times (e.g., Haug *et al*. 2014; Laville *et al*. 2021a), including for *D. ingens* (Secrétan 1985). Usually, eye stalks are considered to be long and narrow connecting structures, but here, the stalks are quite massive and short. This is not uncommon among arthropods, for which stalks can be variously developed from a short, massive structure to a narrow, elongate and flexible structure (e.g., Schoenemann *et al*. 2011; Strausfeld *et al*. 2016).

Cephalic appendages

Several flagellate structures have been previously interpreted as antennules or antennae in thylacocephalans. Haug *et al*. (2014) and Laville *et al*. (2021a) described two antenniform structures from specimens of *Mayrocaris bucculata* (Late Jurassic, Solnhofen Lagerstätten, Germany). They interpreted these structures as antennula and antenna, although an interpretation as a biflagellate antennula was not ruled out. Antenniform structures were also described in Triassic Malagasy thylacocephalans (Laville *et al*. 2021c). In our study, we describe similar flagellate appendages in specimens of *Mayrocaris* sp, *Ostenocaris ribeti*, *Paraostenia voultensis*, and *Paraclausocaris harpa* gen. et sp. nov. These structures are often located on the side of the large compound eyes but, except for *Mayrocaris* sp., their exact morphology and origin are unknown, preventing further interpretation of their nature.

Secrétan & Riou (1983: fig. 3) previously mentioned cephalic appendages, including antennae, in La Voulte thylacocephalans (*Dollocaris ingens*). On two specimens (MNHN.F.R50937, R50938), they described putative bases of several cephalic appendages. After re-examining these specimens, we can conclude that the first three elements, interpreted as the bases of the mandibula, the maxillula and the maxilla, actually belong to raptorial appendages. Concerning the first element, i.e., the putative antenna, it is unlikely to be an antenna due to its position just anterior to the raptorial appendages. It is probably a part of a masticatory appendages (i.e., the mandibula, the maxillula or the maxilla).

Adductor muscles and muscle scar

A bundle of radially arranged muscles is often found in the antero-ventral area of the shield of *Mayrocaris* sp. and *Paraclausocaris harpa* gen. et sp. nov. (Figs 10, 14). Similar structures have been described in other thylacocephalan taxa. Schram *et al.* (1999) interpreted similar muscles in *Protozoea hilgendorfi* Dames, 1886 as gastric muscles. In *Ostenocaris cypriformis* (Arduini *et al*. 1980), a similar bundle associated with a circular mark is present on the shield. Here, the muscles are interpreted as adductor muscles and thus, the rounded mark is believed to be a muscle scar. This would be consistent with the position and the morphology of the muscles found in *Mayrocaris* sp and *Pc. harpa*.

Another structure found on the shield of thylacocephalans might be interpreted as a muscle scar. A large rounded protuberance, located on the central area of the shield has been described as muscle scar on multiple species of thylacocephalan species (*Ligulacaris parisiana* [see Charbonnier *et al.* 2019]; *Dollocaris ingens* [see Secrétan & Riou 1983]; *Paraostenia voultensis* [see Secrétan 1985]; *Victoriacaris muhiensis* [see Hegna *et al*. 2014]; *Paradollocaris vannieri*, *Globulocaris garassinoi*, *Keelicaris deborae* [see Charbonnier *et al.* 2017]; *Mayrocaris bucculata* [see Laville *et al.* 2021a]). However, no muscles are found associated with these protuberances, making unlikely that they are muscle scars. Instead, Secrétan (1985) suggested that this protuberance might serve as a "pocket" for the raptorial appendages. The raptorial appendages, which are protruding from the shield just under the protuberance, could have been folded in the gap formed by the protuberance. This would be consistent with the fact that thylacocephalans might have been ambush predators and thus were lying on the seafloor, waiting for prey (Vannier *et al.* 2016). In modern ambush predators, such as stomatopods, the raptorial appendages are retracted under the margin of the shield when the organism is resting (Kunze & Anderson 1981).

This would also be consistent with the fact that thylacocephalans were swimming, at least occasionally. Having their raptorial appendages hidden under the shield would have given a more streamlined shape to the body, and thus the organism would have swum more efficiently.

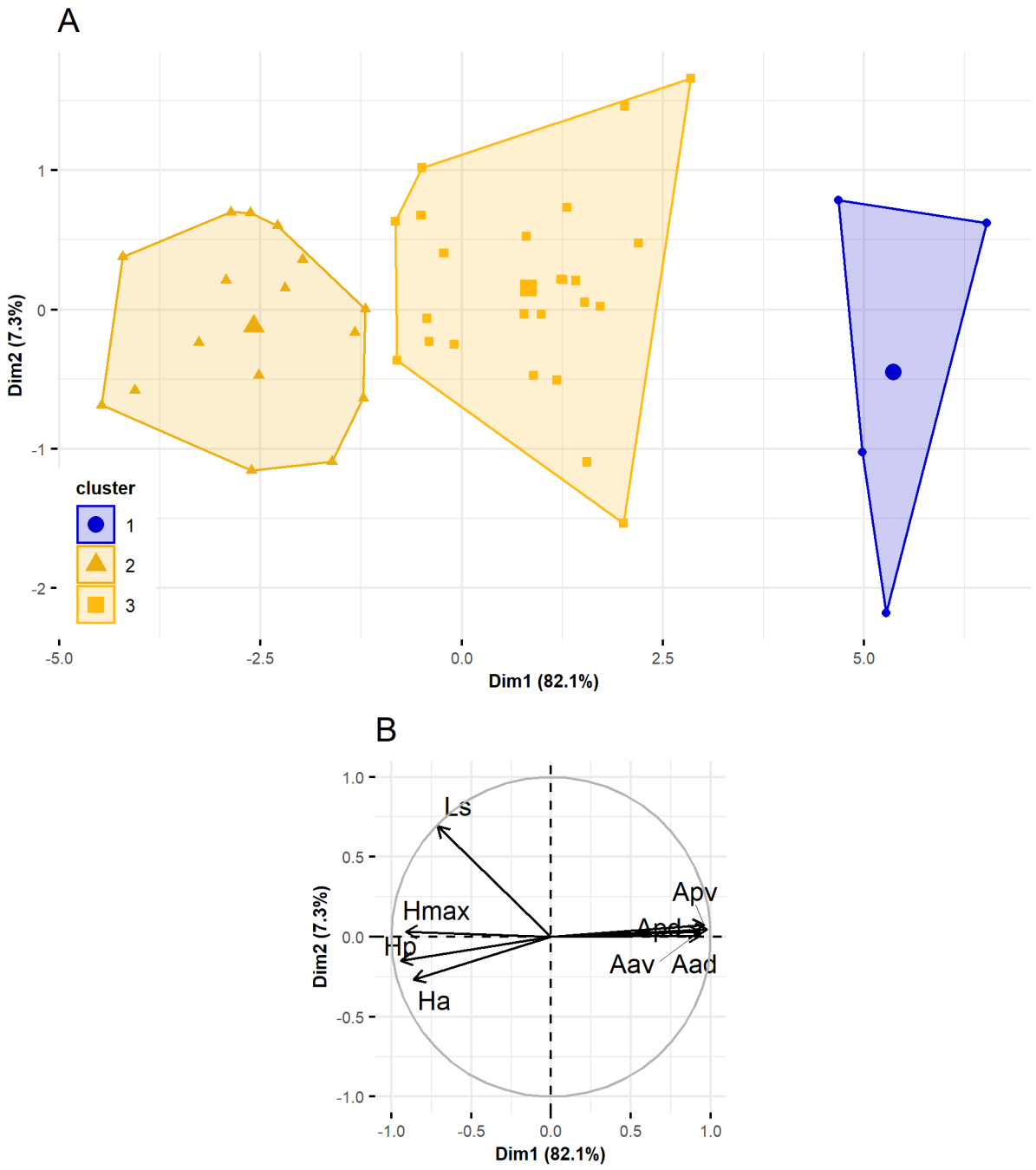

Fig. 22. Complex allometry for *Paraostenia voultensis* Secrétan, 1985 (morphospace). **A**. Principal component analysis projection of morphospace on principal components 1 and 2. **B**. Correlation circle of variables for principal components 1 and 2. Abbreviations: Aad = antero-dorsal angle; Aav = antero-ventral angle; Apd = postero-dorsal angle; Apv = postero-ventral angle; Ha = anterior height; Hmax = maximal shield height; Hp = posterior height; Ls = shield length.

Oval structure

In *Austriocaris secretanae* sp. nov., *Kilianicaris lerichei*, *Paraclausocaris harpa* gen. et sp. nov. and *Paraostenia voultensis*, a large oval sclerotised structure is protruding between the raptorial appendages and the posterior trunk appendages (Fig. 23). This feature has already been reported by Secrétan & Riou (1983) in *Dollocaris ingens* and by Polz (1990: 108) in *Clausocaris lithographica* from Solnhofen Lagerstätten (Fig. 24), where it was referred to as "additional leaf-shaped limbs". It has a rounded distal margin ornamented with a row of setae. It appears associated with the posterior trunk, as seen in the specimens on which the posterior trunk is detached from the shield. The structure does not appear segmented or related to any appendage, making unlikely that it represents an appendage, or a part of an appendage. Therefore, it probably represents an enlarged sclerite or a modified posterior trunk segment.

In terms of function, with its large surface with setose margins, this oval feature could have acted as a paddle, producing a thrust for swimming, similarly to the phyllopodous appendages of branchiopods (Hessler 1985). Another interpretation may be that of ventilatory function. Indeed, the oval structure resembles scaphognathite of decapod pancrustaceans, which corresponds to the exopod of the maxilla. It has a well-developed oval morphology and has setose margins (e.g., Boxshall & Jaume 2009). By

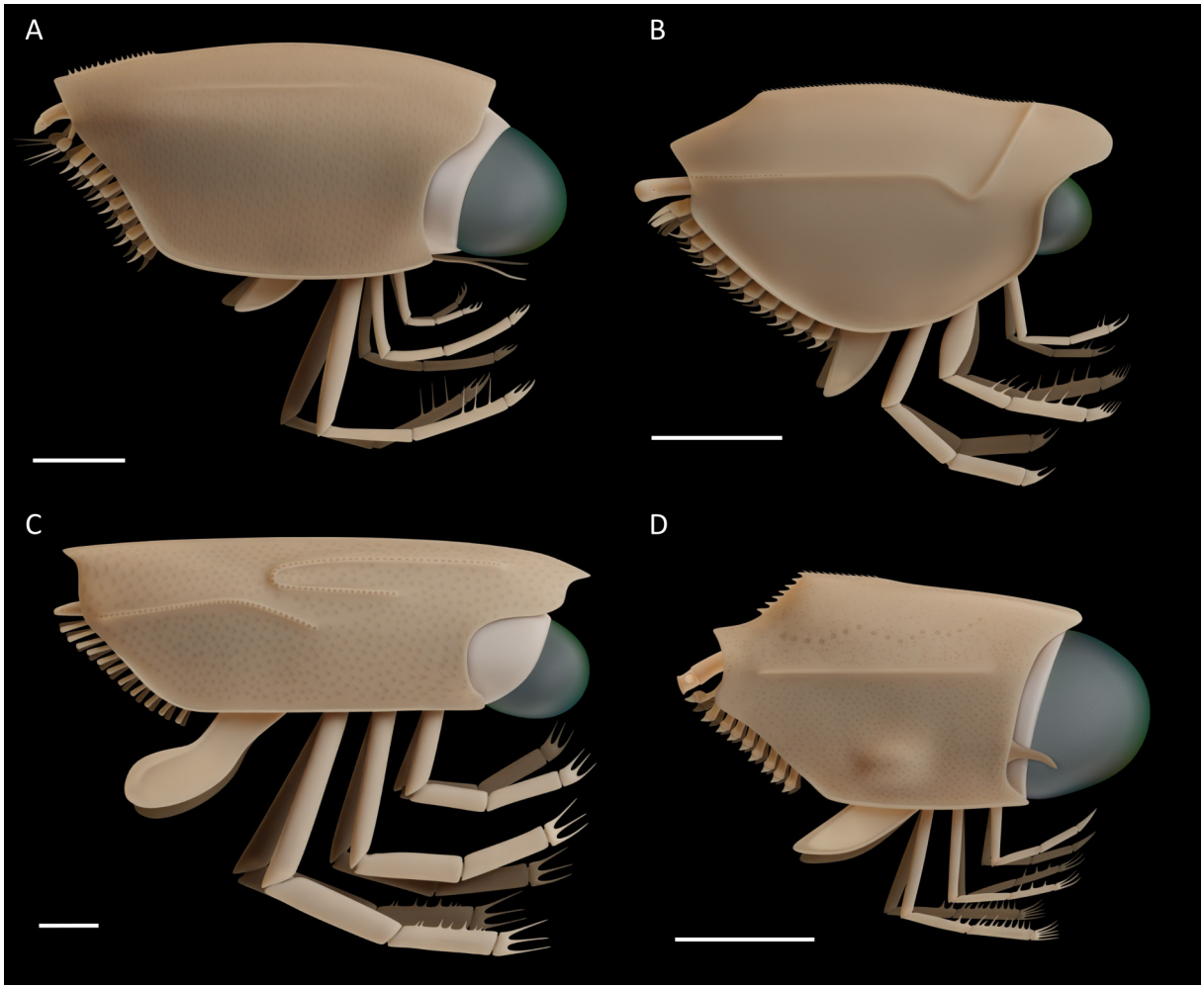

Fig. 23. Reconstruction of La Voulte thylacocephalans. **A**. *Paralausocaris harpa* gen. et sp. nov. **B**. *Kilianicaris lerichei* Van Straelen, 1923. **C**. *Austriocaris secretanae* sp. nov. **D**. *Paraostenia voultensis* Secrétan, 1985. Scale bars = 10 mm. Reconstructions: Alexandre Lethiers (made with Blender).

beating, it produces a water flow that brings water into the shield and helps ventilate the gills. In La Voulte-sur-Rhône thylacocephalans, the oval structure is located just beneath the gills, which would be a good position for ventilating them. Therefore, the oval structure might be analogous to the scaphognathite.

Posterior trunk appendages

Already mentioned in multiple other thylacocephalan species (Schram 1990; Haug *et al.* 2014; Laville *et al.* 2021a), a long and probably biramous terminal trunk appendage is also quite common in La Voulte thylacocephalans (*Kilianicaris lerichei*, *Paraclausocaris harpa* gen. et sp. nov.). A more interesting observation is the possible presence of other biramous posterior trunk appendages. Indeed, one specimen of *Pc. harpa* seems to display a biramous first posterior trunk appendage (Fig. 13A, C). Such detail has never been observed in thylacocephalans before.

Telson

Two particular posterior trunk segments drew our attention during the study of the La Voulte thylacocephalans: the 10th segment in *Paraclausocaris harpa* gen. et sp. nov. and *Paraostenia voultensis* (Figs 13, 17) and the 12th in *Austriocaris secretanae* sp. nov. and *Kilianicaris lerichei* (Figs 4, 6). These segments have a peculiar morphology compared to the rest of the posterior trunk segments: they have a squared shape, do not bear any appendage and displays a unique rounded structure on their dorsal surface. On one specimen of *P. voultensis* (MNHN.F.A29300), setae can be observed on its distal part.

Dorsally to these particular segments, the segments change orientation and appear symmetrical to the ventral ones. These 'dorsal' segments probably correspond to the other pleural parts of the 'ventral' segments. Thus, these peculiar segments represent the terminal segment of the posterior trunk. Based on their position and their morphology, the presence of marginal setae and the absence of appendages attached to these segments, we interpret them as the telson. It probably corresponds to the "reduced, unsegmented abdomen" of *Ostenocaris cypriformis* (Pinna *et al*. 1985).

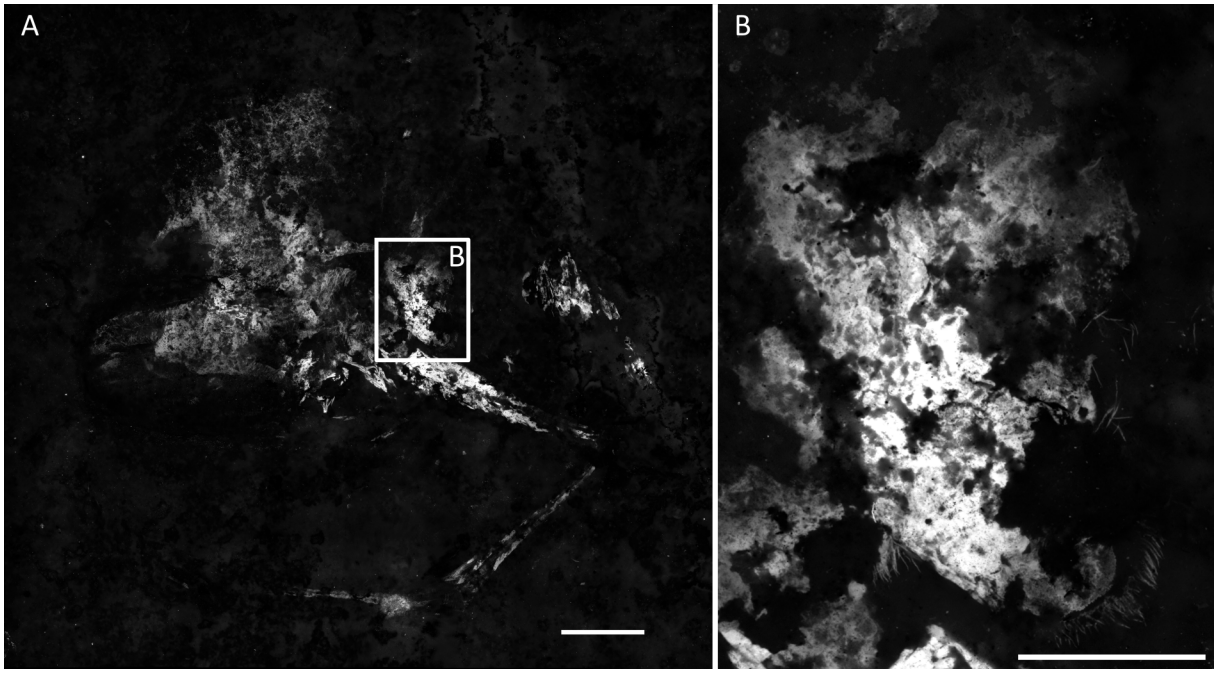

Fig. 24. *Clausocaris lithographica* (Oppenheim, 1888). **A–B**. Specimen JM SOS 972. **A**. General view. **B**. Close-up of oval setose structure. Scale bars: A = 5 mm; B = 2 mm. Photos: T. Laville.

On the telson, a large, circular structure can be distinguished. This structure consists of two circles: a large one, occupying most of the width of the telson, surrounding a smaller one. Such a structure was already mentioned by Secrétan & Riou (1983) for *Dollocaris ingens*. A rounded structure on the telson could be the anus. However, in pancrustaceans, the anus is usually located ventrally or at the posterior end on the telson (Bowman 1971). Here, the circular structure is dorsally located which makes it unlikely to be the anus. The circular structure could also be a tubercle or the basis of a spine, although it is unlikely as it does not rise from the telson and looks more depressed. One hypothesis would be that it represents a statocyst, a balance organ common among malacostracans (Espeel 1985; Sekiguchi & Terazawa 1997; Meland *et al.* 2015; Bober *et al.* 2018), and already described in fossil mysids (e.g., Voicu 1974; Schlacher *et al.* 1992; Wittmann *et al.* 1993; Vicente & Cartanyà 2017). It corresponds to a rounded invagination of soft-tissue that encloses ambient water and a rounded biomineralised statolith. This can give the impression of being formed by two concentric circles, such as what is found in La Voulte-sur-Rhône thylacocephalans. It usually serves for stabilising the body in the water and for orientation while swimming. In macrostylid isopods, two symmetric statocysts can be found on the dorsal surface of the telson (Bober *et al.* 2018). Therefore, it would not be surprising to find such an organ on the telson of thylacocephalans. As it is, better-preserved specimens remain necessary before being able to determine precisely the nature of this circular structure.

Pores

Two different kinds of pores are recorded in La Voulte-sur-Rhône thylacocephalans: 1) canal-like pores (*Mayrocaris* sp., *Paraclausocaris harpa* gen. et sp. nov. and *Paraostenia voultensis*), which are formed by a rim surrounding a hollow part (Figs 13, 19); 2) unrimmed pores on carina (*Austriocaris secretanae* sp. nov.; *Kilianicaris lerichei*). The canal-like pores are quite common among thylacocephalans (Lange & Schram 2002; Broda & Zatoń 2017; Laville *et al.* 2021a). They have been suggested to be sensory structures acting in a similar way as the sensory dorsal organs of pancrustaceans (Broda & Zatoń 2017). Among species with canal-like pores in La Voulte Lagerstätte, one is of particular interest: *P. voultensis*. Indeed, Secrétan (1985) reported that the canal-like pores forming a sinuous line enclosed somewhat of a capsule, that has been interpreted by Rolfe (1985) as putative photophores. While studying the numerous specimens of *P. voultensis*, no capsules have been found in the pores. Moreover, the morphology of these pores is different from the bioluminescent pores of halocyprid myodocops (Angel 1968), which form tubercles. In *P. voultensis*, the pores are flat and not raised. For these reasons, we consider the photophores hypothesis as unlikely.

The second kind of pores only occurs on the carina of *Austriocaris secretanae* sp. nov. and *Kilianicaris lerichei*. They lack a rim and appear filled with sediment. Unrimmed pores have been reported by Broda & Zatoń (2017) and interpreted as setal lumina, i.e., a simple pore (lumen) in the cuticle, that provides intracuticular articulation to the setae (Garm 2004). However, the pores found in *A. secretanae* and in *K. lerichei* (~100 µm) are much bigger than the previously mentioned setal lumina (~1 µm). Another hypothesis could be that the pores represent the bases of broken spines. Spines on the lateral area of the shield have only been reported on putative thylacocephalan cuticular fragments from the Middle Devonian of Czech Republic (Mergl 2020). On these remains, the spines, when broken, form pits. If these pits would have been filled by sediment, they could probably have a similar morphology as the pores found on *A. secretanae* and on *K. lerichei*. We cannot conclude definitively on the nature of such pores but the spine hypothesis should be kept in mind.

Phylogenetic affinities of thylacocephalans

Usually considered as pan/eucrustaceans (Haug *et al*. 2014; Vannier *et al*. 2016), a recent phylogenetic analysis has positioned thylacocephalans as stem-mandibulates in a clade with two enigmatic Palaeozoic euarthropods bearing raptorial appendages (Pulsipher *et al*. 2022): *Acheronauta stimulapis* Pulsipher *et al*., 2022 and *Captopodus poschmanni* Kühl & Rust, 2012. A position within mandibulates is not surprising as it

now seems certain that thylacocephalans had antenniform appendages (possibly antennula and/or antenna) and mandibula. However, a placement as a stem-mandibulates is more unexpected. Indeed, in addition to the cephalic appendages, several anatomical details suggest a close relationship with pancrustaceans: presence of proximal endites on raptorial appendages (Haug *et al*. 2014), sensory dorsal organs (Broda & Zatoń 2017), similarities of organic systems with these of pancrustaceans (Vannier *et al*. 2016).

Moreover, some uncertainties on the anatomy of thylacocephalans, in particular concerning the raptorial appendages, seems to preclude any firm conclusion as to their phylogenetic affinities. Indeed, the nature of raptorial appendages is still debated. They have been interpreted as being antennula, antenna and mandibula (Arduini *et al*. 1980), mandibula, maxillula and maxilla (Vannier *et al*. 2016) or as maxillula, maxilla and maxillipeds (Schram 1990; Haug *et al*. 2014). Some authors also suggested that they were entirely part of the trunk (Secrétan 1985; Rolfe 1985; Polz 1993). These various interpretations impact the tagmatisation of thylacocephalans. If the raptorial appendages are mostly or entirely considered as cephalic, it would imply that thylacocephalans consist of two regions, a cephalon and an undifferentiated trunk, which would be similar to *Ca. poschmanni* and to *Ac. stimulapsis*. In the case of thoracic raptorial appendages, thylacocephalans would have been formed by three tagma: a cephalon, an anterior trunk bearing raptorial appendages and a posterior trunk. In their phylogenetic analysis, Pulsipher *et al*. (2022) favoured the interpretation of the raptorial appendages of thylacocephalans as the maxillula, the maxilla and a maxilliped, and thus of a two-tagma body. They did not test alternative interpretations which would probably have led to a different phylogenetic position for thylacocephalans. Pending confirmation of the nature of the raptorial appendages, the results of Pulsipher *et al*. (2022) should thus be taken with caution, leaving the question of the phylogenetic affinities of thylacocephalans open.

Palaeoecology

Sensing

The antenniform appendages of La Voulte thylacocephalans appear quite small in comparison to their hypertrophied compound eyes (Fig, 14A–D). The combination of large eyes and short antenniform appendages is common among thylacocephalans (Haug *et al*. 2014; Laville *et al*. 2021c). As mentioned by Schram & Koenemann (2022), an analogy can be made with hyperiid amphipods, which also have large eyes and atrophied antennulae and antennae (e.g., Bowman & Gruner 1973; Stenvers *et al*. 2021). With hypertrophied compound eyes that allow for an acute vision, the antennula might have been less useful and thus, would have been replaced by eyes as the primary sensory structure. Moreover, a complex sensory system formed of the canal-like pores has been reported in thylacocephalans (Broda & Zatoń (2017). Such sensory system may have supplemented the eyes, thus reducing the importance of antenniform appendages as sensory structures.

Locomotion

Several lifestyles have been proposed for thylacocephalans: endobenthic (Briggs & Rolfe 1983), epibenthic crawler (Pinna *et al*. 1982; Secrétan 1985), necktobenthic (Vannier *et al*. 2016) or nektonic (Rolfe 1985; Schram *et al*. 1999; Haug *et al*. 2014). It is most likely that thylacocephalans adopted several lifestyles during their evolution.

Concerning La Voulte-sur-Rhône thylacocephalans, several features seems to indicate a nektonic or nektobenthic lifestyle (Fig. 23). First, they appear to have a streamlined shield (Vannier *et al*. 2016), as exemplified in specimens preserved in 3D or dorso-ventrally compressed (Fig. 7). This type of shield is likely to have reduced the drag effect. In addition to the streamlined aspect, the shield appears flexible and thin: it is often wrinkled but not broken and the underlying structures can often be distinguished. This combination is often indicative of a nektonic or nektobenthic lifestyle in extant pancrustaceans such as in *Nebalia* Leach, 1814 (Vannier *et al*. 1997) and halocyprid myodocops (Vannier & Chen 2000).

La Voulte thylacocephalans also seem to have a complex circulatory and respiratory system. They display eight large gills, allowing for efficient gas exchange that might have been ventilated by the oval structure mentioned above. The gills are connected by efferent and afferent vessels to the heart, which itself is connected to large arteries (Vannier *et al*. 2016; Schram & Koenemann 2022). According to Vannier *et al*. (2016), this system might be associated to a complex integumental circulatory system, such as what is known in extant myodocopids (Abe & Vannier 1995). This complex circulatory and respiratory system is indicative of an active lifestyle, consistent with a nektonic or nektobenthic lifestyle.

Some structures on the posterior trunk could also be related to a nektonic or nektobenthic lifestyle. The first of these structures is the combination of the square-shaped and flattened telson, with long terminal trunk appendages (Fig. 23). This recalls the tailfan of extant malacostracans which plays an important role for locomotion, either allowing for escape reaction (Neil & Ansell 1995), or for elevating from the seafloor (Vannier *et al*. 1997). A similar function is likely in thylacocephalans. Another structure of the posterior trunk might play a role in locomotion, the putative statocyst. In mysids and decapods, the statocyst has an important function during locomotion, as it allows for stabilisation of the body and for directional swimming (Neil 1975). If this circular structure is confirmed to be a statocyst, it probably played an important role for swimming in thylacocephalans.

Finally, the only missing information to confirm the swimming ability of La Voulte thylacocephalans is the morphology of the trunk appendages. Indeed, except for *Austriocaris secretanae* sp. nov. for which they appear rod-like (Fig. 4E, H), they are poorly preserved, preventing from determining their exact morphology and thus, from confirming the swimming ability of thylacocephalans. Despite these uncertainties, the morphological evidence largely supports an active nektonic or nektobenthic lifestyle for La Voulte thylacocephalans.

Diversity of Jurassic thylacocephalans

With seven different taxa described, the La Voulte-sur-Rhône Lagerstätte is the most taxonomically diverse thylacocephalan fauna known so far (Fig. 23). Looking at the distribution of thylacocephalan species along the stratigraphic column of this outcrop (Fig. 1), it appears that these thylacocephalans form a unique assemblage. Indeed, the distribution of all taxa spans the entire stratigraphic layer and more importantly, they co-occur in layer g-8-9 (Fig. 1C).

In terms of diversity, the description of two new species, *Austriocaris secretanae* sp. nov. and *Paraclausocaris harpa* gen. et sp. nov. from La Voulte Lagerstätte greatly increase the specific diversity of Jurassic thylacocephalans. Even though only four thylacocephalan-bearing localities are known in the Jurassic, they preserve an important specific diversity with 11 species described (Table 1). Another Jurassic species was previously assigned to thylacocephalans: *Rugocaris indunensis* Tintori, Bigi, Crugnola & Danini, 1986. The affinities of this species with thylacocephalans has always been doubtful (e.g., Schram 2014). Indeed, this species displays a unique morphology among thylacocephalan: it has a sub-triangular shield with rugations. Recently, we were informed that the holotype and only specimen of *R. indunensis* actually represents a fragment of a cephalopod (G. Teruzzi, pers. com.). Thus, we no longer consider this species as a thylacocephalan.

In addition to the important specific diversity, Jurassic thylacocephalans also preserve a large morphological diversity, with unique anatomical details and a huge diversity of shield and appendage morphologies. The Jurassic is also most probably the period with the longest thylacocephalans, as exemplified by *Austriocaris secretanae* sp. nov. or *O. cypriformis* (see Vannier *et al*. 2006).

In terms of palaeogeographic distribution, all known Jurassic localities are restricted to the Tethys Ocean, as are most of the Triassic thylacocephalan-bearing outcrops (Ehiro *et al*. 2019). This can

explain the similarities between these Jurassic faunas, being geographically close. Indeed, the La Voulte thylacocephalan assemblage shares many taxa with other Jurassic assemblages: *Mayrocaris* and *Dollocaris* are also known from the Solnhofen Lithographic Limestones (Polz 1988, 1989, 1997, 2001) while *Paraostenia* and *Ostenocaris* are also known from the Osteno Lagerstätte (Arduini *et al.* 1980; Pinna *et al.* 1985). However, the small number of known localities throughout the Jurassic prevents a biogeographic synthesis of thylacocephalans during the Jurassic.

Conclusion

The reappraisal of the La Voulte thylacocephalans provides important insight into the diversity and morphology of Jurassic thylacocephalans. It reveals an unexpected diversity, with the description of two new species, *Austriocaris secretanae* sp. nov. and *Paraclausocaris harpa* gen. et sp. nov., and the occurence of *Mayrocaris* sp.

La Voulte thylacocephalans also greatly improve our knowledge of the anatomy of the group. We recognised new key anatomical features, such as an oval structure or putative statocyst on the telson, which provide additional pieces of evidence for nektonic or nektobenthic lifestyle in La Voulte thylacocephalans.

Finally, the re-investigation of La Voulte thylacocephalans also provides information concerning their ontogeny. A juvenile stage of *Paraostenia voultensis* is reported for the first time, which indicates that this species had, at least partly during its post-embryonic development, an epimorphic growth.

Acknowledgements

We thank Jean-Michel Pacaud (MNHN, Paris) and Anna Alessandrello (MSNM, Milano) for their curatorial assistance. We would also like to acknowledge Lilian Cazes and Philippe Loubry (MNHN, Paris) as well as Joachim T. Haug and Carolin Haug (LMU, Munich) for their photographic assistance. We also thank Alexandre Lethiers (Sorbonne Université, Paris) for the reconstructions of thylacocephalans and Christopher P.A. Smith (Université de Bourgogne, Dijon) for correcting the manuscript. Finally, we would like to thank two anonymous reviewers and the editors, Christian de Muizon (MNHN, Paris) and Pepe Fernández (Museo Nacional Ciencias Naturales, Madrid) for their remarks that greatly improved the manuscript.

References

Abe K. & Vannier J. 1995. Functional morphology and significance of the circulatory system of Ostracoda, exemplified by *Vargula hilgendorfii* (Myodocopida). *Marine Biology* 124 (1): 51–58. https://doi.org/10.1007/BF00349146

Alessandrello A., Bracchi G. & Riou B. 2004. Polychaete, sipunculan and enteropneust worms from the lower Callovian (Middle Jurassic) of La Voulte-Sur-Rhône (Ardèche, France). *Memorie della Società italiana di Scienze naturali e del Museo civico di Storia naturale di Milano* 32 (1): 3–16.

Angel M.V. 1968. Bioluminescence in planktonic halocyprid ostracods. *Journal of the Marine Biological Association of the United Kingdom* 48 (1): 255–257. https://doi.org/10.1017/S0025315400032562

Arduini P. 1992. *Clausocaris pinnai* n. sp., (Order Clausocarida nov.), thylacocephalan crustacean from the Norian of the Preone Valley (Udine, N. Italy) and morphological considerations on Thylacocephala. *Atti della Società italiana di Scienze naturali e del Museo civico di Storia naturale di Milano* 132 (21): 265–272.

Arduini P. & Brasca A. 1984. *Atropicaris*: nuovo genere della classe Thylacocephala. *Atti della Società italiana di Scienze naturali e del Museo civico di Storia naturale di Milano* 125: 87–93.

Arduini P., Pinna G. & Teruzzi G. 1980. A new and unusual Lower Jurassic cirriped from Osteno in Lombardy: *Ostenia cypriformis* n.g. n. sp. *Atti della Società italiana di scienze naturali e del museo civico di storia naturale di Milano* 121: 360–370.

Audo D. & Schweigert G. 2018. Large polychelidan lobsters with a rounded carapace from the Middle Jurassic La Voulte-sur-Rhône Lagerstätte: taxonomic clarifications. *Geodiversitas* 40 (2): 183–194. https://doi.org/10.5252/geodiversitas2018v40a9

Audo D., Schweigert G., Martin J.-P.S. & Charbonnier S. 2014. High biodiversity in Polychelida crustaceans from the Jurassic La Voulte-sur-Rhône Lagerstätte. *Geodiversitas* 36 (4): 489–525. https://doi.org/10.5252/g2014n4a1

Auguie B. 2017. *gridExtra: Miscellaneous Functions for 'Grid' Graphics*. Available from https://rdrr.io/cran/gridExtra/ [accessed 1 Aug. 2023].

Bachmayer F. 1960. Eine fossile Cumaceenart (Crustacea, Malacostraca) aus dem Callovien von La Voulte-sur-Rhône (Ardèche). *Eclogae geologicae Helvetiae* 53 (1): 421–429.

Blankers T., Adams D.C. & Wiens J.J. 2012. Ecological radiation with limited morphological diversification in salamanders. *Journal of Evolutionary Biology* 25 (4): 634–646. https://doi.org/10.1111/j.1420-9101.2012.02458.x

Bober S., Riehl T. & Brandt A. 2018. An organ of equilibrium in deep-sea isopods revealed: the statocyst of Macrostylidae (Crustacea, Peracarida, Janiroidea). *Zoomorphology* 137 (1): 71–82. https://doi.org/10.1007/s00435-017-0376-5

Bowman T.E. 1971. The case of the nonubiquitous telson and the fraudulent furca. *Crustaceana* 21 (2): 165–175.

Bowman T.E. & Gruner H.E. 1973. The families and genera of Hyperiidea (Crustacea: Amphipoda). *Smithsonian Contributions to Zoology* 146: 1–64. https://doi.org/10.5479/si.00810282.146

Boxshall G.A. & Jaume D. 2009. Exopodites, epipodites and gills in crustaceans. *Arthropod Systematics & Phylogeny* 67 (2): 229–254. https://doi.org/10.3897/asp.67.e31699

Braig F., Haug J.T., Schädel M. & Haug C. 2019. A new thylacocephalan crustacean from the Upper Jurassic lithographic limestones of southern Germany and the diversity of Thylacocephala. *Palaeodiversity* 12 (1): 69–87. https://doi.org/10.18476/pale.v12.a6

Briggs D.E.G. & Rolfe W.D.I. 1983. New Concavicarida (new order:? Crustacea) from the Upper Devonian of Gogo, Western Australia, and the palaeoecology and affinities of the group. *Special Papers in Palaeontology* 30: 249–276.

Broda K. & Zatoń M. 2017. A set of possible sensory system preserved in cuticle of Late Devonian thylacocephalan arthropods from Poland. *Historical Biology* 29 (8): 1045–1055. https://doi.org/10.1080/08912963.2017.1284834

Burnaby T.P. 1966. Growth-invariant discriminant functions and generalized distances. *Biometrics* 22 (1): 96–110. https://doi.org/10.2307/2528217

Carriol R.-P. & Riou B. 1991. Les Dendrobranchiata (Crustacea, Decapoda) du Callovien de La Voulte-sur-Rhône. *Annales de Paléontologie* 77 (3): 143–160.

Charbonnier S. 2009. Le Lagerstätte de La Voulte: un environnement bathyal au Jurassique. *Mémoires du Muséum national d'histoire naturelle* 199: 1–272.

Charbonnier S., Vannier J., Gaillard C., Bourseau J.-P. & Hantzpergue P. 2007a. The La Voulte Lagerstätte (Callovian): evidence for a deep water setting from sponge and crinoid communities. *Palaeogeography, Palaeoclimatology, Palaeoecology* 250 (1–4): 216–236. https://doi.org/10.1016/j.palaeo.2007.03.013

Charbonnier S., Vannier J. & Riou B. 2007b. New sea spiders from the Jurassic La Voulte-sur-Rhône Lagerstätte. *Proceedings of the Royal Society B: Biological Sciences* 274 (1625): 2555–2561. https://doi.org/10.1098/rspb.2007.0848

Charbonnier S., Vannier J., Hantzpergue P. & Gaillard C. 2010. Ecological significance of the arthropod fauna from the Jurassic (Callovian) La Voulte Lagerstätte. *Acta Palaeontologica Polonica* 55 (1): 111–132. https://doi.org/10.4202/app.2009.0036

Charbonnier S., Garassino A., Schweigert G. & Simpson M. 2013. *A Worldwide Review of Fossil and Extant Glypheid and Litogastrid Lobsters (Crustacea, Decapoda, Glypheoidea)*. Muséum national d'Histoire naturelle, Paris.

Charbonnier S., Audo D., Caze B. & Biot V. 2014. The La Voulte-sur-Rhône Lagerstätte (Middle Jurassic, France). *Comptes Rendus Palevol* 13 (5): 369–381. https://doi.org/10.1016/j.crpv.2014.03.001

Charbonnier S., Teruzzi G., Audo D., Lasseron M., Haug C. & Haug J.T. 2017. New thylacocephalans from the Cretaceous Lagerstätten of Lebanon. *Bulletin de la Société géologique de France* 188 (3): 19. https://doi.org/10.1051/bsgf/2017176

Charbonnier S., Brayard A. & The Paris Biota Team. 2019. New thylacocephalans from the Early Triassic Paris Biota (Bear Lake County, Idaho, USA). *Geobios* 54: 37–43. https://doi.org/10.1016/j.geobios.2019.04.005

Charrad M., Ghazzali N., Boiteau V. & Niknafs A. 2014. NbClust: an R package for determining the relevant number of clusters in a data set. *Journal of Statistical Software* 61 (6): 1–36. https://doi.org/10.18637/jss.v061.i06

Dalla Vecchia F.M. 2012. *Il Friuli 215 milioni di anni fa. Gli straordinari fossili di Preone: finestra su di un mondo scomparso*. Comune di Preone.

Dames W. 1886. Ueber einige Crustaceen aus den Kreideablagerungen des Libanon. *Zeitschrift der Deutschen Geologischen Gesellschaft* 38 (3): 551–576.

Eberle J., Myburgh R. & Ahrens D. 2014. The evolution of morphospace in phytophagous scarab chafers: no competition - no divergence? *PLoS ONE* 9 (5): e98536. https://doi.org/10.1371/journal.pone.0098536

Ehiro M., Sasaki O., Kano H. & Nagase T. 2019. Additional thylacocephalans (Arthropoda) from the Lower Triassic (upper Olenekian) Osawa Formation of the South Kitakami Belt, Northeast Japan. *Palaeoworld* 28 (3): 320–333. https://doi.org/10.1016/j.palwor.2019.03.001

Elmi S. 1967. Le Lias supérieur et le Jurassique moyen de l'Ardèche. *Travaux et Documents des Laboratoires de Géologie de Lyon* 19: 1–845.

Enay R. 1993. Les apports sud-téthysiens parmi les faunes jurassiques nord-ouest européennes: interprétation paléobiogéographique. *Comptes rendus de l'Académie des Sciences. Série 2, Mécanique, Physique, Chimie, Sciences de l'Univers, Sciences de la Terre* 317 (1): 115–121.

Enay R., Guiraud R., Ricou L.E., Mangold C., Thierry J., Cariou E., Bellion Y. & Dercourt J. 1993. Callovian (162 to 158 Ma). *In*: Dercourt J., Ricou L.E. & Vrielynck B. (eds) *Atlas Tethys Palaeoenvironmental Maps. Explanatory Notes*: 81–95. Gauthier-Villars, Paris.

Espeel M. 1985. Fine structure of the statocyst sensilla of the mysid shrimp *Neomysis integer* (Leach, 1814) (Crustacea, Mysidacea). *Journal of Morphology* 186 (2): 149–165. https://doi.org/10.1002/jmor.1051860203

Fairbairn D.J. 1997. Allometry for sexual size dimorphism: pattern and process in the coevolution of body size in males and females. *Annual Review of Ecology and Systematics* 28: 659–687. https://doi.org/10.1146/annurev.ecolsys.28.1.659

Fischer J.-C. & Riou B. 1982. Les Teuthoïdes (Cephalopoda, Dibranchiata) du Callovien inférieur de La Voulte-sur-Rhône (Ardèche, France). *Annales de Paléontologie* 68 (4): 295–325.

Fischer J.-C. & Riou B. 2002. *Vampyronassa rhodanica* nov. gen. nov. sp., vampyromorphe (Cephalopoda, Coleoidea) du Callovien inférieur de la Voulte-sur-Rhône (Ardèche, France). *Annales de Paléontologie* 88 (1): 1–17. https://doi.org/10.1016/S0753-3969(02)01037-6

Fischer J.-C. 2003. Invertébrés remarquables du Callovien inférieur de la Voulte-sur-Rhône (Ardèche, France). *Annales de Paléontologie* 89 (4): 223–252. https://doi.org/10.1016/j.annpal.2003.09.001

Flury B.N. 1984. Common principal components in k groups. *Journal of the American Statistical Association* 79 (388): 892–898. https://doi.org/10.1080/01621459.1984.10477108

Fournet J.J.-B.X. 1843. Études sur le terrain jurassique et les minerais de fer de l'Ardèche. *Annales de la Société d'Agriculture, des Sciences de Lyon* 6 (1): 1–35.

Fröhlich F., Mayrat A., Riou B. & Secrétan S. 1992. Structures rétiniennes phosphatisées dans l'oeil géant de *Dollocaris*, un crustacé fossile. *Annales de Paléontologie (1992)* 78 (4): 193–204.

Fuchs D. 2014. First evidence of *Mastigophora* (Cephalopoda: Coleoidea) from the early Callovian of La Voulte-sur-Rhône (France). *Göttingen Contributions to Geosciences* 77: 21–27.

Garm A. 2004. Revising the definition of the crustacean seta and setal classification systems based on examinations of the mouthpart setae of seven species of decapods. *Zoological Journal of the Linnean Society* 142 (2): 233–252. https://doi.org/10.1111/j.1096-3642.2004.00132.x

Gidaszewski N.A., Baylac M. & Klingenberg C.P. 2009. Evolution of sexual dimorphism of wing shape in the *Drosophila melanogaster* subgroup. *BMC Evolutionary Biology* 9 (1): 110. https://doi.org/10.1186/1471-2148-9-110

Gould S.J. 1966. Allometry and size in ontogeny and phylogeny. *Biological Reviews* 41 (4): 587–638. https://doi.org/10.1111/j.1469-185X.1966.tb01624.x

Hallam A. 2001. A review of the broad pattern of Jurassic sea-level changes and their possible causes in the light of current knowledge. *Palaeogeography, Palaeoclimatology, Palaeoecology* 167 (1): 23–37. https://doi.org/10.1016/S0031-0182(00)00229-7

Haug C., Briggs D.E.G., Mikulic D.G., Kluessendorf J. & Haug J.T. 2014. The implications of a Silurian and other thylacocephalan crustaceans for the functional morphology and systematic affinities of the group. *BMC Evolutionary Biology* 14: 159. https://doi.org/10.1186/s12862-014-0159-2

Hegna T.A., Vega F.J. & González-Rodríguez K.A. 2014. First Mesozoic Thylacocephalans (Arthropoda, ?Crustacea; Cretaceous) in the Western Hemisphere: new discoveries from the Muhi Quarry Lagerstätte. *Journal of Paleontology* 88 (3): 606–616. https://doi.org/10.1666/13-131

Hessler R.R. 1985. Swimming in Crustacea. *Earth and Environmental Science Transactions of the Royal Society of Edinburgh* 76 (2–3): 115–122. https://doi.org/10.1017/S0263593300010385

Jacquin T. & Graciansky P.-C. de 1999. Major transgressive/regressive cycles: the stratigraphic signature of European basin development. *In*: Graciansky P.-C. de, Hardenbol J., Jacquin T. & Vail P.R. (eds) *Mesozoic and Cenozoic Sequence Stratigraphy of European Basins*: 15–30. Society for Sedimentary Geology, Tulsa, Oklahoma, USA.

Jauvion C., Audo D., Charbonnier S. & Vannier J. 2016. Virtual dissection and lifestyle of a 165-million-year-old female polychelidan lobster. *Arthropod Structure & Development* 45 (2): 122–132. https://doi.org/10.1016/j.asd.2015.10.004

Jauvion C., Charbonnier S. & Bernard S. 2017. A new look at the shrimps (Crustacea, Decapoda, Penaeoidea) from the Middle Jurassic La Voulte-sur-Rhône Lagerstätte. *Geodiversitas* 39 (4): 705–716. https://doi.org/10.5252/g2017n4a3

Jauvion C., Bernard S., Gueriau P., Mocuta C., Pont S., Benzerara K. & Charbonnier S. 2019. Exceptional preservation requires fast biodegradation: thylacocephalan specimens from La Voulte-sur-Rhône (Callovian, Jurassic, France). *Palaeontology* 63 (3): 395–413. https://doi.org/10.1111/pala.12456

Jauvion C., Audo D., Bernard S., Vannier J., Daley A.C. & Charbonnier S. 2020. A new polychelidan lobster preserved with its eggs in a 165 Ma nodule. *Scientific Reports* 10 (1): 3574. https://doi.org/10.1038/s41598-020-60282-1

Ji C., Tintori A., Jiang D. & Motani R. 2017. New species of Thylacocephala (Arthropoda) from the Spathian (Lower Triassic) of Chaohu, Anhui Province of China. *PalZ* 91 (2): 171–184. https://doi.org/10.1007/s12542-017-0347-7

Jolicoeur P. 1963. 193. Note: the multivariate generalization of the allometry equation. *Biometrics* 19 (3): 497–499. https://doi.org/10.2307/2527939

Josse J. & Husson F. 2016. missMDA: a package for handling missing values in multivariate data analysis. *Journal of Statistical Software* 70 (1): 1–31. https://doi.org/10.18637/jss.v070.i01

Kassambara A. & Mundt F. 2019. *factoextra: Extract and Visualize the Results of Multivariate Data Analyses*. R Package Version 1.0.7. Available from https://CRAN.R-project.org/package=factoextra [accessed 2 Aug, 2023].

Kiers H.A.L. 1997. Weighted least squares fitting using ordinary least squares algorithms. *Psychometrika* 62 (2): 251–266. https://doi.org/10.1007/BF02295279

Klingenberg C.P. 1998. Heterochrony and allometry: the analysis of evolutionary change in ontogeny. *Biological Reviews* 73 (1): 79–123. https://doi.org/10.1111/j.1469-185X.1997.tb00026.x

Kruta I., Rouget I., Charbonnier S., Bardin J., Fernandez V., Germain D., Brayard A. & Landman N. 2016. *Proteroctopus ribeti* in coleoid evolution. *Palaeontology* 59 (6): 767–773. https://doi.org/10.1111/pala.12265

Kühl G. & Rust J. 2012. *Captopodus poschmanni* gen. et sp. nov. a new stem-group arthropod from the Lower Devonian Hunsrück Slate (Germany). *Arthropod Structure & Development* 41 (6): 609–622. https://doi.org/10.1016/j.asd.2012.06.004

Kunze J. & Anderson D.T. 1981. The functional morphology of stomatopod Crustacea. *Philosophical Transactions of the Royal Society of London. B, Biological Sciences* 292 (1059): 255–328. https://doi.org/10.1098/rstb.1981.0032

Lange S. & Schram F.R. 2002. Possible lattice organs in Cretaceous Thylacocephala. *Contributions to Zoology* 71 (4): 159–169. https://doi.org/10.1163/18759866-07104006

Laville T., Haug C., Haug J.T., Forel M.-B. & Charbonnier S. 2021a. Morphology and anatomy of the Late Jurassic *Mayrocaris bucculata* (Eucrustacea?, Thylacocephala) with comments on the tagmosis of Thylacocephala. *Journal of Systematic Palaeontology* 19 (4): 289–320. https://doi.org/10.1080/14772019.2021.1910584

Laville T., Haug J.T. & Haug C. 2021b. New species of Thylacocephala, *Eodollocaris keithflinti* n. gen., n. sp., from the Mazon Creek Lagerstätte, Illinois, United States (c. 307 Ma) and redescription of other Mazon Creek thylacocephalans. *Geodiversitas* 43 (10): 295–310. https://doi.org/10.5252/geodiversitas2021v43a10

Laville T., Smith C.P.A., Forel M.-B., Brayard A. & Charbonnier S. 2021c. Review of Early Triassic Thylacocephala. *Rivista Italiana di Paleontologia e Stratigrafia* 127 (1): 73–101. https://doi.org/10.13130/2039-4942/15188

Lê S., Josse J. & Husson F. 2008. FactoMineR: a package for multivariate analysis. *Journal of Statistical Software* 25 (1): 1–18. https://doi.org/10.18637/jss.v025.i01

Meland K., Mees J., Porter M. & Wittmann K. 2015. Taxonomic review of the orders Mysida and Stygiomysida (Crustacea, Peracarida). *PLoS ONE* 10: e0124656. https://doi.org/10.1371/journal.pone.0124656

Mergl M. 2020. The Cuticles of (?) Thylacocephalan arthropod from the Basal Choteč Event (Choteč Formation, Eifelian; Barrandian Area, Czech Republic). *Folia Musei rerum naturalium Bohemiae occidentalis. Geologica et Paleobiologica* 54 (1–2): 1–12. https://doi.org/10.2478/fbgp-2020-0001

Minelli A. & Fusco G. 2013. Arthropod post-embryonic development. *In*: Minelli A., Boxshall G. & Fusco G. (eds) *Arthropod Biology and Evolution: Molecules, Development, Morphology*: 91–122. Springer, Berlin, Heidelberg. https://doi.org/10.1007/978-3-642-36160-9_5

Neil D.M. 1975. The mechanism of statocyst operation in the mysid shrimp *Praunus flexuosus*. *Journal of Experimental Biology* 62 (3): 685–700. https://doi.org/10.1242/jeb.62.3.685

Neil D.M. & Ansell A.D. 1995. The orientation of tail-flip escape swimming in decapod and mysid crustaceans. *Journal of the Marine Biological Association of the United Kingdom* 75 (1): 55–70. https://doi.org/10.1017/S0025315400015198

Oppenheim P. 1888. Neue Crustaceenlarven aus dem lithographischen Schiefer Bayerns. *Zeitschrift der Deutschen Geologischen Gesellschaft* 40 (4): 709–719.

Packard G.C. 2018. A new research paradigm for bivariate allometry: combining ANOVA and non-linear regression. *Journal of Experimental Biology* 221 (7): jeb177519. https://doi.org/10.1242/jeb.177519

Pélabon C., Bolstad G.H., Egset C.K., Cheverud J.M., Pavlicev M. & Rosenqvist G. 2013. On the relationship between ontogenetic and static allometry. *The American Naturalist* 181 (2): 195–212. https://doi.org/10.1086/668820

Pélabon C., Tidière M., Lemaître J.-F. & Gaillard J.-M. 2018. Modelling allometry: statistical and biological considerations – a reply to Packard. *Biological Journal of the Linnean Society* 125 (3): 664–671. https://doi.org/10.1093/biolinnean/bly141

Pinna G., Arduini P., Pesarini C. & Teruzzi G. 1982. Thylacocephala: una nuova classe di crostacei fossili. *Atti della Società italiana di Scienze naturali e del Museo civico di Storia naturale di Milano* 123 (4): 469–482.

Pinna G., Arduini P., Pesarini C. & Teruzzi G. 1985. Some controversial aspects of the morphology and anatomy of *Ostenocaris cypriformis* (Crustacea, Thylacocephala). *Transactions of the Royal Society of Edinburgh: Earth Sciences* 76 (2–3): 373–379. https://doi.org/10.1017/S0263593300010580

Polz H. 1988. *Clausia lithographica* Oppenheim (? Crustacea). *Archaeopteryx* 6: 69–73.

Polz H. 1989. *Clausocaris* nom. nov. pro *Clausia* Oppenheim 1888. *Archaeopteryx* 7: 73.

Polz H. 1990. *Clausocaris lithographica* (? Crustacea, Thylacocephala). *Archaeopteryx* 8: 93–109.

Polz H. 1993. Zur Metamerie von *Clausocaris lithographica* (Thylacocephala,? Crustacea). *Archaeopteryx* 11: 105–112.

Polz H. 1994. *Mayrocaris bucculata* gen. et sp. nov. (Thylacocephala, Conchyliocarida) aus den Solnhofener Plattenkalken. *Archaeopteryx* 12: 35–44.

Polz H. 1997. Der Carapax von *Mayrocaris bucculata* (Thylacocephala, Conchyliocarida). *Archaeopteryx* 15: 59–71.

Polz H. 2001. *Dollocaris michelorum*, sp. nov. (Thylacocephala, Concavicarida) aus den Solnhofener Plattenkalken. *Archaeopteryx* 19: 45–55.

Pulsipher M.A., Anderson E.P., Wright L.S., Kluessendorf J., Mikulic D.G. & Schiffbauer J.D. 2022. Description of *Acheronauta* gen. nov., a possible mandibulate from the Silurian Waukesha Lagerstätte, Wisconsin, USA. *Journal of Systematic Palaeontology* 20 (1): 2109216. https://doi.org/10.1080/14772019.2022.2109216

R Core Team 2021. *R: A Language and Environment for Statistical Computing*. R Foundation for Statistical Computing, Vienna, Austria. Available from https://www.R-project.org/ [accessed 2 Aug. 2023].

Rak Š., Broda K. & Kumpan T. 2018. First Carboniferous thylacocephalan from Europe and its significance for the understanding of functional morphology of Concavicarididae Schram, 2014. *Crustaceana* 91 (3): 265–285. https://doi.org/10.1163/15685403-00003771

Rao C.R. 1973. *Linear Statistical Inference and its Applications: Second Edition*. Wiley, New York.

Rolfe W.D.I. 1969. Phyllocarida. *In*: Moore R.C. (ed.) *Treatise on invertebrate paleontology, Part R, Arthropoda 4* 1: R296–R331. Geological Society of America & University of Kansas Press, Lawrence, KS.

Rolfe W.D.I. 1985. Form and function in Thylacocephala, Conchyliocarida and Concavicarida (?Crustacea): a problem of interpretation. *Transactions of the Royal Society of Edinburgh: Earth Sciences* 76 (2–3): 391–399. https://doi.org/10.1017/S0263593300010609

Rolfe W.D.I. 1992. Not yet proven Crustacea: the Thylacocephala. *Acta Zoologica* 73 (5): 301–304. https://doi.org/10.1111/j.1463-6395.1992.tb01095.x

Schlacher T.A., Wittmann K.J. & Ariani A.P. 1992. Comparative morphology and actuopalaeontology of mysid statoliths (Crustacea, Mysidacea). *Zoomorphology* 112 (2): 67–79. https://doi.org/10.1007/BF01673808

Schneider C.A., Rasband W.S. & Eliceiri K.W. 2012. NIH Image to ImageJ: 25 years of image analysis. *Nature Methods* 9 (7): 671–675. https://doi.org/10.1038/nmeth.2089

Schoenemann B. & Clarkson E.N. K. 2011. Eyes and vision in the Chengjiang arthropod *Isoxys* indicating adaptation to habitat. *Lethaia* 44 (2): 223–230. https://doi.org/10.1111/j.1502-3931.2010.00239.x

Schram F.R. 1990. On Mazon Creek Thylacocephala. *Proceedings of the San Diego Society of Natural History* 3: 1–16.

Schram F.R. 2014. Family level classification within Thylacocephala, with comments on their evolution and possible relationships. *Crustaceana* 87 (3): 340–363. https://doi.org/10.1163/15685403-00003289

Schram F.R. & Koenemann S. 2022. Infraclass Thylacocephala. *In*: *Evolution and Phylogeny of Pancrustacea: A Story of Scientific Method*: 603–624. Oxford University Press, New York.

Schram F.R., Hof C.H.J. & Steeman F.A. 1999. Thylacocephala (Arthropoda: Crustacea?) from the Cretaceous of Lebanon and implications for thylacocephalan systematics. *Palaeontology* 42 (5): 769–797. https://doi.org/10.1111/1475-4983.00097

Secrétan S. 1985. Conchyliocarida, a class of fossil crustaceans: relationships to Malacostraca and postulated behaviour. *Transactions of the Royal Society of Edinburgh: Earth Sciences* 76 (2–3): 381–389. https://doi.org/10.1017/S0263593300010592

Secrétan S. & Riou B. 1983. Un groupe énigmatique de Crustacés: ses représentants du Callovien de la Voulte-sur-Rhône (France). *Annales de Paléontologie* 69 (4): 59–97.

Secrétan S. & Riou B. 1986. Les Mysidacés (Crustacea, Peracarida) du Callovien de la Voulte-sur-Rhône. *Annales de Paléontologie* 72 (4): 295–323.

Sekiguchi H. & Terazawa T. 1997. Statocyst of *Jasus edwardsii pueruli* (Crustacea, Palinuridae), with a review of crustacean statocysts. *Marine and Freshwater Research* 48 (8): 715–720. https://doi.org/10.1071/mf97131

Sjoberg D.D., Whiting K., Curry M., Lavery J.A. & Larmarange J. 2021. Reproducible summary tables with the gtsummary package. *The R Journal* 13 (1): 570–580. https://doi.org/10.32614/RJ-2021-053

Stenvers V.I., Gonzalez B.C., Goetz F.E., Hemmi J.M., Jessop A.-L., Lin C., Hoving H.-J.T. & Osborn K.J. 2021. Extraordinary eyes reveal hidden diversity within the holopelagic genus *Paraphronima* (Amphipoda: Hyperiidea). *Deep Sea Research Part I: Oceanographic Research Papers* 177: 103610. https://doi.org/10.1016/j.dsr.2021.103610

Strausfeld N.J., Ma X., Edgecombe G.D., Fortey R.A., Land M.F., Liu Y., Cong P. & Hou X. 2016. Arthropod eyes: The early Cambrian fossil record and divergent evolution of visual systems. *Arthropod Structure & Development* 45 (2): 152–172. https://doi.org/10.1016/j.asd.2015.07.005

Tintori A., Bigi E., Crugnola G. & Danini G. 1986. A new Jurassic Thylacocephala *Rugocaris indunensis* gen. n. sp. n. and its paleoecological significance. *Rivista Italiana di Paleontologia e Stratigrafia* 92 (2): 239–250.

Van Roy P., Rak Š., Budil P. & Fatka O. 2021. Upper Ordovician Thylacocephala (Euarthropoda, Eucrustacea) from Bohemia indicate early ecological differentiation. *Papers in Palaeontology* 7 (3): 1727–1751. https://doi.org/10.1002/spp2.1363

Van Straelen V. 1922. Les crustacés décapodes du Callovien de la Voulte-sur-Rhône (Ardèche). *Comptes Rendus des séances de l'Académie des Sciences, Paris* 175: 982–983.

Van Straelen V. 1923a. Les mysidacés du Callovien de la Voulte-sur-Rhône. *Bulletin de la Société géologique de France* 23: 431–439.

Van Straelen V. 1923b. Description de crustacés décapodes macroures nouveaux des terrains secondaires. *Annales de la Société royale zoologique de Belgique* 53: 84–93.

Van Straelen V. 1925. Contribution à l'étude des crustacés décapodes de la période Jurassique. *Mémoires de la Classe des Sciences de l'Académie royale de Belgique* 7 (2): 1–462.

Vannier J. & Chen J.-Y. 2000. The Early Cambrian colonization of pelagic niches exemplified by *Isoxys* (Arthropoda). *Lethaia* 33 (4): 295–311. https://doi.org/10.1080/002411600750053862

Vannier J., Boissy P. & Racheboeuf P.R. 1997. Locomotion in *Nebalia bipes*: a possible model for Palaeozoic phyllocarid crustaceans. *Lethaia* 30 (2): 89–104. https://doi.org/10.1111/j.1502-3931.1997.tb00449.x

Vannier J., Chen Y., Huang Y., Charbonnier S. & Wang Q. 2006. The Early Cambrian origin of thylacocephalan arthropods. *Acta Palaeontologica Polonica* 51 (2): 201–214.

Vannier J., Schoenemann B., Gillot T., Charbonnier S. & Clarkson E. 2016. Exceptional preservation of eye structure in arthropod visual predators from the Middle Jurassic. *Nature Communications* 7: 10320. https://doi.org/10.1038/ncomms10320

Vicente C.S. & Cartanyà J. 2017. A new mysid (Crustacea, Mysida) from the Ladinian Stage (Middle Triassic) of Conca de Barberà (Catalonia, NE Iberian Peninsula). *Journal of Paleontology* 91 (5): 968–980. https://doi.org/10.1017/jpa.2017.24

Villier L., Charbonnier S. & Riou B. 2009. Sea stars from Middle Jurassic Lagerstätte of La Voulte-sur-Rhone (Ardèche, France). *Journal of Paleontology* 83 (3): 389–398. https://doi.org/10.1666/08-030.1

Voicu G. 1974. Identification des Mysidés fossiles dans les dépôts du Miocène supérieur de la Paratéthys Centrale et Orientale et leur importance paléontologique, stratigraphique et paléogéographique. *Geologicky Zborník. Geologica Carpathica* 25: 231–239.

Warton D.I., Wright I.J., Falster D.S. & Westoby M. 2006. Bivariate line-fitting methods for allometry. *Biological Reviews* 81 (2): 259. https://doi.org/10.1017/S1464793106007007

Warton D.I., Duursma R.A., Falster D.S. & Taskinen S. 2012. smatr 3 - an R package for estimation and inference about allometric lines. *Methods in Ecology and Evolution* 3 (2): 257–259. https://doi.org/10.1111/j.2041-210X.2011.00153.x

Wilby P.R., Briggs D.E.G. & Riou B. 1996. Mineralization of soft-bodied invertebrates in a Jurassic metalliferous deposit. *Geology* 24 (9): 847–850. https://doi.org/10.1130/0091-7613(1996)024<0847:MOSBII>2.3.CO;2

Wilke C.O. 2019. *cowplot: Streamlined Plot Theme and Plot Annotations for 'ggplot2'*. Available from https://cran.r-project.org/web/packages/cowplot/index.html [accessed 2 Aug. 2023].

Williams M., Benton M.J. & Ross A. 2015. The Strawberry Bank Lagerstätte reveals insights into Early Jurassic life. *Journal of the Geological Society* 172 (6): 683–692. https://doi.org/10.1144/jgs2014-144

Wittmann K.J., Schlacher T.A. & Ariani A.P. 1993. Structure of recent and fossil mysid statoliths (Crustacea, Mysidacea). *Journal of Morphology* 215 (1): 31–49. https://doi.org/10.1002/jmor.1052150103

Manuscript received: 10 March 2022
Manuscript accepted: 17 April 2023
Published on: 5 October 2023
Topic editor: Tony Robillard
Section editor: Christian de Muizon
Desk editor: Pepe Fernández

Supplementary material

Supp. file 1. List of the material studied. https://doi.org/10.5852/ejt.2023.898.2295.9935

Supp. file 2. Measurements data and R scripts. Available from https://doi.org/10.5281/zenodo.6341180 https://doi.org/10.5852/ejt.2023.898.2295.9937

Supp. file 3. Eigenvalues and factor loadings of principal component analysis. https://doi.org/10.5852/ejt.2023.898.2295.9939